Detection of metals using Bi-modified glassy carbon electrodes: an insight into their performance

A thesis submitted for the degree of Doctor of Philosophy

By

Arlete Nkoko Bambuwu

Chemistry - School of Natural and Environmental Sciences, Newcastle University

Newcastle Upon Tyne NE1 7RU, United Kingdom

December, 2022

Abstract

Heavy metals are well known as a source of several contamination problems for humans, marine life, and animals. Their detection and quantification are extremely important to suppress negative effects such as diseases caused by them. Conventionally, spectrometric techniques such as AAS and ICPs are the most recommended due to their sensitivity and accuracy. However, the main drawbacks of those techniques are the cost and the specialized training required for its operator. Electroanalytical techniques have been an important substitute for spectrometric methods due to their cost-effectiveness and simplicity of their operation. Bi-modified electrodes introduced recently produced results that can be comparable to those obtained by spectrometric techniques. Glassy carbon has been widely used as the substrate on which Bi is electrodeposited, and in this work glassy carbon Bi-modified electrodes have been explored. The roughness factor of the bare electrode has been estimated using two different methods, however, only the recalibration technique provided values in the expected range which is from 1.5 to 2.0. In this research, two heavy metals are targeted namely Zn and Pb. Trials with several reference electrodes have been done such as mercury-mercurous sulfate electrode MSE (K_2SO_4 saturated) and MSE (1 M H_2SO4) and finally calomel (1M KCl). the latter showed the capacity for the detection of both Zn and Pb. Acetate buffer, pH 4.5, was employed since it is the most used and recommended. The study of the influence of the addition of another electrolyte to increase the ionic strength and consequently the improvement of the sensitivity has been realized in this work. $NaClO_4$ and Na_2SO_4 chosen to undergo this study showed the peak shift in the case of Zn. Higher Zn peaks are mainly obtained under stirring conditions, particularly in the case of $NaClO_4$.

Among other factors, the plating solution preparation also influences the performance of the stripping analysis, Zn stripping peak heights obtained from Bi prepared in acetate buffer are lower than those from Bi prepared in HNO_3. Although the irreproducibility problem was consistently observed throughout this research, the calibration curve obtained for the 1-6 µM range for both Pb and Zn requires a series of treatments until it reaches the one that fulfills the requirements, for Zn two calibration curves were produced, a drop in sensitivity is recorded on the second, therefore the first and an average curve are maintained for sample calculations showing r= 0.979 and r= 0.943 respectively. The detection of Pb has been

extremely difficult due to the issue of multiple peaks which was addressed by applying an extensive electrochemical cleaning. The calibration curve generated presented a correlation factor of r = 0.969.

Real samples were used to fulfil the purpose of this work, natural and tap water from different sources are used. Samples analysed have not shown any Pb peak, only Zn peaks could be detected. Zn stripping peaks have suffered some shifts compared to the position of the peaks from the standard solution. The concentration of Zn(II) was estimated based on the first and average calibration curves respectively, for tap water: Stanton Street presented 13.5±6.8 and 14.3±7.2 µg/L, and Morpeth Street 24.6±8.3 and 25.7±8.7 µg/L, for natural water: Blaydon Bridge 5.9±0.5 and 6.3±0.5 µg/L and Blaydon Burn 14.5±3.5 to 15.4±3.7 µg/L The results obtained from the electroanalytical technique through calibration curve calculation technique are comparable to the ones obtained in standard addition, ICP-OES and ICP-MS. The matrix effect is observed as the differences in charges registered during calibration curves experiments are extremely lower than in standard addition. Additionally, the LOD and LOQ were estimated for Pb as 1.17 µg/L and 3.56 µg/L, and for Zn as 0.252 µg/L and 0.764 µg/L respectively, using the regression parameters and the conditions of the sample applied in this research work.

Acknowledgement

In the first place, I would like to thank God for the life and strength to endure all the difficulties throughout this journey.

My special gratitude to INAGBE for the funding, the opportunity, and all the support offered.

I would like to thank Prof. Ulrich Stimming for accepting me as his PhD student.

I would like to express my gratitude to Dr Ben Horrocks for all the help provided throughout this work, and for encouragement during all the difficult times I have been through.

A huge thanks to Dr Elizabeth Gibson, who intervened during a desperate time, and I would also like to thank Dr Martin Cooke for his support in uncertain times.

I would also like to thank my compatriot Nelson Manzanza for being supportive and encouraging as we were facing a similar situation.

I would like to thank my family, my late father Nkoko Zola Fernando, my mother Vinda Clementina, and my brothers Benjamin, Briguel, and Massamba for caring for my daughters Victoria and Graciete during almost five years of absence.

Special thanks to the Faculty of Natural Sciences of Agostinho Neto University, particularly my mentors Dr Vila Famila and Dr Massuquinini Ines.

I would also like to thank Dr Jochen who was fundamental at the beginning of this research, and Dr Arup who as a research associate contributed enormously to the successful sample results in the last phase of this work.

I would also like to thank all my colleagues at Stimming Group; I have enjoyed having them around as a family. Thanks for all the support received.

Thanks to Nexus especially Jose Portoles and Michael Foster for allowing me to obtain XPS and SEM results; and Clair Roper for ICP-OES and ICP-MS.

I would also like to thank the SNES PGR staff, particularly Brian Shields and Craig Hinds for their prompt help in all my inquiries.

Table of Contents

List of Figures

List of Tables

Abbreviations and Symbols

A: surface area

AFM: Atomic Force Microscopy

ASV: Anodic Stripping voltammetry

A^{ECSA}: Electrochemically active surface area

A^{geo}: Geometric surface area

b: intercept

BFE: Bi film electrode

BSE: back scattered electrons

C_a: concentration of the amalgam (alloy)

CA: Chronoamperometry

C_b: bulk concentration of the metal

$C_{b,0}$: bulk concentration of the metal ion at the beginning of the pulse

$C_{b,t}$: bulk concentration of the metal ion after a given time

C_d: differential capacity of the double layer

CL: Cathodoluminescence

cm^3: cubic centimetre

C_{ox}: concentration of oxidizing specie

CPEs: Carbon Paste Electrodes

CV: Cyclic voltammetry

d: diameter

D: diffusion coefficient

DPV: differential pulse voltammetry

E_i: initial potential

E_v: final potential

EDX: Energy dispersive X-ray analysis

eV: electronvolt

E_d: deposition potential

E (U): electric potential

F: faraday's constant

g/cm^3: gram per cubic centimetre

GCEs: Glassy carbon electrodes

i_{bkgd}: background current

i_c: charging current

ICP-OES: Inductively coupled Plasma-Optical Emission Spectrometry

ICP-MS: Inductively Coupled Plasma-Mass Spectrometry

$i_{f,r}$: background current associated with redox reaction of impurities

i_L: limiting current.

i_t: total current

i_p: stripping peak current

I_{s+x}: Analytical signal provided by the final solution (containing both the analyte and the standard)

I_x: Analytical signal provided by $[X]_i$

j: current density

K: constant dependent on the flow regime

LOD: limit of detection

m: moles accumulated on the surface

m: slope

mm: millimetre

MSE: mercury-mercurous sulfate electrode

mC: milli Coulomb

mM: milli molar

mV: milli volt

ms: milli second

mL: milli litre

mg: milligram

min: minutes

mA: milli Ampere

mm: millimetre

n: number of electrons transferred.

NA: atomic number

NCBFE: Nafion coated Bi film electrode

P_W: pulse width

P_H: pulse height

ppb: part per billion

ppm: part per million

PSPD: position-sensitive photodiode

q_{ad}: the adsorption charge associated with a known adsorbate on the electrode surface.

q_m: the charge associated with a monolayer coverage of the said adsorbate

r: correlation factor

R: gas constant

R_F: roughness factor

rpm: rotation per minute

RSF: relative sensitivity factor

s: second

$[S]_i$: Concentration initial of the standard

$[S]_f$: Concentration of the standard in the final solution

S_H: step height

S_T: step time

Sat'd: saturated

SE: secondary electrons

SEM: Scanning electron microscopy

SHE: Standard Hydrogen Electrode

t_d: deposition time

T: temperature

U: Convection rate

U^0: Standard potential

V: volt

V: total volume containing both the analyte and the standard

V_{Hg}: volume of a mercury electrode

V_0: initial volume (volume of the unknown which may be the analyte)

V_s: volume of the standard

vs: versus

$W_{1/2}$: peak width at half height.

w/w: weight per weight

$[X]_i$: Initial concentration of the solution containing the analyte

$[X]_f$: Concentration of the analyte in the final solution

XPS: X-ray Photoelectron Spectroscopy

δ: thickness of the diffusion layer

α: constant dependent on the electrode geometry

ν: Scan rate

Δi_p: differential current

ΔE: pulse height

σ: electronic conductivity

µC: micro Coulomb

µM: micro molar

µA: micro-Ampere

µL: micro-litre

µg: micro gram

Chapter 1: Introduction

Detection and quantification of heavy metals are fundamental to evaluate the level of pollution generated by them. Heavy metals constitute a source of pollution in the environment. Some of them are a major threat to public health, for example Pb [193]. This element can be a source of carcinogenic diseases. Pb quantification is extremely important for safety reasons in industrial processes, food supply, and in the environment. It is also important in medicine, especially clinical diagnosis, and toxicology. According to WHO regulations, permissible concentration limits in water for Pb and Zn are respectively 0.01 mg/L and 3-5 mg/L. One of the metals studied in this thesis is Zn, which is an important cofactor for many enzymes essential for normal physiological function. However, high levels of Zn can produce toxic effects [192]. Zn is an essential mineral for the function of hundreds of enzymes throughout the body. Zn operates as a cofactor for enzymes responsible for aspects of DNA expression. It is important in membrane stabilization, the metabolism of vitamin A, gustatory and olfactory systems. In natural, unpolluted surface waters, the concentration of Zn recorded is low and commonly reported below 10 µg/L. Groundwaters may contain larger concentrations of 10-40 µg/L. However, in tap water, the Zn(II) concentration may be increased because Zn is commonly used to protect pipework against corrosion. Leaching of Zn from pipework (mainly in older galvanized plumbing materials) may result in drinking water containing Zn at concentrations above 0.1 mg/L. At levels above 3-5 mg/L in water (drinking) containing Zn, the liquid tends to be opalescent, to have an "unwanted astringent taste" and the deposition of a "greasy film" has been reported on boiling the water with high Zn levels [192].

The second metal mentioned in this work is Pb (lead) which can sometimes be found in tap water due to its dissolution from natural sources. However, Pb contamination is predominantly a result of corrosion of household plumbing systems that contain Pb. The use of plastic plumbing materials has not entirely solved this problem; Pb compounds are also encountered in polyvinyl chloride (PVC) pipework. Pb can be stripped (leached) from parts of the plumbing system and consequently, a high lead concentration in drinking water can still be observed. The extent of Pb dissolved in the plumbing system is influenced by several factors related to the corrosion of Pb and the solubility of Pb compounds. These include the

presence of chloride and dissolved oxygen (influences corrosion rate), pH which influences both the corrosion rate and solubility, and temperature. The water softness and the standing time of the water in the pipework also matter - high flow rates will dilute the Pb ions. Soft, acidic water is considered (being) the most plumbosolvent. While Pb leaching can essentially continue indefinitely, it declines with time for soldered joints and brass taps. However, newly-constructed homes that contain soldered connections of copper piping can discharge Pb at levels of 210–390 μg/L [193].

Heavy metals are generally described as metals with relatively high densities, atomic weights, or atomic numbers. A density of more than 5 g/cm^3 is sometimes quoted as the common criterion for an element to be denoted as a heavy metal [95]. Some heavy metals are either nutrients, for example Zn, or relatively harmless, but can be toxic in larger amounts or in certain forms [151]. Other heavy metals are poisonous in small quantities and not essential. Examples include Hg and Pb, which are extremely toxic and do not have known useful biological functions. Mining, tailings, industrial waste, agricultural runoff, occupational exposure, paints, and treated timber are considered possible sources of heavy metals [149]. The bioavailability and toxicity of the metal rely essentially on its speciation - the nature of the ligands bound to the metal ion. Metal complexes which can enter biological cells across the negatively charged cell membrane are more bioavailable and more toxic. The cation aquo-ions and lipid-soluble complexes pose the greatest threat to living organisms. Anionic complexes may be excluded from cells and their toxicity reduced.

Because of their wide utilisation, toxicity of the combined or elemental form as well as the extensive distribution in the environment of the metals like Pb and Hg, it is most likely to observe the degree of contamination caused by those metals [9]. In the human body, metals such as Cr, As, and Pb have a strong ability to bind to proteins. These soft metals interact strongly with sulfur through thiol groups on cysteine residues and affect the performance of enzymes that regulate metabolic reactions. As a result of this union of sulfur metal enzymes, the operation of the latter is restrained leading to health degradation, which frequently terminates in death [157]. Pb is the utmost ubiquitous pollutant heavy metal, and alongside Hg, they are known to harm the central nervous system [46]. Heavy metals assessments in aquatic environments of industrialised societies showed to be two to three times levels higher than in case of the pre-industrial era, a considerable growth is observed [147].

Because of the industrial activities, a surge in the concentration of heavy metals is reported, deteriorating the air, water, and soil quality; therefore, human beings' health, flora, and fauna are negatively affected [163]. General origins of heavy metals in this context involve mining and industrial wastes, vehicles emissions, motor oil, fuels used by ships and heavy machineries, construction works, fertilisers, pesticides, paints, dyes and pigments, renovation, illegal depositing of construction and demolition waste, open-top roll-off dumpster, welding, brazing and soldering, glassworking, concrete works, roadworks, use of recycled ventilation system, food contaminated by the environment or by the packaging, armaments, lead-acid batteries, electronic waste recycling yard, and treated timber [25], ageing water supply infrastructure [79] and microplastics floating in the world's oceans [38]. Electrical conductivity and reflectivity (characteristics of metals) or density, strength, and durability (characteristics of heavy metals) determine some general applications of heavy metals [57].

Normally, the detection and quantification of heavy metals are mainly executed using spectrometric methods such as atomic absorption and ICPs (ICP-OES and ICP-MS). Although all these spectrometric methods can reach a detection limit concentration of ppb, the ICP-MS apparatus can lower it to the ppt range. For analysis, these techniques require samples to be processed and analysed in a laboratory. Nevertheless, the equipment is large, extremely costly, and its operation requires specialized training. Electrochemical stripping analysis is also known as a powerful technique to detect heavy metals, and it is remarkably sensitive as well [24,139]. However, electrochemical techniques are low-priced and simple to be operated although not recommended for routine analysis due to their extended experiments. Some advantages of anodic stripping voltammetry (ASV) include its capacity to achieve comparable sub-ppb limits of detection (LOD) with its inexpensive, unsophisticated, and smaller footprint equipment. In addition to that, approximately thirty different elements are detectable using ASV, although some of them demand a special protocol for the purpose as is the case of As. The concentration of free/labile at a specific pH according to the solution in study can be estimated through ASV and the acidification of this solution in study is not a requirement contrary to ICP [123,146]. Currently, considerable ASV literature is available; however, due to disadvantages such as extensive operation time, the technique use is not as frequent as expected. One of the most recent improvements to electrochemical stripping analyses is the

use of Bi modified electrode which is currently considered a substitute for mercury electrodes since the latter is no longer in use due to its toxicity [13].

The effectiveness of the stripping analysis using Bi is a question that needs to be answered because there are inconveniences in using this technique compared to certified ones such as ICPs and AAS. Metal deposition and stripping are a major challenge on a solid electrode for several motives since a change in the surface properties is registered once the metal is deposited. The exploration of some overlooked insights while executing this technique especially when the glassy carbon electrode is used as substrate. These insights include the surface characteristics which are a combination of the deposit including the underlying solid electrode, deposition potentials, onset potentials for HER, and water reduction [24,127]. The application of this technique in using real samples is fundamental for situations where specialized techniques cannot be used due to financial issues. One of the objectives of this work is to deliver a simple approach for the detection and quantitation of heavy metals in real samples and environmental samples.

One of the milestones established in this work is the detection of heavy metals using Bi film-modified electrodes employing a simple and cost-effective technique. Many third countries such as Angola are developing countries. Bi-modified electrodes have been recently one of the most prominent electroanalytical techniques used. The effectiveness of the Bi film produced is also an issue that needs to be investigated.

The detection of heavy metals is as important as their quantification. In many countries, water quality is still an issue; in some regions, the consumption of water straight from rivers and wells occurs without submitting the water to any prior treatment. This can lead to poisoning of those consuming this water. Conventional techniques used for this purpose are extremely expensive and the possibility to obtain them is limited. Besides, those conventional techniques require specific training for their operation as referred to earlier.

It is crucial to examine a technique that competes with conventional techniques (spectrometric techniques) and provides reliable results without having to spend a fortune. Electroanalytical techniques can be considered a good substitute for spectrometric techniques; however, Hg electrodes are widely banned due to their high toxicity. The Bi-modified electrode is a promising alternative for stripping voltammetric determination of

heavy metals [183]. This technique has shown some effectiveness in its behaviour. This research aims to evaluate some insights into its performance closely. In this work, a closer look at Bi films produced under room temperature conditions is taken.

Although, there is some good information on Bi electrode performance. There are some inconveniences in using this method that has been overlooked. This research focuses on aspects that affect the detection of Zn with Bi-modified electrodes using glassy carbon as the substrate. The consequences of this irreproducible behaviour affect the accuracy and reliability of the results of the quantification and detection. In this work, the aim was to demonstrate through changes in the behaviour of glassy carbon electrodes, that it is nevertheless possible to detect and quantify Zn and Pb reliably.

The pH recommended for Bi-modified electrodes is normally 4-6, and some works suggest pH=4.5 and acetate buffer as the supporting electrolyte. However, the plating solution in which Bi is prepared can influence the stripping peaks of the analyte, consequently, the sensitivity of the technique may be affected. A study on the behaviour of the stripping when Bi is prepared in acetate buffer and HNO_3 was made. The differences in the analytical results will provide an insight into the fact that several previous works prepare the plating solution in mineral acids such as HNO_3 and HCl. This study is detailed in Chapter 5.

This research also investigates the influence of the electrolyte which can affect positively the stripping signal, which means, increasing the analyte peak current and improving the sensitivity of the technique. In this work, Na_2SO_4 and $NaClO_4$ were evaluated for their effect on the sensitivity. Na_2SO_4 is a common, readily available electrolyte and $NaClO_4$ is of interest because perchlorate anion is known to be weakly coordinating with many metals.

The state of the electrode is fundamental since all the processes occur on the surface of the electrode, in chapter 4, the electrode is studied thoroughly by first estimating the roughness factor and then by microscopic characterization.

For reliable results, apart from electroanalytical techniques, the results must be compared to sensitive techniques such as ICP-based spectroscopies in Chapter 6. In this work, this comparison between the results of electroanalytical and spectrometric (ICP-OES and ICP-MS) in this case) techniques. To increase the reliability and accuracy of the results, standard

addition was also introduced to compare with the calibration curve and also examine the matrix effect.

Chapter 2: Fundamentals

Propagation of heavy metal contamination has raised awareness of methods for their determination and characterization [53]. It is recognized that heavy metals are hugely toxic and dangerous pollutants, perhaps only second to pesticides in environmental significance. In comparison to pesticides, an important feature distinguishing metals is that many metals are biodegradable. Nevertheless, they are life threatening and can reach humans from numerous environmental sources via respiration and, the continental and marine food chains. A handful of metals are entirely not lethal (toxic) at any level [182]. In general, however, many metal ions have important biological functions and are therefore essential at some level but produce toxic effects at higher levels [66]. As a consequence of their biodegradable nature, heavy metals may be transported as ions and accumulate in vital organs of a human being where they exert toxic effects. In case of Zn, the difference between the concentrations at which it is poisonous and the concentration that is essential for normal physiological processes is small. Because of this narrow concentration difference, reliable knowledge of the matrix is compulsory. Information on the chemical state of the trace metal in natural waters or biological fluids is important for the understanding of their reactivity, transport, and toxicity [182].

Bi is known as an environmentally friendly element, with lower toxicity and is widely used in the pharmaceutical industry. According to some works realized, bismuth-modified electrodes are well-suited for analysis of Zn. They are claimed to show well-defined, reproducible stripping peaks without distortion. In addition, excellent resolution of neighbouring peaks, a large hydrogen evolution overpotential, a wide linear dynamic range, and a ratio of the analytical signal to the background that is comparable to those of mercury electrodes [181].

Bi is a semi-metal with a rhombohedral structure and, because of its distinctive physical and chemical properties [190], bismuth has attracted much interest from physicists and chemists. Bi also displays beneficial electrochemical properties related to the low electrocatalytic activity for hydrogen evolution and oxygen reduction; these properties reduce the level of the background signals and interference of undesirable faradaic currents at negative potentials during the electrodeposition of Zn. In addition to that, Bi can produce alloys with heavy metals

such as Pb and Zn at ambient temperature during the deposition step from an aqueous solution [120]. The alloy formation enhances the nucleation process that is required to deposit heavy metals in the first step of a stripping analysis. These factors are responsible for the choice of Bi electrodes of various forms for the detection of heavy metals by stripping voltammetry [181].

2.1. Electroanalytical methods

Electroanalytical methods are extensively applied in scientific research and the monitoring of industrial materials and the environment. Voltammetry is a class of techniques that includes many common electroanalytical methods, it involves the application of a controlled potential and measurement of the current produced. Limits of detection of the order of 10^{-6} M (10^{-10} M with pre-concentration) as mentioned in Chapter 11, section 11.8 of the reference [12], can be attained using voltammetric methods and a large number of metallic ions and organic compounds may be determined. The concept of preconcentrating analytes on the electrode to lower the detection limit has been demonstrated to be extremely advantageous. Stripping electroanalytical methods (SEAM) are used for the analysis of trace metal ions in solutions [27]. The first phase in any SEAM is the accumulation of the electroactive substance on the surface or in the bulk of the electrode. The second phase is informative and is operated under various modes of electrode polarization: potentiodynamic conditions, including superposition of pulses of different shapes and amplitude and galvanostatic and potentiostatic conditions. Accordingly, the information sources in SEAM are cathodic or anodic voltammograms (stripping voltammetry), potential-time dependences (stripping chronopotentiometry), or current-time dependences (stripping chronoamperometry and coulometry). The electrochemical reaction has always been the source of information in SEAM [27].

In numerous matrices, the normal concentration of several important metals is most of the time near the detection limit of the respective technique used. The suitability of an individual technique for trace analysis depends on several factors: detection limit, capital and running costs of the instrumentation, analysis time, sample preparation and selectivity. Compared to atomic spectroscopy, stripping analysis provides the benefit of species characterization (determination of the chemical identity of the metal complex not merely the elemental identity). Methods based on atomisation of the sample destroy the information on the

chemical speciation of the elements which may be relevant to applications in which the bioavailability of the heavy metal is crucial [182].

In several situations, the defining factor in selecting analytical techniques is the issue of interferences. Interference may be understood as any effect that alters the response when the concentration of the analyte remains unaffected. In stripping analysis, the formation of intermetallic compounds, adsorption of organic substances on the electrode and overlapping peaks are included as causes of the interference [50]. Stripping analysis is an analytical technique which employs a bulk electrolytic step to preconcentrate the metal of interest from the sample solution into or onto the working electrode. Anodic stripping voltammetry (ASV) is the form (type) of stripping analysis extensively used as explained in section 11.8 of the reference [12]. Fundamental knowledge of voltammetry is necessary for a good understanding of ASV.

Electrochemical stripping analysis has found widespread use in the measurement of trace metals owing to its effectiveness and low capital cost [40]. The technique achieves much greater sensitivity than direct polarography or voltammetry by pre-concentration of the analyte. This takes the form of an electrodeposition step. The analytical performance of the detection may also be enhanced by the use of pulse techniques (DPV, SWV) to discriminate against undesirable contributions to the current, such as double-layer charging. The combination of pre-concentration and enhancement of the faradaic signal is responsible for the impressive sensitivity of the electrochemical stripping analysis. ASV instruments are low priced and can be portable and execute the simultaneous analysis of four to six metals in various matrixes at concentration levels down to 10^{-10} M [179].

Anodic stripping voltammetry (ASV) is known as a technique which occurs in two stages. (Figure 2.1). The preconcentration (or deposition), the first step, is the reduction of the analyte in the sample solution at a negative potential and its concentration into an electrode (traditionally, mercury electrode, but may be a solid metal such as bismuth or any other electrode). This step takes credit for the outstanding sensitivity of the technique and this technique can achieve extremely low detection limits (LOD) competitive with atomic spectroscopy. A consideration of the reasons for the enhanced sensitivity of stripping analysis compared to direct polarography indicates that, as a result of the implementation of the preconcentration step, the concentration of the metal (analyte) in the mercury (or bismuth

alloy) is 100-1000 times greater than that of the analyte in the sample solution. The second step, known as the stripping step, consists of the application of a positive potential scan, the alloys produced previously are dissolved back into the solution, and the peak currents obtained when the system achieves the oxidation of the analyte, are then measured. The peak current (peak height) i_p is proportional to the metal concentration in the sample solution providing the deposition conditions are reproducible; this relation is used to estimate the concentration of an analyte in the sample [182]. The proportionality between peak stripping current and scan rate is also more favourable for analysis than the square root dependence of peak currents on scan rate for direct voltammetric detection of dissolved species.

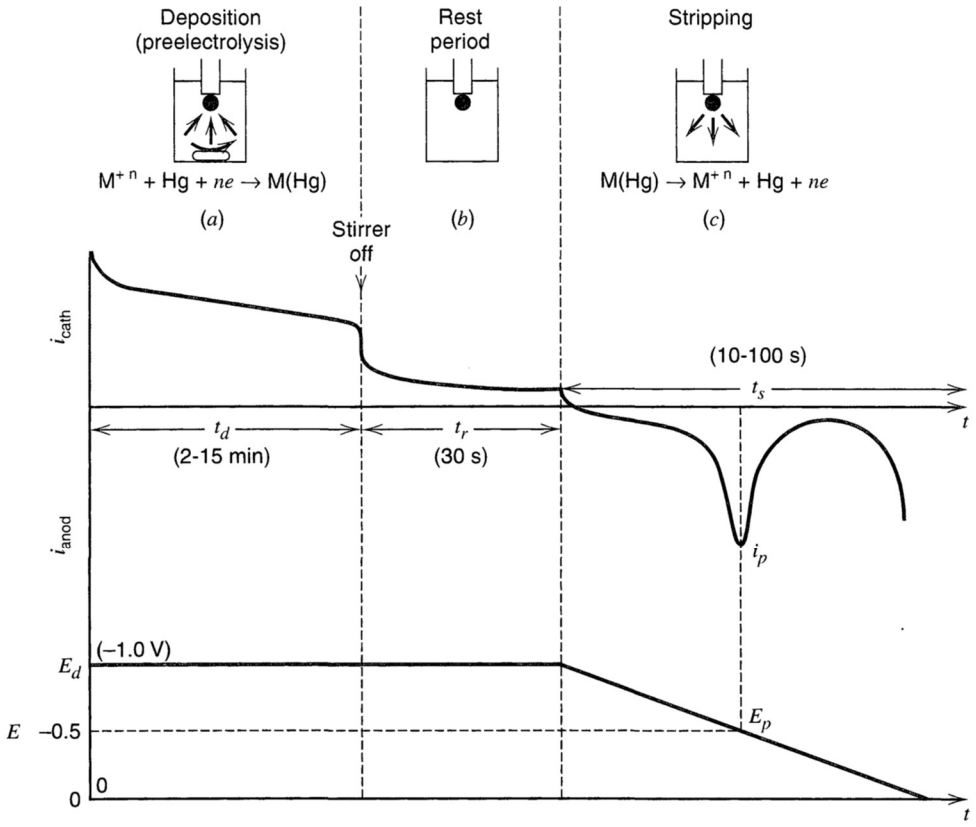

Figure 2.1: Stripping voltammetry process **(Barendrecht, 1967)** Principles of anodic stripping. Values shown are typical ones used; potentials and E_p are typical of Cu^{2+} analysis. (a) Preelectrolysis at E_d: stirred solution. (b) Rest period: stirrer off. (c) Anodic scan (v=10-100 mV/s). [Adapted from E. Barendrecht, Electranal.Chem.,2, 53 (1967), by courtesy of Marcel Dekker, Inc.]. Figure taken from reference [12].

The deposition step is a fundamental stage for the performance of the stripping analysis in which the deposition potential, E_d, is applied to the working electrode to provoke the

deposition of the analyte (through the reduction process) onto or into the surface. It is recommended that this potential should range several tenths of a volt ≈ 0.3-0.5 V more negative than the reversible potential calculated from the Nernst equation for the ion with the most negative standard potential for reduction to the element. The current during this electrodeposition step may be too small to measure, but the electrodeposit may be accumulated over a long period (several minutes) and then, when the metal is stripped in the positive scan, the current will be enhanced because the time taken for the stripping step is much shorter (of order a few seconds) [12].

In most cases, the polarographic half-wave potential $E_{1/2}$, can be used instead of the reversible potential to estimate the required deposition potential. The practical requirement of an overpotential of 0.3-0.5V is due to the low concentration of the ion in the solution compared to the high concentration in the deposited alloy (generally 100-1000 times). This concentration ratio can be related to a potential via the Nernst equation and results in a negative contribution of (0.059/n) V per decade of concentration ratio (n is the number of electrons in the reaction). To overcome the entropic factor favouring the dissolution of the metal and to drive the deposition at a useful rate an overpotential greater than 0.180/n V is necessary [182].

The overpotential also takes into account the ***IR*** drop, which is the small potential drop caused by the cell resistance (R). In this manner, the maximum plating efficiency of the desired metal ions is attained. Deposition potentials of -0.6 V and -1.4 V (vs. Ag/AgCl electrode) are used for the deposition of Pb and Zn respectively. In practice, it is recommended to verify experimentally the effect of the deposition potential on the stripping peak to diminish side reactions. Due to the hydrogen evolution background reaction that develops at negative potentials, it is worth taking care not to apply the deposition potentials more negative than about -1.5 V (in neutral media) or -1.2 V (in acidic media). This would mean a progressive loss in the sensitivity toward ions with negative peak potentials. For example Zn, as the solution acidity increases, lower hydrogen evolution overpotentials are observed when solid electrodes are used instead of Hg, this may be considered as one reason that Hg electrodes were favoured for ASV for many years [27,182]. The selectivity of the measurement can be determined by the selection of the deposition potential to some extent. If the peak current of interest is closely spaced with a second and more negative peak, the selectivity can be

improved by making the deposition potential more positive to reduce the signal from the second species.

The deposition time (t_d) requires to be controlled carefully, evidently the longer the deposition steps the larger the amount of analyte that is available at the electrode during the stripping (measurement) step. Generally, for concentrations of the order of 10^{-9}, 10^{-8}, and 10^{-7} M of the metal ion solutions, deposition periods of 12, 5 and 2 min, respectively are sufficient. Since the amount of metal plated is proportional to the deposition time, the resulting stripping peak current (i_p) yields a straight when plotted against the deposition time. It is suggested to apply deposition periods no longer than those required to obtain well-defined analyte (metal -ion) stripping peaks.

The deposition step is a coulometric one, therefore it can be treated according to Equation 2.1 suggested by Lingane:

$$C_{b,t} = C_{b,0} \exp\left(-\frac{ADt}{V\delta}\right) \qquad Equation\ 2.1$$

Where $C_{b,0}$ and $C_{b,t}$ are the bulk concentrations of the metal ion at the beginning of the deposition strep step and after a given time, t. A is the electrode area, V: the solution volume, D: the diffusion coefficient of the ion, and δ: the thickness of the diffusion layer. Equation 2.1 implicitly assumes the deposition reaction is diffusion limited and the diffusion layer thickness is maintained by stirring, other types of forced convection or the use of an ultramicroelectrode [27,119].

Mass transport

The deposition step is normally aided by convective transport of the metal ions to the surface of the working electrode. The convective transport can be attained by the electrode rotation, solution flow or by solution stirring. The global sensitivity and precision are primarily determined by the efficacy of the hydrodynamics, this also acts as a regulator of the extent of the metal deposited throughout the preconcentration step.

For any working electrode and convection transport employed in stripping analysis, the same general deposition theory applies. Use of Faraday's law facilitates the concentration of the metal in the amalgam, C_a, to be calculated:

$$C_a = \frac{i_L t_d}{nFV_{Hg}} \qquad Equation\ 2.2$$

Where i_L is the limiting current for the deposition of the metal, F the Faraday constant, and V_{Hg} the volume of the mercury electrode. In the case of metallic films deposited on an inert solid electrode, the amount, in moles, of metal accumulated on the surface (M) is given by:

$$M = \frac{i_L t_d}{nF} \qquad Equation\ 2.3$$

The deposition current typically remains basically constant during the deposition step since the electrolysis is not exhaustive for the time period and electrode area employed, and it is expected to be reproducible.

Under the forced convection conditions applied in stripping analysis, both diffusion and convection contribute to the deposition current. When the deposition potential is applied, the concentration of the ion on the surface becomes effectively zero. According to the Nernst diffusion layer model, the convection maintains the concentration of the metal ion uniform, at the bulk value, until a certain distance from the electrode δ (δ is the thickness of the diffusion layer, the region within which the maximum change in concentration occurs and the mode of transport is diffusion rather than convection). As a result of this concentration gradient, ions are moving by diffusion toward the electrode surface [182]. The rate at which this transfer occurs is proportional to the slope of the concentration profile at the electrode surface and can be described by:

$$i_L = \frac{nFADC_b}{\delta} \qquad Equation\ 2.4$$

The equation above indicates that any means of reducing the value of δ will increase the deposition current. Empirically, δ is related to the convection rate by:

$$\delta = \frac{K}{U^{\alpha}} \qquad Equation\ 2.5$$

Where U is the convection rate and K and α are constants dependent on the flow regime and electrode geometry. The increase of the convection rate leads to the decrease of the diffusion layer thickness; as a result, the concentration gradient becomes steeper, thus increasing the

deposition current. It is also obvious to precise that control of convection rates is vital for obtaining reproducible deposition.

The rest period

To enable the production of a uniform concentration of the metals in the mercury electrode or any other, a rest period is imposed between the preconcentration and the stripping steps. Because the forced convection is halted at the end of the deposition period, the deposition current declines to nearly zero, and a uniform concentration distribution is established very promptly. The rest period also guarantees that the following stripping step is performed in a quiescent solution, which means, after convection in the solution stopped. Electrodeposition is facilitated by the diffusion transport, which persists during the rest period.

Stripping step

The second stage of ASV is the stripping, which is described as the anodic potential scan (positive potential), linear or another potential waveform such as pulsed (DPV, SWV…). As soon as the potential achieve the standard potential of the analyte (metal-metal ion couple), this metal is stripped from the electrode through oxidation reaction and back to the solution, then the current flow, the process can be described as the equation below:

$$M(Hg) \rightarrow M^{n+} + ne^{-} \qquad Equation\ 2.6$$

At the end, the signal obtained is a voltammogram (current potential) which reports paramount analytical information, useful for metal detection and quantification (in short, metal qualitative and quantitative analysis). The voltammogram of a every single metal is a peak shaped, its current is directly proportional to the concentration of this analyte in or on the electrode, and hence in the sample solution. Besides, apart from the peak current, its potentials are useful for the identification of the metals in a sample solution, this means, the qualitative analysis of the metals in study. Though, the deposition step of the analyte is usually connected with the methodology adopted throughout the stripping step.

During the stripping step, the analyte or metal of interest is determined through the utilisation of various techniques (linear scan, normal pulse, differential pulse, and square wave voltammetry). Some works have compared these techniques, it was observed that in normal pulse voltammetry, an inadequate signal is obtained because of its specific excitation-

signal mode and subsequent background. On the other hand, all the remaining techniques demonstrated sharp and well-defined peaks in this order: square wave > differential pulse > linear pulse voltammetry (Conclusion based on an investigation with Pb peaks).

It was observed a very low current background, although the presence of dissolved oxygen in the solution was registered [85]. Square wave voltammetry shows high sensitivity and allows the detection of Pb at µg/L levels with low interference from dissolved oxygen. The parameters of the SWV technique (frequency, pulse height and step increment) require optimization to achieve such performance [4].

The Background currents

The total current recorded during the stripping step in linear scan ASV is given by:

$$i_t = i_p + i_{bkgd} \qquad Equation\ 2.7$$

Where i_p is the stripping peak current and i_{bkgd} is the background current unrelated to the stripping reaction of interest.

In practice, the limit of detection and accuracy of voltammetry is determined by uncertainty in measuring the peak current of the desired metal ion caused by the background current. The background current must be subtracted from the total current to get an accurate measurement. The background current is given by:

$$i_{bkgd} = i_c + i_{f,r} \qquad Equation\ 2.8$$

Where i_c is the charging current and $i_{f,r}$ is the background component associated with redox reactions of impurities, or decomposition, of electrolyte (or solvent) or reactions of the electrode itself.

The most important background component is the charging current. At the electrode-solution interface, a separation of charge arises, making the electrode to behave as a capacitor. At a specific given potential, there is a charge on the electrode and an opposite of the same magnitude in the solution. The array of charged species and oriented dipoles existing at the interface is called the electrical double layer and has the electrical behaviour of a capacitor. The change in the potential of the working electrode, results in the circulation of the current with the function to charge and discharge the capacitor. This charging current is non faradaic

because it flows in the absence of accompanying redox reaction. The charging current in a linear scan stripping measurement is given by:

$$i_c = C_d A v \qquad Equation\ 2.9$$

Where C_d is the differential capacity of the doubled layer at the given potential, A is the electrode area and v is the scan rate. The significance of the charging current depends upon its relative size to the stripping peak current. Whereas one can increase the peak current by increasing the scan rate or the surface area, the charging current is increased as well. The Faradaic background component $i_{f,r}$ is composed of currents that limit the working potential range, as well as the currents within this range. When using bare solid electrodes, the anodic range is usually limited by the oxidation of water. In aqueous solutions, the negative (cathodic) potential range is limited by the reduction of hydrogen ions. Which are the most readily reduced species present:

$$2H^+ + 2e^- \rightarrow H_2 \qquad Equation\ 2.10$$

The resulting current is often called the hydrogen evolution current. The reversible potential of this reaction (at 298 K) can be expressed by:

$$E = E^0{}_{H_2/H^+} - 0.059\ pH \qquad Equation\ 2.11$$

Therefore, the more acidic is the solution, the more positive is the potential of the hydrogen evolution current (59-mV shift per pH unit). In neutral or basic solutions, the direct reduction of water to hydrogen may also be important.

Within the working potential range, the faradaic background current is triggered mainly by redox reactions of trace impurities that are nearly unavoidably found in the blank solution. Some aspects responsible include small amounts of dissolved oxygen, heavy metal ions from distilled water, and impurities present in the salt used as supporting electrolytes. In addition, when bare solid electrodes are used, various electrode surface reactions yield faradaic background currents within the working potential range, these include redox reactions of surface functionalities present at carbon surfaces and the oxide and/or hydrogen films present at the metallic surfaces.

2.1.1. Differential Pulse Voltammetry

Differential pulse voltammetry is one of the most broadly used stripping modes; one of its advantages is the ability to discriminate against the double-layer-charging background current. In DPV stripping mode, pulses of equal amplitude are superimposed on an anodic potential scan. Typical choices for the pulse characteristics are an amplitude of 25 or 50 mV, a duration of 50 ms, and a repetition rate of 0.5-5 s. With these choices, the basic potential scan rate is low for example 2-10 mV/s, thus, no substantial change in the ramp potential associated with the underlying anodic scan will be observed throughout the pulse duration. The currents are sampled twice: immediately before the pulse (at 1) and towards the end of the pulse (after ≈ 40 ms, at 2), to allow time for the charging current stimulated by the pulse to decay. The first current is subtracted instrumentally from the second one, and the current difference (differential current) [$\Delta i = i(t_2) - i(t_1)$ is obtained and plotted against the potential. The DPV voltammogram consists of a peak, whose potential correlates with the maximum difference in rates of the metal oxidation between points (1) and (2) [179].

The immediate application of the potential pulse to the total current rises as a consequence of the growth in the Faradaic and charging currents. The induced charging current declines faster compared to the faradaic current ($i_c \approx e^{-t/RCd}$ versus $i_f \approx t^{-1/2}$), where t is the time, R is the resistance and C_d is the differential capacity (double layer capacitance). Therefore, the sampled current is mainly faradaic for t greater than several times RC_d. Since the charging current at the sampling points (prior to the pulse and at its end) is essentially the same, the difference between the readings is credited primarily to the faradaic reaction (metal oxidation). The method offers a high discrimination against the charging current.

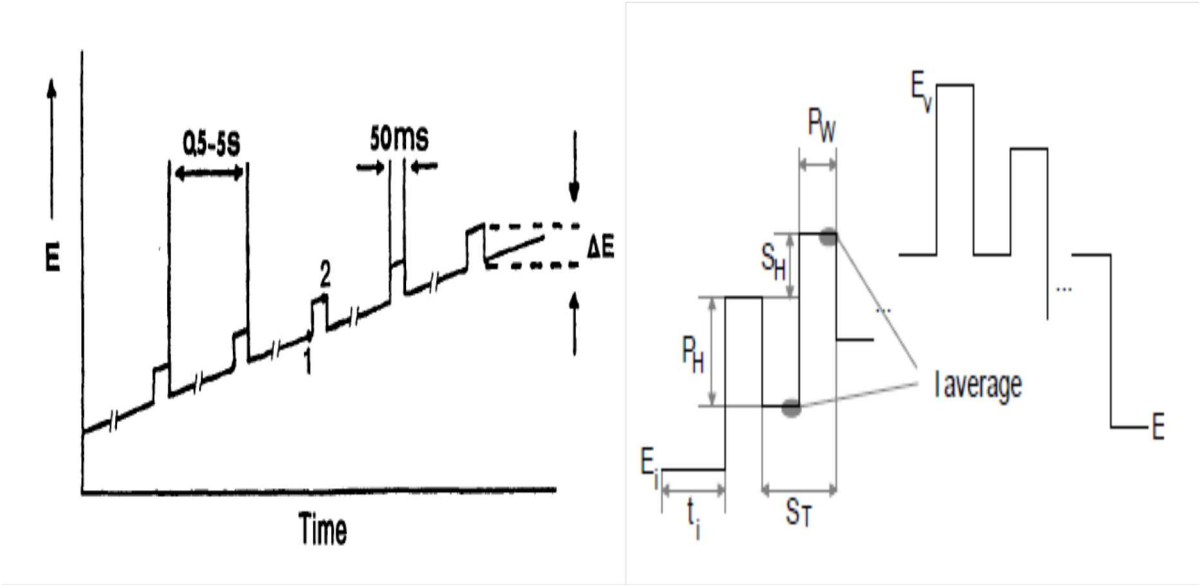

Figure 2.2: Excitation signal for DPV (waveform), potential-time sequence, pulse and parameters. Figures taken from references [21,179].

Where **: P_W (t_p)**: pulse width (ms), **,P_H (ΔE)**: pulse height (V), **E_i**: initial potential, **E_v**: final potential, **S_H (ΔE_s)**: step height (V), **S_T**: step time (ms) or pulse period.

According to the potential wave form for DPV technique shown in Fig 2.2, the output from the potentiostat, which means the voltammogram corresponds to the difference between the two current values. The shape of differential pulse voltammogram is a peak as cited previously as a result of the double sampling, which is characteristic to DPV mode. The current peak height is directly proportional to the concentration of the electroactive species in the electrochemical cell. In case of a reversible system, the peak height, Δi_p of a differential pulse voltammogram is:

$$\Delta i_p = \frac{nFAD_{Ox}^{\frac{1}{2}} C_{Ox}^{*}}{\pi^{\frac{1}{2}} t_p^{\frac{1}{2}}} \left(\frac{1-\sigma}{1+\sigma}\right) \qquad Equation\ 2.12$$

Where: $$\sigma = exp\left(\frac{nF\Delta E_p}{2RT}\right) \qquad Equation\ 2.13$$

As ΔE_p decreases, the magnitude of the quotient (1-σ)/(1+σ) also diminishes monotonically, and tends to zero as ΔE_p reaches zero. When ΔE_p is negative Δi_p is positive (or cathodic), and vice versa. The quotient's maximum magnitude is unity, it applies (assigns) at significant magnitudes. In that limit, Δi_p corresponds to the faradaic current sampled on top of the

normal pulse voltammetric wave (in case of the use of this waveform) attained, maintaining the timing conditions. Under normal conditions, ΔE_p value is not high suficient to accomplish this maximum (greatest) possible Δi_p. For analysis, ΔE_p is usually 50 mV, which delivers a peak current from 45% to 90% of the limiting value, depending on *n*.

The width of the peak at half height, $W_{1/2}$ improves as the pulse height turns greater, since the differential behaviour can be observed over a larger range of base potential. The recommendation to abstain from increasing ΔE_p much past 100 mV is due to the unacceptable degradation of the resolution. The peak width at half height , $W_{1/2}$ for small values of ΔE_p turn out to be:

$$w_{1/2} = 3.52\frac{RT}{nF} \qquad Equation\ 2.14$$

According to the equation above, for 25° C and n=1, 2 and 3, the values would be 90.4, 45.2, 30.1 mV respectively. In DPV, real peaks are wider, particularly in case of the pulse height being comparable to or larger than the limiting width [143].

Part of the metal-ions stripped from the electrode during the pulse are replated into the electrode during the waiting period between pulses, this replating behaviour results in a supplementary increase in the signal-to-background ratio (S/N or S/B), the latter is an indicator of the quality of the peak generated. Consequently, the same metal-ion is oxidated and re-reduced repeatedly (as long as the potential during the waiting period is cathodic enough) between pulses and so, repetitive contributions generated to the measured the current. As the waiting period between pulses is declined, the peak current decreases due to the increased frequency of pulsing and the reduced amount of the material plated back. When the pulse duration is reduced from 56 to 29 ms, the metal (analyte) is more effectively replated near the electrode before it can diffuse to the bulk solution [12,141].

In general, the differential pulse stripping voltammetry provides improved signal to background response. The enhanced sensitivity of DPV is attributed to the reduced contribution from the background currents. Assuming that the background current from interfacial capacitance or from competing faradaic processes does not shift much from the first current sample to the second, then the subtractive process generating Δi_p tends to supress the background contribution [12]. The price paid for the enhanced sensitivity of the

method is also its slow scan rate, which means, the total stripping step may last 2-3 minutes. Hence, this may make the technique unappealing for routine analysis especially at relatively large concentrations (> 50 ppb), for which a short deposition time and fast linear scans are sufficient to obtain good stripping peaks. The differential pulse voltammetry technique offers the capacity to solely eliminate non-faradaic charging current, but this effect is not extended to various faradaic components of the background current. The differential pulse stripping peak currents are more susceptible to interferences by surface-active materials than the corresponding linear scan peaks because of the sensitivity of the differential pulse measurements to small changes in the rate of the electrode reaction [182].

2.1.2. Bismuth modified electrode

The composition (design) of a Bi modified electrode is fundamental in the prospective stripping performance. Bi films can be produced via ex situ (pre-plated) or in situ (generally through addition of nearly 0.25-1.00 ppm Bi (III)) straight to the sample or solution containing the analyte and consequently, depositing simultaneously the metal of interest and Bi). The formation of the Bi film and the alloy can chemically be explained in the reactions below:

$$Bi^{3+} + 3e^{-} \rightarrow Bi^{0} \qquad Equation\ 2.15$$

$$M^{n+} + ne^{-} \rightarrow M(Bi) \qquad Equation\ 2.16$$

Equation 2.15 illustrates the formation of a Bi-modified electrode through the reduction of Bi^{3+} into Bi^{0}, when this process is be done separately, which means, in a solution without the analyte (metal-ion), it is called the ex-situ electrodeposition. Equation 2.16 refers to the alloy formation between the metal-ion and Bi, the metal reduces and forms the alloy with Bi, this process represents the preconcentration step in the stripping analysis procedure. When both equations 2.15 and 2.16 occur simultaneously, which means, the solution in the cell contain the analyte (metal-ion) and Bi, the process is named in-situ electrodeposition.

The ASV response on a glassy carbon substrate increase with the concentration of the bismuth ions (above 200 ppb). Frequently, an acetate buffer pH 4.5 solution containing Bi ions is used as the plating solution. Such electrodes are able to accomplish reproducible multiple stripping runs adding to that an electrochemical cleaning after the stripping step.

Microscopic imaging reveals that the subsequent bismuth films are not homogeneous, with

the exact morphology relying on the plating potential. Besides, the nature and condition of the carbon substrate influence deeply in the nucleation and growth of Bi, and consequently in the structural features of the produced film.

Bismuth electrodes can be further modified by coverage with polymeric layers. To minimize interferences from surface-active materials, it is recommended to employ Nafion coated bismuth film electrodes (Nafion is a sulfonated fluoropolymer). The preparation of these electrodes is simple and executed through the application of a drop of Nafion solution onto the glassy carbon surface, which afterward is taken for Bi electrodeposition via in-situ or ex-situ [101,181].

Potential window and scope of Bismuth Electrodes

Concerning Bismuth film electrodes, an ample cathodic potential range (in the vicinity of -1.25 V vs. Ag/AgCl, pH 4.5) owing to the low electrocatalytic activity of Bi for hydrogen evolution, but a quite limited anodic region (due to the oxidation of bismuth) is observed. The thickness of the Bi film determines the cathodic range. In general, 4-5 non overlapping analytes (metal-ions) stripping peaks can be analysed simultaneously because of the potential window of around 1.0V. Overall, Bi electrodes are mainly able to provide measurements for electrodeposited metals with standard potentials more negative than bismuth (for example Zn, Ga, Cd, Tl, Sn, Pb). In comparison to measurements at mercury electrodes, most of the heavy metal ASV measurements includes a deposition potential of -1.10 V vs. Ag/AgCl [183] (excluding of Zn measurements that demands a deposition potential of -1.4 V because of the electropositive nature of Zn). Note that this value of deposition potential is adjusted depending on the reference electrode used.

The deposition potential as an important parameter in stripping analysis, was studied by Kokkinos et al [105]. The choice of the appropriate deposition potential determines the emergence and intensity of the metal (analyte) stripping peak. The effect of the deposition potential was investigated with Pb as the metal ion (analyte) using a sputtered Bi-electrode in the chosen range -0.5 to -1.2V vs. Ag/AgCl. The results of this investigation concluded that applying a potential more positive than E^0 of the metal (in this case Pb), the stripping peak corresponds to zero because the reduction of the metal does not start when the potential is not sufficiently negative. Then, the emergence and the growth of the metal stripping peak is

observed as the deposition potential applied is more negative than -0.6 V vs. Ag/AgCl, and afterward at deposition more negative potentials (-1.1 V vs. Ag/AgCl), the stripping peak levelled-off. Owing to the risk of reaching the background hydrogen evolution region at more negative potential, it is recommended to apply a deposition potential more positive than -1.5 V vs. Ag/AgCl.

Besides, the deposition potential influences the quality of the film formed. As a useful recommendation, it is important to investigate the potential at which the hydrogen evolution begins by recording a cyclic voltammogram on the selected modified Bi. Following this suggestion, the choice of deposition potential to obtain the greatest peak (The study mentioned refers to Pb peaks) as well as the lowest yield of hydrogen gas would be achievable [108].

During the deposition time, the heavy metal (Pb or Zn) is reduced at the Bi electrode to produce the M (Bi) alloy. Commonly, it can be assumed that lower detection (LODs) limits are associated with lengthy deposition potential [33]. In such manner, as for every single analysis the best choice is a compromise between sensitivity and reasonable analysis time. Peak potentials of the analyte arbitrate the resolution of the stripping measurements and its sharp peaks facilitates the selectivity while using Bi-modified electrodes. The detection of Pb (Zn or any other metal of interest) at the surface of a Bi electrode is attributed to its ability to produces a fused alloy with certain heavy metals. Bi modified electrodes do not demand the removal of oxygen during stripping analyses, and displays large negative potential window, this is advantageous for analyses.

ASV is a two-phased technique as referred earlier, in case of a Bi-modified electrode and Pb as heavy metal:

- The deposition step in which occurs the reduction of Pb^{2+}, forming a Pb-Bi alloy, Pb (Bi);

- The reoxidation of Pb and its return to the solution occurs in the stripping step, as illustrated in the equation below:

$$Pb(Bi) \rightarrow Pb^{2+} + 2e^{-} \qquad Equation\ 2.17$$

Sensitive electroanalytical techniques (as DPV and SWV) are employed in the stripping step, to estimate the extent (can be the concentration) of the analyte in the sample.

Influence of dissolved oxygen

One of the contributors to the increase of the background currents is the presence of dissolved oxygen in the stripping analysis for example in some cases, the dissolved oxygen can strip Zn and interfere that way. Therefore, it is generally advised to deaerate the sample prior to ASV operation. However, oxygen does not constitute a threat to Bi-film electrodes as they are not significantly affected by their presence in the system [183]. Besides, Bi films demonstrate the capacity of its stripping analysis operation being executed in a non-deaerated solution, since hugely reproducible results are attainable in these conditions.

In recent times, the improvement of trustable and effective non-mercury electrodes in electroanalysis have been a challenge [181]. Some of the advantages of Bismuth electrodes include their interesting signal-to-background characteristics and peak resolution. The distinctive and beneficial stripping behaviour involves the capacity of Bi electrodes to produce fused alloys with metals as referred at the beginning of this section 2.1.2. The successful analytical utility of the Bi coated electrodes depends upon understanding their fundamental behaviour.

Bi electrodeposition on GCEs at sufficiently negative potentials is a diffusion-controlled reaction which means the reaction rate corresponds to the rate of transport of the reactants through the reaction medium. Cyclic voltammetry (CV) and Chronoamperometry (CA) are electrochemical techniques which have the ability to perform as both metal electrodeposition method and as an indicative to estimate the reaction mechanism. Glassy carbon has been largely employed as a substrate for the formation of Bi-modified electrodes, this choice is also attributed to its extensive use in the investigations of electrochemical nuclear growth phenomena and the fact of containing arbitrary locations of active sites for the film nucleation (this applies at a mechanically polished GCE) [199].

Choice of Glassy carbon substrate

Apart from nucleation studies appointed as part of the reasons of the choice of glassy carbon electrodes as a substrate, the surface area is also taken into account for the same purpose.

GC electrode is considered as the most appropriate working electrode for Bi-modified electrodes, due to its high current density (conclusion brought from Zn, Cd and Pb studies), sharp Zn peaks, display of a flat (horizontal) baseline, and minor noise level.

In most of the cases, 0.1M acetate buffer pH 4.5 is used as supporting electrolyte, the thickness of Bi film produced is determined by the concentration of the plating solution (concentration of Bi in the solution). On the other hand, the position of the peak is not influenced by the thickness of the Bi film. This thickness of the film also regulates the peak height of the metals studied. The growth of the thickness of the film, results in the decrease of the height of Pb peaks, whereas the height of the Zn peak rises to some extent.

The thickness of Bi peaks also determines the background current at negative potentials region; some findings indicated that a more sloping baseline is obtained for Zn since it is the metal that emerges in that region, as the thickness of the film grew. Initially, it was predicted that the background current would be reduced (lower) at the negative potential region (near Zn) as a result of the negative shift of the hydrogen evolution overpotential arising from a large amount of Bi on the surface (high thickness of the film). High thickness of Bi film intensifies the background at the anodic region of Pb because of the onset of the great Bi oxidation peak.

The width of the analyte peaks is also affected by the thickness of the film, in both electrodeposition modes: ex-situ or in-situ, the increase of the thickness of the film leads to the surge on the width of Pb peaks, while the width of Zn remained unchanged. The deposition time influences in the peak height magnitude; therefore, it can be utilized to increase the sensitivity [102].

Bismuth electrode modification

The process of the modification of an electrode with a Bi film, which is useful for metal analysis, consists in the electrodeposition of Bi onto the electrode surface. The operation is carried out using two modes of electrodeposition (ex-situ and in-situ). The ex-situ electrodeposition also known preplating, is described as the electrodeposition of Bi on the surface before being transferred into the solution containing the analyte [102]**.** While, in-situ electrodeposition, represent the process in which the electrodeposition of Bi occurs simultaneously with the analyte, since Bi ions are spiked into the solution containing the

analyte, and then the deposition potential is applied as to complete the preconcentration step [184].

Ex-situ Bi-modified electrodes preparation can be executed in a distinct medium than the one containing the analyte (the plating solution and the analyte solution can be prepared in different medium). A reported limitation (obstacle) for Bi ex-situ electrodeposition involves the deterioration of the modified electrode produced on account of the deficient adhesion of the Bi-film. Bi-film produced ex-situ are less stable than those formed in-situ, in other words, the interaction between Bi and the substrate is stronger in the in-situ electrodeposition mode than the ex-situ. This can be addressed by adding NaBr to the solvent used to prepare the plating solution, frequently acetate buffer is selected. This is because the referred salt facilitates a dense growth of little crystals. as suggested by Hocevar, et al in reference [84] from the investigation undertaken by Ogorevic's group.

Bi films obtained via in-situ mode are more stable than ex-situ, therefore, a high sensitivity is attained for metal analysis. The in-situ versus pre-plating (ex situ) in some electrodes such as screen-printed electrodes (SPEs), display higher, better and more stable peaks for Pb whereas distorted peaks were registered at pre-plated electrodes on SPE substrates [155].

As referred earlier, the in-situ deposition produces a modified electrode, the same applies in the presence of surfactants. The reproducibility of the results depends also on the working conditions alongside with the substrates chosen. Therefore, the substrate must be carefully selected.

Effect of Bi concentration

According to Arduini in reference [4], one of the parameters of utmost importance is the concentration of Bi (III). The thickness of the film produced through deposition at a given potential and for a given duration of the electrodeposition, is regulated by the concentration of Bi and this thickness also influences in the peak height, and thus, the analytical signal. However, there is no clear influence in the peak position. The outcome of the investigations showed that the growth of the thickness of the Bi film led to the decrease of the current intensity of the peak. Furthermore, the increase of the concentration of Bi resulted in the rise of the width of the peak, this can be partly compensated by using the charge passed under

the peak as the analytical signal, the peak width should be be small for the peak to be clearly distinguished from the capacitive current. A wider peak at 1 mg/L concentration of Bi was reported when highly saline samples were investigated. Some studies as Svancara, et al in reference [166] have discovered that a considerable decline in sensitivity is observed when extremely high concentration of Bi ions (greater than 2 mg/L) due to the saturation effect on the surface, then consequently, the height of the peak reduced. In short, the peak of the metal-ion grows at the range of the concentration of Bi (III) of 0.01-1mg/L, this is due to the rise of the extent of the nucleation sites and alloy formation. Notwithstanding, because of the production of a heavy layer of Bi on the electrode surface, moderately obstructing the conductive area, the count of the active sites decreases; therefore, analyte peak signal as well as its current decreases at Bi concentration higher than 1mg/L. Besides, concentrations of Bi as low as 40 µg/L can provide well defined and sharp peaks. Reminding that, the study which provided earlier conclusions, was completed using Pb stripping peaks.

Effect of plating solution

An aspect important while performing the ASV with Bi-modified electrodes is the composition of the Bi solution. Another factor to be taken into consideration is that non complexed Bi (III) ions hydrolyse very easily, illustrated by the following chemical reactions:

$$Bi^{3+} + H_2O \rightarrow BiO^+ + 2H^+ \qquad Equation\ 2.18$$

or

$$Bi^{3+} + 3H_2O \rightarrow Bi(OH)_3 + 3H^+ \qquad Equation\ 2.19$$

The precipitate $Bi(OH)_3$ is formed, $Bi(OH)_3$ is a Bi compound that is so far not fully characterised [154].

However, the substances in eq. 2.18 and 2.19 are not produced in extremely alkaline solutions [166], the probability of the production of water-soluble hydroxo complexes reducible at the electrode surface, makes Bi-CPEs (Carbon Paste Electrodes) capable to operate in NaOH [86]. Generally, in stripping analysis using Bi-modified electrodes, acids, and acetate buffer (pH 4-5) are selected as supporting electrolytes in order to avoid the electrolysis illustrated in equations 2.18 and 2.19; however, acetate buffer is currently the most used medium. The

choice of a suitable pH range for operation with Bi-modified electrodes is essential, investigations in the subject showed that at pH 4, a modest decrease in the analyte peak height is observed, while at pH 6, the analyte peak height decreases quickly because of Bi (III) hydrolysis demonstrated in equations 2.18 and 2.19. In short, the range of pH 4-5 is more appropriate for Bi-modified electrodes experiments, however, at higher pH (especially pH ≥ 6), the sensitivity declines because of Bi (III) hydrolysis. Furthermore, the capacity to dissolve weak organic complexes of the analyte in the sample is one of the advantages of the use of the mineral acids (HNO_3, HCl, and $HClO_4$). It is recommended the bypass of extremely acidic media due to the risk of a high rate of hydrogen evolution, which strongly affects the deposition [106]. In addition to that, in the alkaline solutions, it is reported that the pH influences in the potential window by extending negative cathodic limits [92].

Similar to the pH, throughout the preconcentration, the ionic strength can occasionally promote the rise of the background current or divide the stripping peaks (emergence of multiple peaks for a single metal).

2.2. Scanning Probe Microscopy

2.2.1. SEM and EDX

A scanning electron microscope (SEM) is the form of electron microscope that yields images of a sample through scanning of the surface with a focused beam of electrons. The technique using electric and magnetic fields to accelerate and focus an electron beam in high vacuum. Th ebeam is rastered across the sample and images obtained by mapping the interaction of the electrons with the sample across the surface. The electron beam is scattered by atoms of the sample and may also suffer inelastic collisions in which energy is transferred from the beam to electrons in the sample. The combination of the position of the beam and the intensity of the signal due to scattered electrons yields an image. The atoms excited by the electron beam in inelastic collisions, are responsible for the emission of the electrons called secondary electrons which can be identified using an Everhart-Thornley detector. The specimen topography determines the count of these secondary electrons, and hence the signal intensity. The specimen observation is realized in high vacuum (conventional SEM), low vacuum or wet conditions (in a variable pressure or environmental SEM). Besides, in specially designed SEM, temperature conditions as a broad extent of a cryogenic or high temperature.

Concerning the resolution of the images, Some SEMs instruments are capable to attain a resolution better than 1 nanometre [164].

Numerous categories of signals as secondary electrons (SE), reflected or back-scattered electrons (BSE), characteristic X-rays and light (cathodoluminescence) (CL), absorbed current (specimen current) and transmitted electrons are generated in SEM. Any SEM instrument possess the ability to identify secondary electrons through its detector; however, there is a limitation in detecting all the signal types cited earlier in an individual equipment.

The energy of secondary electrons is reported to be approximately 50 eV, because of this low energy these electrons are simply able to evade from the top few nanometres of the surface of the specimen requiring only the initial electron beam. In addition to that, the SEM micrographs can be collected at a resolution of below 1 nm. Contrary to SEs, back scattered electrons (BSE) display greater energy, and surface from much profound area of the specimen, resulting in a lower image resolution [168]. Nonetheless, BSEs have usually found their application in analytical SEM, through its combination with characteristic X-rays, since its signal intensity is greatly associated (linked) to the atomic number (Z) of the sample. Therefore, BSE images can enlighten about the distribution; however, they are unable to identify different elements in the sample [168]. The emission of characteristic X-rays is described as the removal of an inner shell electron from the specimen by the electron beam, allowing a higher-energy electron to occupy the core-hole and discharge energy. The measurement of this energy released (or wavelength recorded) at the end of the process cited earlier, is executed by Energy-dispersive X-ray spectroscopy or Wavelength-dispersive X-ray spectroscopy and is employed for identification and measurement of element abundance in the specimen and, to plot their distribution.

The characteristic three-dimensional appearance of SEM micrographs facilitates the comprehension of the specimen surface structure. A vast range of magnifications is probable, from around 10 times (approximately equivalent to that of a potent hand-lens) to higher than 500,000 times, nearly 250 times the magnification limit of the outstanding light microscopes [70].

Sample preparation

It is recommended sufficiently small SEM samples should be accommodated and attached strongly on the specimen stage, which consists of a specimen holder or stub using conductive adhesive. Since the electrical conductivity and stability are vital, there is sometimes a need to implement a special sample preparation before the measurement (scanning); as a result of this preparation, the resistance of the sample to the high vacuum and the energy beam of the electrons from SEM instrument is ensured.

Scanning flaws and other image artifacts are reported in secondary electron imaging mode when nonconductive specimens are scanned by the electron beam since they collect charge. For conventional imaging in the SEM, in order to avoid the accumulation of electrostatic charge , specimens are required to have a surface electrically conductive and electrically fitted [168].

Scanning Process and image formation

In a conventional SEM, an electron gun equipped with a tungsten filament cathode is used to emit thermionically an electron beam. Tungsten is normally employed in thermionic gun because of its low priced as well as some of its physical properties such as high melting point and low vapor pressure. These properties favour the metal (tungsten) to be electrically heated for electron emission [128,164,168].

EDX (Energy Dispersive X-ray Spectroscopy) is known as an analytical technique employed mainly for the elemental analysis or chemical characterisation of a specimen, which is described as the interaction of a source of X-ray excitation and a sample. Its characterization abilities are substantially attributed to the important assumption that every single element contain an exclusive atomic structure permitting a distinctive set of peaks on its electromagnetic emission spectrum. The stimulation of characteristic X-rays emission from a sample is realized by focusing a beam of electrons into the specimen in study [70].

An atom within the sample contains fundamental) state (or unexcited) electrons in discrete energy levels or electron shells attached to the nucleus. An electron hole is created when the electron is expelled from inner shell because the incident beam may have excited it in that shell. The hole is filled by an electron from an external, higher-energy shell, and the difference in energy between the higher energy shell and the lower energy shell is discharged as an X-

ray. The amount and energy of the X-rays released from a sample can be measured using an energy dispersive spectrometer. The energies of these X-rays are distinctive expresses the difference between the two shells of the atomic structure of the releasing element, which is unique, thus, EDX allows the elemental composition of the sample to be measured [70,96].

The main modules of the EDX setup are the excitation source (electron beam or x-ray beam), the X-ray detector, the pulse processor and the analyser. The conversion of the X-ray energy into voltage signals is performed at (by) the detector; afterwards, this report reached the pulse processor, which is responsible for the measurement of these signals, which at last arrive into the analyser for data exhibition and analysis. Si (Li) detector cooled to cryogenic temperatures with liquid nitrogen is mostly employed.

Because of the outcome information obtained from the spectrum, EDX allows the determination of chemical elements present in a specimen and the estimation of their extent. Besides, EDX facilitates the measurement of multi-layer coating thickness of metallic coatings and analysis of a variety of alloys. Several factors affect the accuracy of the quantitative analysis of sample composition, for instance, the overlapping X-ray emission peaks (e.g., Ti Kβ and V Kα) and the nature of the sample. The production of X-rays relies on the capacity of an atom in the specimen being excited by an incident beam. The prospect of an X-ray escaping the specimen, and hence, being able to be detected and measured, relies on the energy of the X-ray and the composition, amount, and density of material that must pass through to reach the detector. Due to the X-ray absorption effect and similar effects, accurate estimation of the sample composition from the measured X-ray emission spectrum requires the application of quantitative correction procedures, which are sometimes referred to as matrix corrections [70,96].

2.2.2. XPS

X-ray Photoelectron spectroscopy (XPS) is a surface-sensitive quantitative spectroscopic technique based on the photoelectric effect that allows the identification of the elements existing within the surface of a sample, including their chemical state. XPS may also provide information on the overall electronic structure and density of the electronic states in the material. XPS is widely used because it is not only capable of showing what elements are present but also what other elements they are bonded to and with good sensitivity, typically

0.1 - 1 atom %. The surface sensitivity of XPS arises because the mean free path of the photoelectrons is typically 2-3 nm and therefore only photoelectrons from the top layers of the samples are detected, even though the X rays may penetrate much more deeply.

XPS is employed in line profiling, or in-depth profiling (when paired with ion-beam etching) of the elemental composition across the surface and is repeatedly employed to investigate chemical processes in solid materials.

This technique is one of the photoemission spectroscopies, the incident beam of X-rays on the material produces photoelectrons whose number and energy are analysed. Material properties are inferred from the measurement of the kinetic energy and the number of ejected electrons. Owing to the reliance on the detection of electrons, XPS demands high vacuum (residual gas pressure $p \approx 10^{-6}$ Pa) conditions.

When using laboratory X-rays sources, it is important to remind that XPS may be used to quantify the most common elements excluding hydrogen and helium. The technique can detect in the parts per thousand range; however, it is capable of lower detection limits if the element analysed is at the top surface of the sample and long detection times are employed.

XPS finds its application mainly in the analysis of inorganic compounds: metals and their alloys, semiconductors, glasses, ceramics, and hard materials in general. This is because the ultra-high vacuum conditions do not generally allow for the introduction of materials that contain volatile components. XPS is, however, occasionally employed in the analysis of the hydrated forms of materials such as hydrogels and biological samples after being frozen [73, 80,117,135,150,152,176-177].

XPS spectrum

A classic XPS spectrum is defined as a chart that indicates the number of electrons identified at a specific binding energy for a given duration of detection (counts per second). A set of characteristic XPS peaks are yielded by each chemical element according to the binding energy of the core electrons. This energy is principally determined by the atomic number, and this is the basis of elemental analysis by XPS. For example, 1s electrons of carbon have a binding energy of about 285 eV and if the X-rays have a photon energy of 1500 eV, a strong signal for electrons with kinetic energy of 1225 eV will be observed corresponding to

photoelectrons originating from carbon atoms of the sample. The count of the electrons detected in every single peak is clearly connected to the extent of the element in the sample. The atomic percentage values are obtained through the correction of every raw XPS signal by dividing the intensity by a relative sensitivity factor (RSF) and normalized over the elements identified.

The variation of the detection limits depends significantly on the cross section of the core state in study and the background signal level. Commonly, photoelectron cross sections expand with atomic number and the background enhances with the atomic number of the matrix constituents and the binding energy, this is due to secondary emitted electrons.

XPS can regularly attain detections limits of 0.1-1.0% atomic percent (0.1%=1 part per thousand= 1000 ppm) in case of practical analyses, however, in several instances lower limits may be obtained.

Degradation relies on the sensitivity of the material to the wavelength of X-rays, the entire amount of the X-rays, the temperature of the surface and the level of the vacuum. Metals, alloys, ceramics, and most glasses are typically not measurably affected by either monochromatic or non-monochromatic X-rays during XPS analysis.

Measured area and sample size

The area of analysis is depending on the equipment design and vary from 10 to 200 micrometres. Largest size for a monochromatic beam of X-rays is 1–5 mm, non-monochromatic beams are 10–50 mm in diameter. The resolution of the spectroscopic image can achieve levels of 200 nm or below as reported in XPS equipment that uses synchrotron radiation as X-ray source. Instruments accept small (mm range) and large samples (cm range). The limiting factor is the design of the sample holder, the sample transfer, and the size of the vacuum chamber.

Analysis Time

Normally, the duration of the analysis ranges between 1–20 minutes for a wide survey scan that allows the measurement of the complete detectable elements, and naturally 1–15 minutes for high resolution scan which disclose chemical state differences (for a high

signal/noise ratio for count area result, usually it involves multiple sweeps of the location in study), 1–4 hours for a depth profile for 4–5 elements as a function of etched depth.

Chemical states and Chemical shifts

One particular advantage of XPS is its capacity to provide the chemical state of an element in the sample, which is known as local bonding environment. The observation of slight reproducible shifts in the exact binding energy of a certain element is reported as chemical shift. In general, the higher the oxidation state of an element, the higher is the binding energy of the core electrons and this appears as a shift in the energy of the peak due to that element of the order of 10^{-1} - 10^{0} eV.

Instrumentation

The major elements of an XPS system include the source of X-rays, an ultra-high vacuum (UHV) chamber with mu-metal magnetic shielding, an electron collection lens, an electron energy analyser, an electron detector system, a sample introduction chamber, sample mounts, a sample stage capable to heat or cool the specimen, and a set of stage manipulators.

Peak identification

Each chemical element can produce a range of 1 to more than 20 peaks. Physical and electronic literature sources as well as advanced XPS instruments contain tables of binding energies, identifying the shell and spin-orbit of every single peak generated by a specific element. These binding energies values are precisely employed to disclose the elemental composition of an unknown, through comparison with its measured peaks.

An important recommendation for earlier the start of the peak identification process, the operator should verify if a shift (because of positive or negative charge on the surface) was observed in the binding energies of the survey spectrum (0-1400 eV). It is simply required to observe two peaks which represent the presence of carbon and oxygen. C1s electrons are often observed due to unavoidable contamination of the sample surface in ambient atmosphere prior to insertion in the vacuum chamber of the XPS instrument. The C1s binding energy of methylene (-CH_2-) groups does however provide a useful energy scale calibration at 284.8 eV. Alternatives include adding a small amount of metallic gold on the sample surface

for which there is a characteristic pair of Au4f electron peaks at 84.8 eV [6,73,80,89,134- 135, 150,152,176-177].

2.2.3. AFM and Optical microscopy

- AFM (atomic force microscopy)

The atomic force microscope (AFM) is part of the large group of scanning probe microscopes and consists in a proximal probe being exploited for studying properties of surfaces with sub-nanometre resolution.

AFM is a technique largely applied in the surface chemistry of samples under ambient conditions. It is particularly suited to biology, because it permits the measurement of native biological samples under near-physiological conditions, excluding any complicated sample preparation operation, this constitutes the most alluring benefit of the technique AFM as a high-resolution microscope [2].

AFM operation is described as the raster scan of a smaller tip attached at the extremity of a flexible microcantilever in mild touch with the sample. The technique is completed with sub-Angstrom accuracy by a piezoelectric actuator (mostly a tube, occasionally a tripod). The cantilever deflects when it interacts with the specimen, and the tip-sample interaction can be observed with high resolution using a laser beam at the rear of the cantilever. The beam reflection in the direction of the split photodetector results in the formation of an optical lever capable to enlarge cantilever deflections. The relative intensity of light falling on each portion of the split photodiode is determined by the angle of deflection of light from the cantilever and therefore of the height of the cantilever. The cantilever deflection sensor is linked to a feedback circuit, which holds at a permanent value (rate) the tip–sample interaction monitoring the tip–sample distance. The electric signals from the feedback circuit are mapped across the sample line by line during the raster scan. This information is used to construct a 2D false colour image of the sample topography (Figure 2.3) [2,19,31,67,69,114, 138,142].

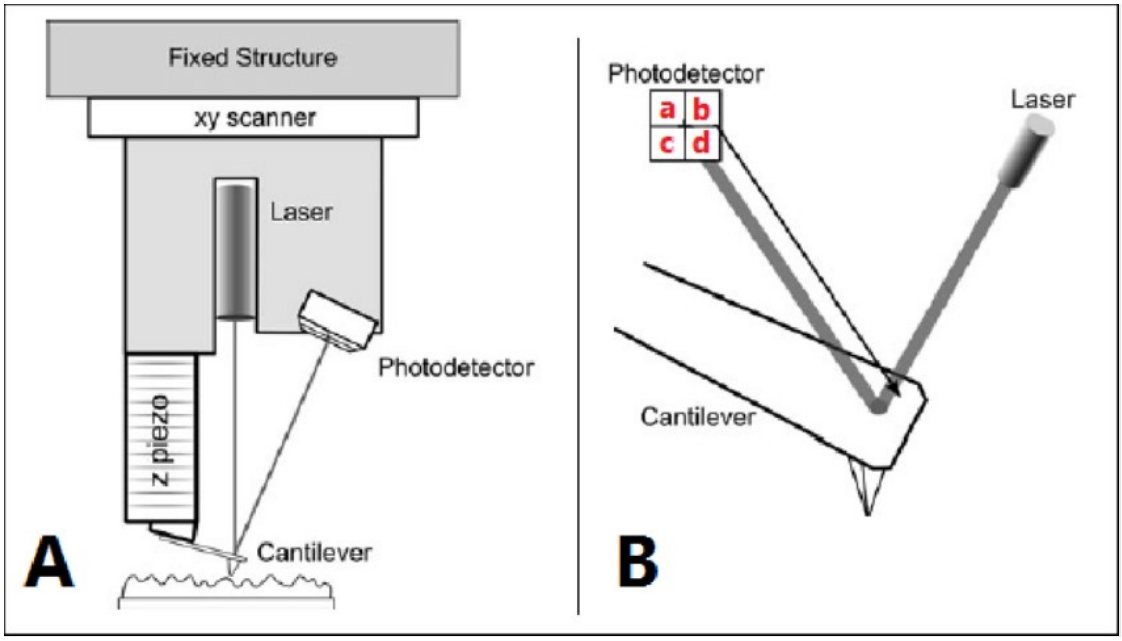

Figure 2.3: Schematic of AFM Operation. Image A Illustrates the standard scanning head configuration. Image B illustrates the laser reflecting off the cantilever onto a position-sensitive photodiode (PSPD) detector. The PSPD is divided into quads a, b, c and d. A PSPD gives an electrical signal proportional to measured light intensity and the relative positioning on the PSPD. Images A & B from reference [49].

- **Optical Microscopy**

The optical microscope, also known as a light microscope, is defined as form of microscopy relying generally on the use of visible light and a system of lenses to produce amplified images of small objects. Classic optical microscopes are modest, while the enhancement on the resolution in advanced instruments constitutes the main ambition.

The observation on a microscope can be described as the following simple procedure, the matter is positioned on the sample holder, then it is promptly viewed by one or two eyepieces of the microscope.

The light on the object in study plays an important role in the microscopy observation. Samples are illuminated in various manner, the light comes from below in case of transparent specimen, while solid samples are illuminated through (bright field) or around (dark field) the objective. Optical microscopies possess a maximum magnification of 1000x.

Optical microscopes can be classified in two categories: - simple microscopes which employs a simple lens or group of lenses to magnify the image, - compound microscopes that makes use of a system of lenses (a group yields the image and the other amplify it) as to obtain much

greater magnification. A simple microscope utilizes a lens or set of lenses to expand an object by using only angular magnification, resulting into an amplified virtual image easily observed by the operator. A compound microscope utilizes the objective lens which is near the object in study for light collection, this lens directs the real image of the sample into the microscope. then, the eyepiece (second lens or group of lenses) captures this image and magnify it, thus, the resulting magnified image can be observed by the operator [187].

Some applications of optical microscopes include areas such as microelectronics, nanophysics, biotechnology, pharmaceutic research, mineralogy and microbiology [72].

2.3. Spectroscopic methods

Spectrophotometry is any technique that uses light to measure chemical concentrations. In atomic spectroscopy, a sample is disintegrated into atoms in a flame, furnace or plasma. A plasma is a gas sufficiently hot to accommodate ions and free electrons. Every single element is measured by absorption or emission of ultraviolet or visible radiation by gaseous atoms.

In atomic spectroscopy, samples are vaporized at 2000-8000 K decomposes into atoms. Concentrations of atoms in the vapor are measured by emission or absorption of characteristic wavelengths of radiation. Because of to its high sensitivity, capacity to perform simultaneous multielement analyses, and the simplicity with which several samples can be automatically analysed. Atomic spectroscopy is considered as a fundamental tool of analytical chemistry, ions on the vapor are measurable in a mass spectrometer. Equipment for atomic spectroscopy is high-priced, however largely available.

Analyte (metal of interest) is measured as ppm (µg/g or mg/L) to parts per trillion (pg/g) [75]. In order to analyse the most important constituents, the sample is required to be diluted. Trace components are able to be measured without preconcentration. Atomic spectroscopy exhibits a precision of normally a few percent (this value is influenced by the type of sample and matrix). Such precision is comparable to that of some wet chemical methods. Inductively coupled plasma atomic emission spectroscopy (ICP-MS) provides an accuracy and precision of 0.1%, providing the appropriate experimental conditions and samples are carefully selected.

In atomic absorption, a liquid sample is aspirated (sucked) into a flame whose temperature is 2000-3000 K. The evaporation of the liquid and the decomposition of the remaining solid into atoms in the flame, act as replacement for the cuvette of the conventional spectrophotometry. The length of the flame is normally 10 cm, the iron cathode contained in the hollow cathode, is bombarded with energetic Ne^+ or Ar^+ ions, excited Fe atoms vaporize and emit light with the same frequencies absorbed by analyte Fe in the flame, then a detector measures the extent of light that passes through the flame. In atomic absorption atoms absorbs portion of the light from the source and the remaining light reaches the detector. Atomic emission results from atoms located in an excited state on account of the high thermal energy of the flame.

Absorption and emission spectra of liquids and solids typically have bandwidth of 10-100. Generally, the spectra comprise sharp lines and show slight overlap between different elements in the specimen. Consequently, various instruments have the capacity to measure more than 70 elements simultaneously. In atomic spectroscopy, analyte is atomized in a flame, an electrically heated furnace, or a plasma. Then, the Types of atomic spectroscopies are AAS with flame, AAS with graphite furnace and ICP [76].

2.3.1. Inductively Coupled Plasma

The inductively coupled plasma is twice hotter than the combustion flame. As one of the advantages of ICP, the eradication of common interferences frequently found in the case of flames is attributed to its high temperature, stability and relatively inert Ar environment. In general, the ICPs apparatus are more expensive than a flame instrument. Simultaneous multi element analysis is routine for inductively coupled plasma-atomic emission spectroscopy.

The cross-sectional view of an inductively coupled plasma burner demonstrates two of a 27 or 41 MHz induction coil wrapped around the upper opening of the quartz instrument. High purity gas is supplied across the plasma inlet, following a spark from the coil ionizes Ar, then the radio frequency field accelerates free electrons. A collision between electrons and atoms, and the energy moves to the entire gas, keeping a temperature of 6000 to 10000 K. Ar coolant gas serve as overheating protector to the quartz [76].

A fine aerosol is generated by a vibrating crystal and then Ar stream using a heated tube that is responsible for the solvent evaporation, transports that aerosol. The removal and

condensation of the solvent occur in the next refrigerated zone. Next, desolvator holding microporous polytetrafluoroethylene membrane in a chamber kept at 160° C receives the stream. Either the diffusion through the membrane or the sweeping by Ar flow are applied in the elimination of the residual solvent vapor. Analytes enters the plasma flame in form of an aerosol of dry, solid particles. Sufficient energy is accessible for the atomization process since the solvent evaporation occurs without using Plasma energy. Besides, the extent of the sample reaching the plasma is greater than in a conventional nebulizer.

ICPs have proven to improve the sensitivity by a factor of a 3 to 10 through the observation of the emission along the length of the plasma (axial view) instead of a across the diameter of the plasma. Mass spectrometer increases significantly compared to optical emission [76, 160-161].

Advantages of inductively coupled plasma

As mentioned previously, a lot of usual interferences are eradicated in the inductively coupled argon plasma. In addition to that, among its advantages, it can be included high temperature of the plasma which is twice hotter than in the conventional flame and twice longer residence time of the analyte in the plasma. Consequently, a more complete atomization is achieved, and signal is improved significantly. Another aspect is that the temperature of the plasma is more uniform outweighing the self-absorption effect which can provide non-linear curves. Plasma emission calibration curves are linear over five orders of magnitude. While in flame and furnaces, the linear range is two orders of magnitude, and it is eight orders of magnitude for ICP-MS [76,161].

Inductively Coupled Plasma atomic emission spectroscopy

This technique also referred as inductively coupled plasma optical emission is a type of emission spectroscopy, specifically ICP, that use as detector an optical spectrometer. ICP-OES instrument is constituted of two parts: ICP and the optical spectrometer. Although its sensitivity is lower than ICP-MS, ICP-OES finds its application in metal determinations of various samples for example food, analysis of trace elements especially in forensics and also in minerals processing to furnish data on the grades of a variety of streams for the construction of mass balances.

Inductively coupled plasma-mass spectrometry

Ar is an inert gas whith an ionization energy of 15.8 eV, which is the highest among all the chemical elements excluding He, Ne and F. The analyte elements ionization occurs through collision with Ar^+, excited Ar or energetic atoms in the plasma. Then, the plasma reaches a mass spectrometer, where the separation and measurement of the ions following their mass-to-charge ratio takes place. The mass spectrometer requires one detector for every single isotope to achieve its better measurement ratio.

Sampling with the spectrometer is challenging due to the requirement of a high vacuum as to prevent clashes between ions and background gas and molecules responsible for the diversion of the ions from their path in a magnetic field [76].

ICP-MS can attain low detection limits of part per trillion, this is attributed to the cleanliness of reagents, glassware and procedures. It is recommended to prepare the solutions by using highly pure metal and trace metal grade HNO_3 in conditions of keeping away from dust. The use of HCl and H_2SO_4 is restrained due to the isobaric interference caused. The plasma-mass spectrometer interface cannot abide high concentrations of dissolved solids that can clog the orifice of the sampling cone. The plasma reduces organic matter to carbon that can clog the orifice. ICP-MS is also capable to analyse organic substances unless O_2 is inserted into the plasmas as a form of oxidation of carbon.

The production of the ions in the plasma is also affected by the matrix effect, therefore calibration standards are prepared according to the matrix of the unknown. On the other hand, Standard addition is recommended as the adequate method [76,160].

Chapter 3: Materials and methods of calculation

This chapter gives details on the working conditions, that means, instruments, materials and calculation methods.

3.1. Chemicals

Throughout this work several chemicals were used to fulfil the purpose of this work, all the chemicals are analytical grade and purchased from Sigma Aldrich.

- Bismuth nitrate pentahydrate $Bi(NO_3)_3.5H_2O$, 98.0 %, reagent grade, F.W: 503.086 g/mol

This salt is fundamental to the formation of Bi film (Bi electrodeposition) on glassy carbon electrode surface. 10 mM Bi (III) required to be prepared as stock solution, so 1.213 g of $Bi(NO_3)_3.5H_2O$ was transferred to 250 mL volumetric flask. The salt was dissolved in either acetate buffer pH 4.5 or 0.1 M HNO_3, then completed with the solvent (deionized water) until the mark in the flask, according to the experimental conditions designed.

- Lead Nitrate $Pb(NO_3)_2$, ACS reagent, ≥ 99.0%, F.W: 331.21 g/mol

$Pb(NO_3)_2$ salt was used to prepare standard solution for Pb detection. The stock solution of 10 mM Pb(II) is prepared in a 100 mL volumetric flask. 331 mg are weighed in an analytical balance then transferred to the volumetric flask.

- Acetic Acid, glacial CH_3COOH, 100%, anhydrous for analysis, ACS reagent, F.W: 429.197 g/mol.

In order to prepare acetate buffer, a solution of acetic acid 0.5 M is required to be prepared in this work. The stock solution from which it should be prepared is glacial acetic acid (17.416 M, based on a density of 1.049 g/mL, a formula weight of 60.05 g/mol, and a concentration of 99.7% w/w). To make a 0.5 M solution, 14.354 mL of the stock solution was slowly added to deionized water. The final volume of solution was adjusted to 500 mL with deionized water.

- Sodium acetate CH_3COONa, reagent sodium acetate trihydrate $CH_3COONa.3H_2O$, p.a, ACS, ≥99.5 %, F.W: 136.08 g/mol.

The acetate buffer solution is mainly prepared using sodium acetate. In this research, 0.5M CH_3COONa is used for the purpose, therefore 6.804 g of $NaCH_3COO.3H_2O$ is dissolved in water and then, transferred into 100 mL volumetric flask and adjusted until the mark with deionized water.

- Potassium Chloride KCl, ACS reagent, 99.0-100.5 %, F.W: 74.56 g/mol.

The solution used throughout this work is 1M concentration, 37.275 weighed in an analytical balance are transferred into a 500 mL volumetric flask. Then, added deionized water until the mark of the volumetric flask.

- Nitric Acid HNO_3 0.1M, ACS reagent, 70%, F.W: 63.013 g/mol.

During this work, HNO_3 has been used as a solvent to prepare Bi (III) solution as well as to remove all the impurities in the glass cell and all the glassware used. Therefore, first a stock solution of 1 M HNO_3 is prepared from $HN0_3$ (concentrated 70%, d=1.42), 15.8 mL of the concentrated acid are added slowly into approximately 100 mL deionized water. Then, transferred to 250 mL volumetric flask and filled until the mark of the flask. After that, 50 mL of 1M HNO_3 prepared is taken and transferred to a 500 mL volumetric flask to obtain 0.1 M HNO_3 solution.

- Sulfuric Acid H_2SO_4 1 M (used for electrode filling), H_2SO_4 concentrated, ACS reagent, 95.0-98.0 %, F.W: 98.078 g/mol.

Sulfuric acid is initially used as electrode filling solution in MSE (1 M H_2SO4), 1 M H_2SO4 solution is prepared from a stock solution H_2SO_4 concentrated which is estimated to be 17.822 M based on a density of 1.84 g/mL, a formula weight of 98.08 g/mol, and a concentration of 95% w/w. To make a 1 M solution, slowly add 28.055 mL of the stock solution deionized water. Then, adjust the final volume of solution to 500 mL with deionized water.

- Sodium sulfate Na_2SO_4 1M, Na_2SO_4 anhydrous, ACS reagent, ≥99.0%, F.W: 142.042 g/mol.

Na_2SO_4 is another salt that is used in the study of the effect of addition of an electrolyte to the analyte stripping peak. 14.204 g of the salt are transferred to a 100 mL volumetric flask and afterward deionized water is added until the mark on the flask.

- Sodium Perchlorate $NaClO_4$ anhydrous, ACS reagent, ≥98.0%, F.W: 122.44 g/mol.

1 M $NaClO_4$ is used in this work when the study of the effect of the addition of an electrolyte to the analyte stripping peak. 12.244 g are transferred into a 100 mL volumetric flask then, added deionized water until the mark in the flask.

- Zinc nitrate hexahydrate $Zn(NO_3)_2.6H_2O$, for analysis, reagent grade, F.W: 297.49 g/mol

A stock solution of 10 mM Zn(II) is prepared in 0.1M Acetate Buffer pH=4.5 as to keep the pH within the recommended working range, 297.49 mg of $Zn(NO_3)_2.6H_20$ are dissolved in acetate buffer and then transferred to 100mL volumetric flask. Consequently, the solvent is added until the mark in the flask.

- Potassium Hexacyanoferrate (II) trihydrate $K_4Fe(CN)_6.3H_2O$, ACS reagente, 98.5-102.0%, F.W: 422.39 g/mol.

The solution of 10 mmol/L of $K_4Fe(CN)_6$ needed to be prepared in 1 M KCl for the study of the roughness factor, for the purpose 0.424 g is then dissolved in 1 M KCl then, transferred to a 200 mL volumetric flask and adjusted until the mark with the solvent used.

- Potassium Hexacyanoferrate (III) trihydrate $K_3Fe(CN)_6.3H_2O$, ACS reagente, 98.5-102.0 %, F.W: 329.26 g/mol.

The solution of 10 mmol/L of $K_3Fe(CN)_6$ is prepared by transferring 0.329 g of the hydrated salt, it is dissolved in 1 M KCl and then transferred to a 100 mL volumetric flask and, the volume is adjusted until the mark with the solvent used.

3.2. Instruments

Several instruments and equipment were used throughout this work, they are all cited below.

Equipment and instruments used:

- Analytical balance: KERN ABJ-NM/ABS-N, ABS 220-4N, max 220 g, d 0.1mg.
- pH Meter: Mettler Toledo Five Easy.
- Electrochemistry instrument: Potentiostat Biologic SP300
- Magnetic Stirrer: AREC VELP SCIENTIFICA
- ICP instruments:

a) ICP-OES: Agilent 7700 ICP-MS

b) ICP-MS: Agilent 5800 ICP-OES

- Filtration:
  a) Filter: All-Glass Filter Holder Assembly with 300 mL funnel, fritted base and cap, clamp, 1 L flask
  b) Membranes: X100 Membrane Circles, Cellulose Acetate, White Plain 0.45 µm, 47 mm.
- Microscopic instruments:

  a) AFM and Optical Microscopy: Multimode 8 SPM base controlled by a Nanoscope V (Bruker, USA) and OMV optical viewing system (Bruker, USA).

  b) SEM and EDX: Hitachi TM 3030 and Quantax 70 from Nexus.

  c) XPS: K-Alpha Spectrometer from Nexus.

3.3. Electrodes and Preparation

During the research, in all the electrochemical experiments, the electrode selected was a glassy carbon electrode. As suggested by the literature Kefala et al in reference [101], glassy carbon electrodes as substrate produce the highest current densities for the metal selected to be studied. Besides, GC electrodes exhibit the flattest baseline and the lowest background current.

The electrode preparation varied throughout the research in order to improve the results, it was mainly treated mechanically, this means, the polishing process. Glassy carbon electrodes are polished using a slurry of alumina (particle size 0.05 µm) in deionized water on a velvet pad. The electrode was rinsed with deionized water and stored in deionized water in a small bottle. In preliminary experiments, the electrode was subject to mild ultrasonication in a cleaning bath for 5 minutes after polishing.

Following several trials, it was observed that the sonication did not improve data quality and therefore it was deemed unnecessary.

3.4. Calculation Methods

3.4.1. Calibration curve

A calibration curve demonstrates the response of an analytical method to known quantities of the analytes. Solutions that contain known concentrations of the analytes are described as standard solutions. Solutions that consist of all the reagents and the solvents utilized in the analysis except the analyte, are denoted as blank solutions. The analytical response obtained from the blank solution refers to impurities and interfering species in the reagents [76].

Steps for a calibration curve:

- A series of standards whose concentrations cover the expected range for unknown samples, are prepared. Those standards are then measured to obtain the analytical response and produce data.

- Those analytical responses are used to generate a graph of response against the concentration of the standards.

- The method of least squares is applied to establish the best straight line using the set of data. The method of least squares determines the best fit line by minimization of the sum of the squares of the vertical deviations.

- The sample containing the unknown concentration of the analyte is then prepared and its analytical signal obtained through measurement. After that, the straight line acquired previously is then used through interpolation (or extrapolation if the value lies outside the calibration range) to obtain the unknown concentration value of the analyte in the sample. Figure 3.1 depicts important parameters that can be obtained from a calibration curve.

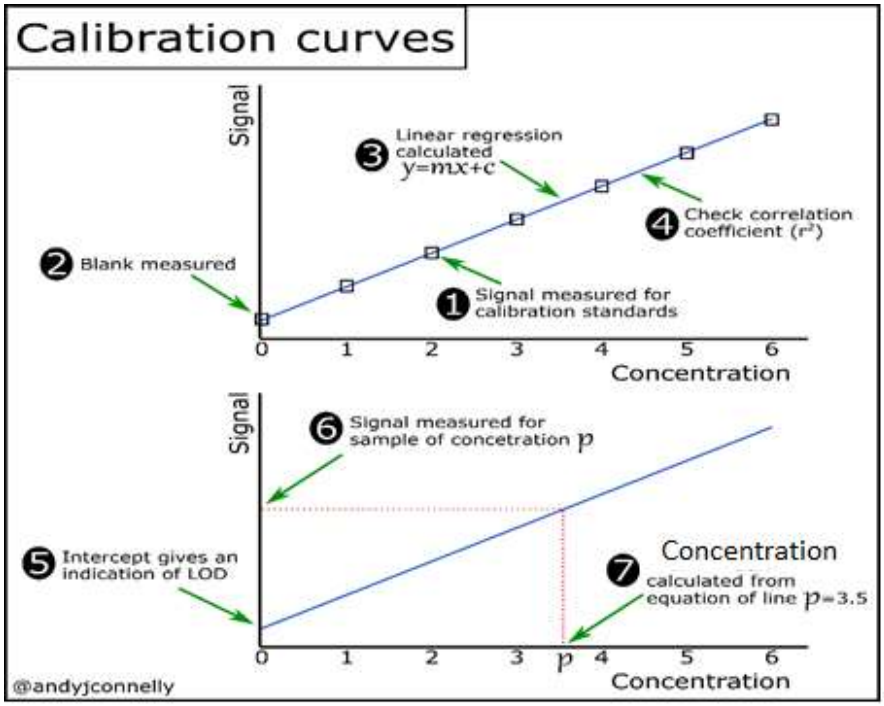

Figure 3.1: Important parameters obtained from a calibration curve. The best straight line from the method of least squares for a calibration curve.

Any calibration curve, linear or nonlinear, is less trustworthy (inaccurate) if it is extrapolated outside the range of calibration standards. Thus, the standards are best prepared over the entire range of concentration of the interest. It is suggested to prepare at least six standards and two replicate measurements for each sample and while making a rigorous procedure, it must include the preparation of each standard for calibration curve independently from a certified material (solution). It is important that serial dilution should be avoided where possible because of the propagation of any systematic error in the stock solution, however this is not always possible in trace analysis. Standard solutions for a calibration curve should be measured randomly not following a monotonic variation of concentration which may introduce systematic errors. Figure 3.2 exhibits an example of different regions found in a typical calibration curve.

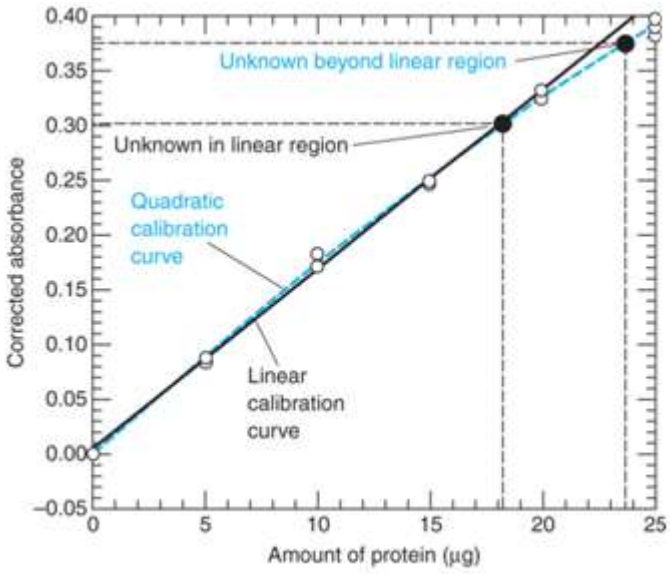

Figure 3.2: An example of regions in calibration curves of a UV-Vis spectrophotometric analysis of a protein, an image taken from reference [75].

3.4.2. Standard Addition

Standard addition is a method of calculation in which a certain quantity of the standard is spiked into the sample containing unknown concentration of the analyte. The concentration of the analyte in the original sample can be inferred from the increase of the analytical signal. It is a requirement for this method to obtain a linear response which does not pass through the origin. Moreover, higher precision can be attained when the addition of the standards is performed by mass instead of volume.

The standard addition method is principally convenient once the sample composition or its complexity strongly upsets the analytical signal, this is called matrix effects. The matrix comprises all the substances in the sample excluding the analyte. A matrix effect consists in the alteration in the analytical signal generated by any other component of the sample other than the analyte. In such cases, a simple calibration may result in a poor match of the background in the calibration standards to the sample.

There are common methods to perform standard addition:

a) Standard addition to a single solution

The standard addition to a single solution is a procedure in which a sample containing an unknown initial concentration of the analyte $[X]_i$ provides a signal intensity I_x. Next, a known

concentration (or volume) of the standard S is spiked into the aliquot of the sample and a signal I_{s+x} is generated for this second solution. Besides, addition of a standard to the concentration of the analyte $[X]_f$, where f stands for final. The concentration of the standard in the final solution as $[S]_f$. Note that the subscripts X and S refer to similar species, the analyte, but denote different concentrations.

The analytical signal is directly proportional to the analyte concentration, so:

$$\frac{Concentration\ of\ the\ analyte\ in\ initial\ solution}{Concentration\ \ of\ analyte\ plus\ standard\ in\ final\ solution} = \frac{signal\ from\ initial\ solution}{signal\ from\ final\ solution} \quad Equation\ 3.1$$

Standard Addition equation:

$$\frac{[X]_i}{[S]_f + [X]_f} = \frac{I_x}{I_{s+x}} \qquad Equation\ 3.2$$

For an initial volume V_0 of unknown and added (spiked) volume V_s of standard with concentration $[S]_i$, the total volume is $V=V_0+V_s$ and the concentrations are:

$$[X]_f = [X]_i \left(\frac{V_0}{V}\right) \qquad Equation\ 3.3$$

$$[S]_f = [S]_i \left(\frac{V_s}{V}\right) \qquad Equation\ 3.4$$

By expressing the diluted concentration of the analyte $[X]_i$, it is possible to determine $[X]_i$, as all the other quantities in the equation above are known.

In case the analysis does not consume solution, the recommendation is to start with the sample containing the analyte with an unknown concentration and measure its analytical signal. Afterwards, a small volume of concentrated standard is added and its analytical signal registered one more time. Various smaller volumes of the standard are added, and the analytical signal measured after each addition. Figure 3.3 exhibits an illustration of a standard addition to a single solution.

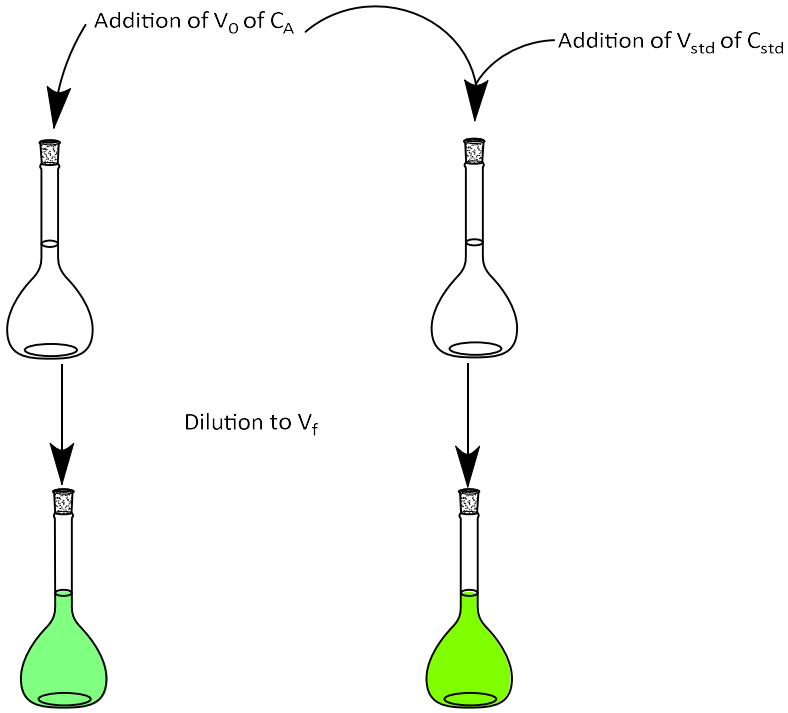

Figure 3.3: illustration of a standard addition for a single solution.

It is beneficial the standards to be concentrated so that the addition of small volumes would be possible, as a result the sample matrix would not substantially change. It is expected that the addition of the standards to intensify the analytical signal by a factor of 1.5 to 3.

b) **multiple solutions used for standard addition, successive standard addition**.

Procedure for multiple solutions with constant volume

The other type of the standard addition is illustrated in the figure below. Identical volumes of the samples are measured and transferred into certain volumetric flasks. To every single flask, growing volumes of the standard are added, and then the same flasks are diluted to the corresponding final volume. Each one of these flasks holds the same concentration of analyte in the sample (unknown) and different concentrations of standard as seen in Figure 3.4. The analytical signal I_{s+x} is measured for each flask; this method is recommended in the case of the analysis consumes some of the solution.

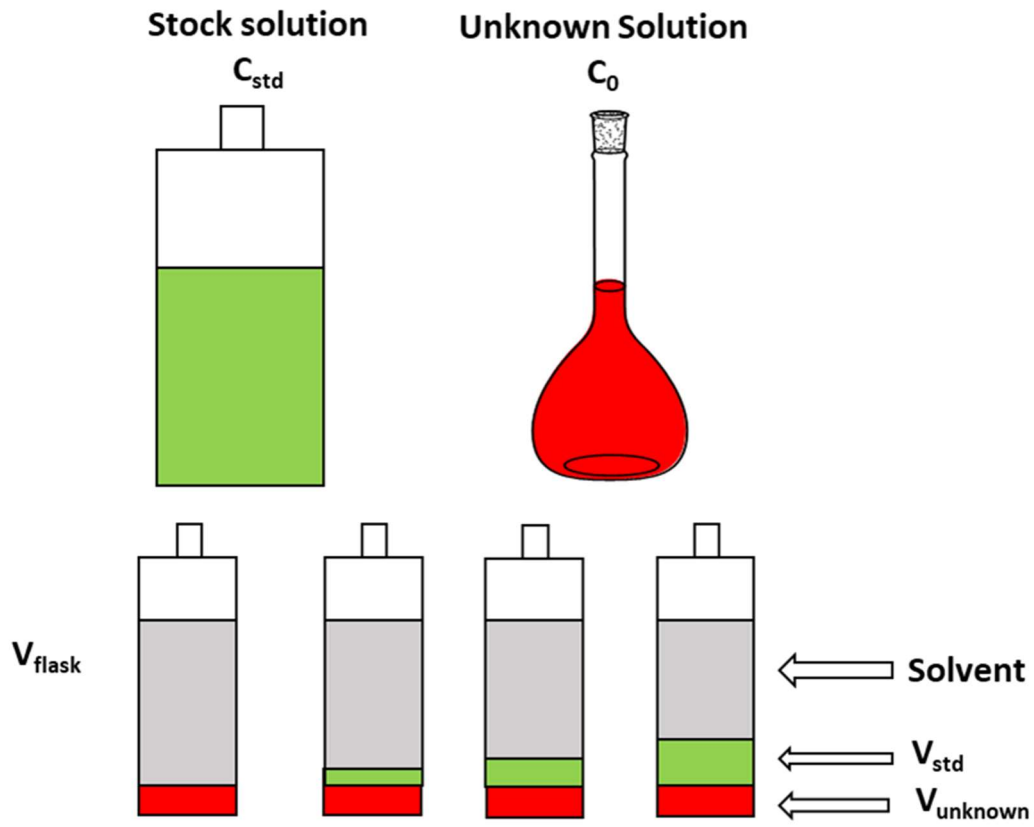

Figure 3.4: Illustration of a standard addition for multiple solutions.

As all standard additions are meant to be prepared to a constant volume, the plot signal I_{s+x} versus the concentration of diluted standard, $[S]_f$ is generated. Though, the x-intercept is the final concentration of unknown $[X]_f$, following the dilution to the final sample volume. The initial concentration of unknown $[X]_i$ is estimated from the dilution used to obtain the final sample. Sometimes, the plot is also generated as the analytical signal I_{s+x} versus the volume of the standard added in each volumetric flask. Figure 3.5 shows the standard addition curves in terms of concentration and volume spiked.

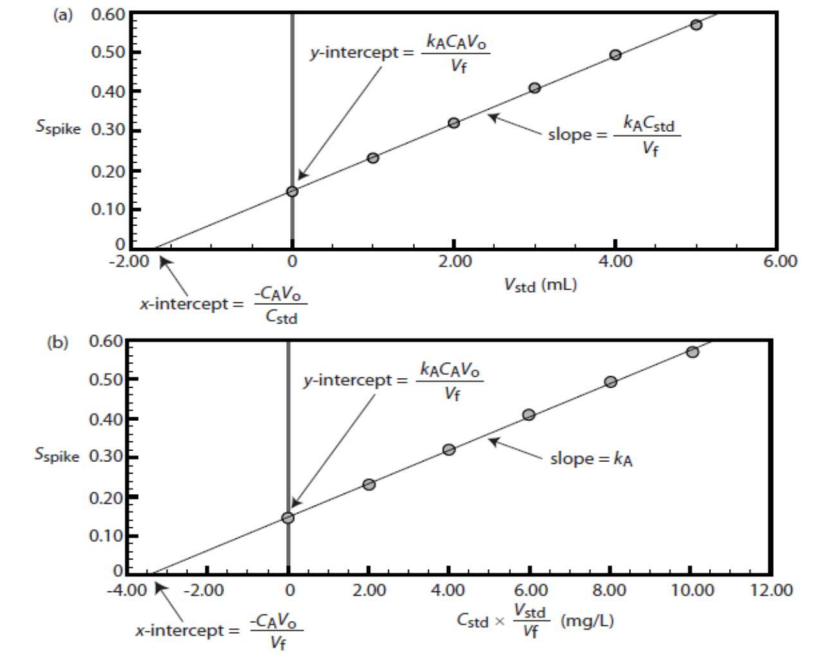

Figure 3.5: Standard addition curves in terms of concentration and volume added taken from reference [77].

The equation of the best straight line is $y = mx + b$ The x-intercept is obtained by setting:

$$y = 0 \quad \rightarrow \quad 0 = mx + b \quad \rightarrow \quad x = -\frac{b}{m} \qquad Equation\ 3.5$$

Figure 3.6 explains how to find the original concentration of the analyte. The theoretical response is determined through substitution of the expressions for $[X]_f$ and $[S]_f$ from the equation mentioned earlier.

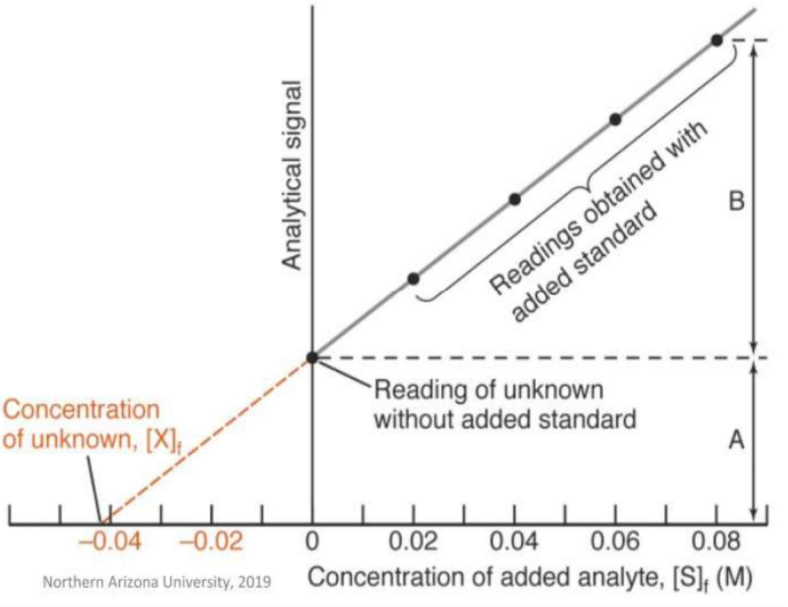

Figure 3.6: Parameters in a standard addition curve taken from reference [76].

For successive standard additions to one solution:

$$\underbrace{I_s + x\left(\frac{V}{V_0}\right)}_{\text{Function to plot on y-axis}} = I_x + \frac{I_x}{[X]_i}\underbrace{[S]_i\left(\frac{V_s}{V_0}\right)}_{\text{Function to plot on x-axis}} \qquad Equation\ 3.6$$

Successive standard additions to one solution:

Plot $I_s + x(\frac{V}{V_0})$ versus $[S]_i(\frac{V_s}{V_0})$ x: intercept is $[X]_i$.

A graph of $I_{s+x}(V/V_0)$ which is the corrected response on the y-axis versus $[S]_i(V_s/V_0)$ on the x-axis should be a straight line. The right side of the of the equation above corresponds to zero as $[S]_i\left(\frac{V_s}{V_0}\right) = -[X]_i$. The magnitude of the intercept on the x-axis equals the original concentration of the analyte in the sample.

Chapter 4: Characterization of the glassy carbon electrode surface

4.1. Microscopic characterization of the Glassy carbon electrode

A set of glassy carbon disk electrodes (GCEs) (Geometric area: 0.196 cm^2, diameter: 5mm) was employed in all the experiments. The electrodes were submitted to a microscopic analysis before undergoing Bi electrodeposition on the surface. The electrodes were pre-treated by polishing with alumina (0.05 μm) on a polishing pad (tan velvet). Afterwards, the electrode was sonicated in deionized water and washed with ethanol.

4.1.1. Optical microscopy and AFM analysis

The first microscopy test on the GCEs was performed using optical and atomic force microscopy. The instrument used is Bruker Multimode 8. The electrodes are scanned one by one, taking a large number of micrographs. The results showed a flat surface with parallel scratches, which may have been produced during the original cutting process as all the GCEs were from a set of ten provided by the supplier Alvatek and the scratches were observed before any polishing steps had been applied at Newcastle University. In addition to that technique, AFM provided information regarding the roughness and some imperfection on the electrode surface (some holes). Figure 4.1 depicts the above statements.

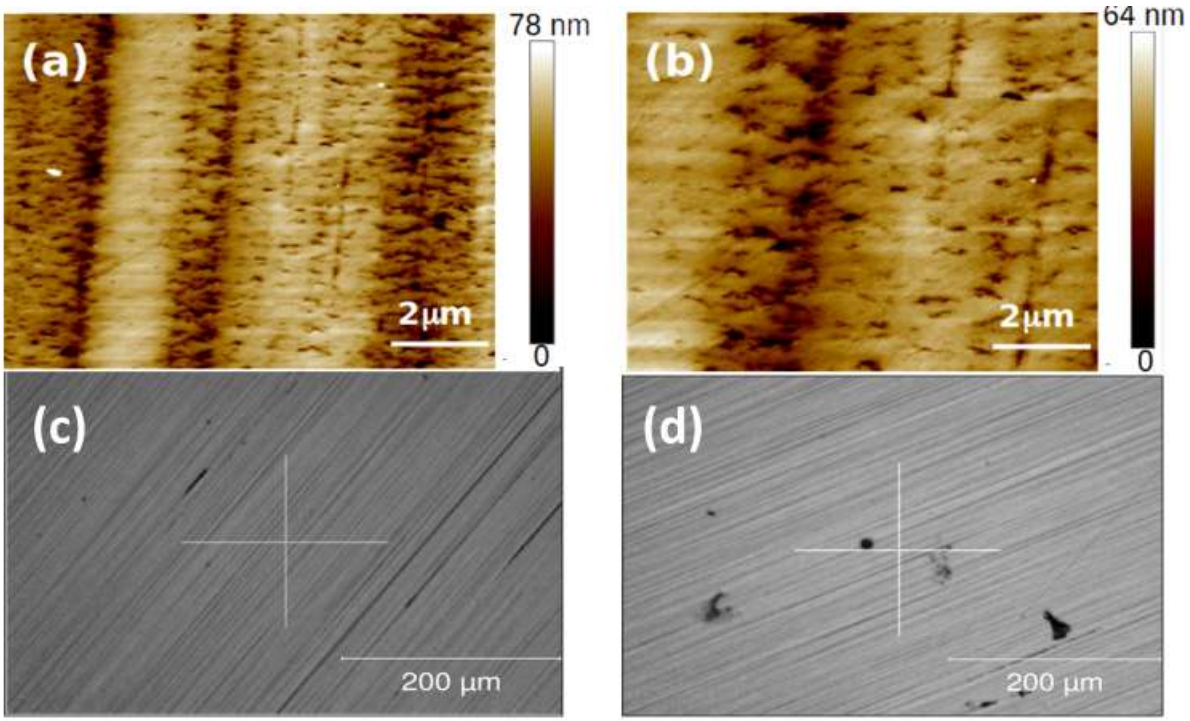

Figure 4.1: Optical Microscopy and AFM images of a bare GCE showing the scratches on its surface. (a) and (b) are AFM micrographs of the same bare GC, (c) and (d) optical microscopy images at different locations of the same bare GCE.

4.1.2. SEM and EDX

After AFM and Optical Microscopy, the electrodes were taken for another microscopy characterization. SEM and EDX analyses are performed for the purpose after the polishing process. The experiment was executed in NEXUS laboratory, Stephenson building and the instrument used was a Hitachi TM3030 operating at 15 kV. This microscopic observation showed the presence of some white spots on the surface, the whole surface scanned showed the presence of carbon, aluminium and oxygen. However, quantifying specifically the white spots mentioned, there is a considerable drop on carbon and a rise on aluminium and oxygen, which indicates that the surface is covered by the elements cited as illustrated in Figure 4.2. The percentage of aluminium and oxygen are variable depending on the location; hence, there is not uniformity (Figure 4.3). The large quantity of oxygen found on the surface of the electrode may have come either from the polishing process or from the air. Since the presence of Al is confirmed in EDX element identification images, it is very likely that particles of alumina have remained on the surface of the electrode despite washing and sonication.

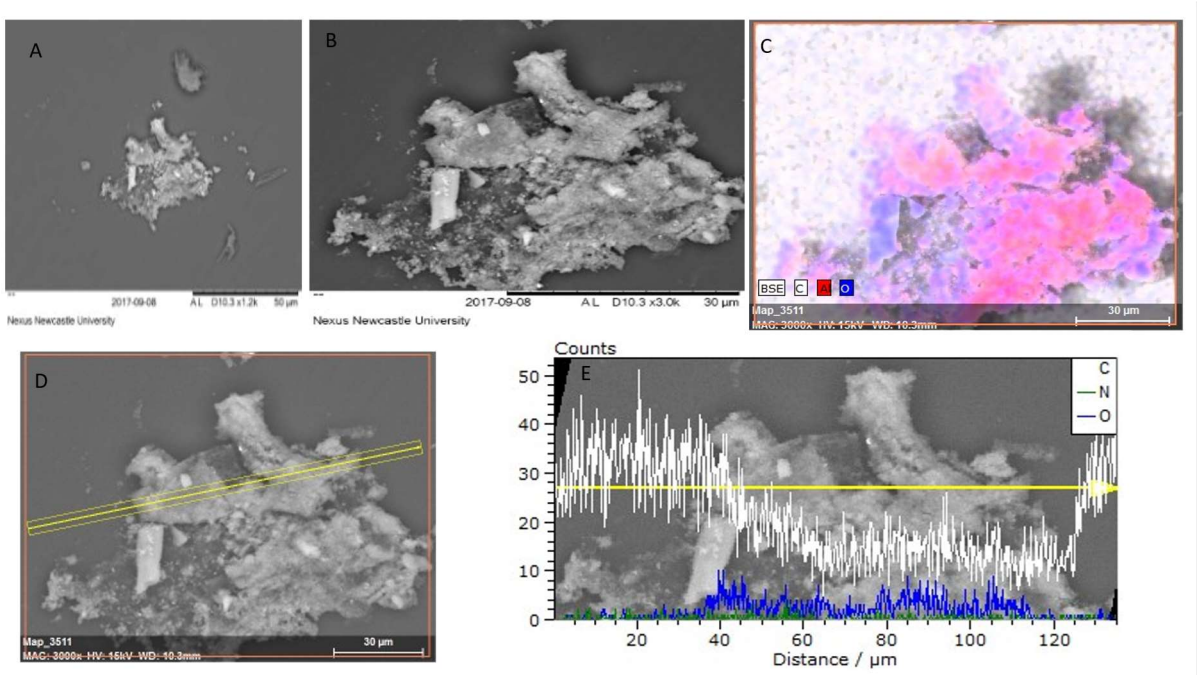

Figure 4.2: SEM and EDX images of a bare GCE after polishing and sonication. A: is a SEM image (magnification x1.2k and size 50µm) of a location of the surface on which some particles are seen; B: a SEM image of the particle observed in A at increased magnification (x3.0k) and reduced size (30 µm); C: is an EDX image of the surface at the same magnification and size of B, showing elements identification of carbon in white, aluminium in red and oxygen in blue; D and F: are EDX images showing a section selected area in yellow for elements quantification of carbon, oxygen and nitrogen. In E, it can be seen clearly that a drop on the count of carbon is observed while an increase on oxygen counts is noticed exactly on the particle.

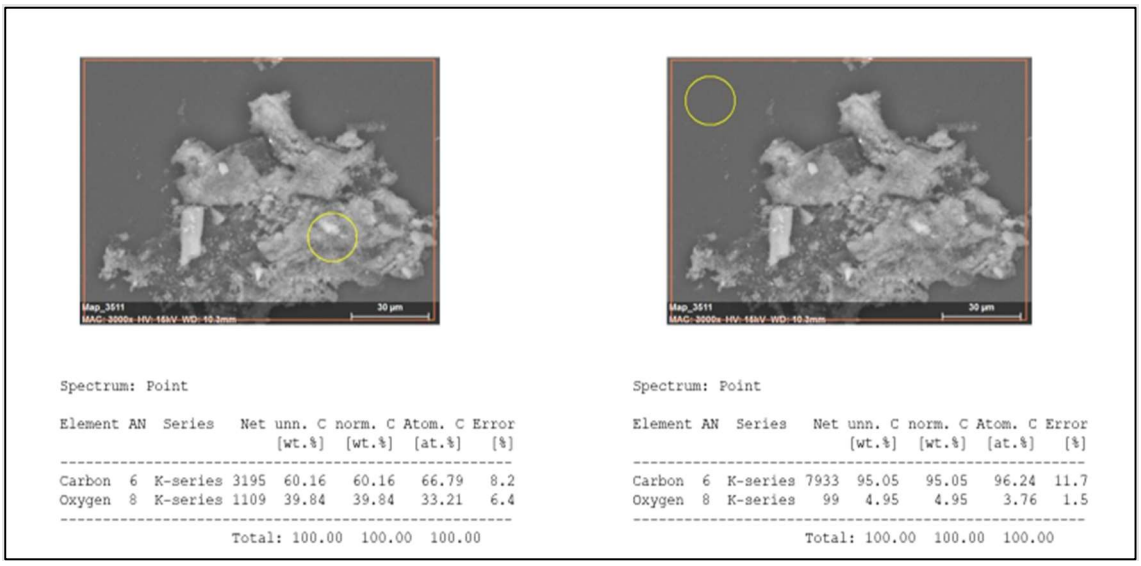

Spectrum: Point

Element	AN	Series	Net unn. C [wt.%]	norm. C [wt.%]	Atom. C [at.%]	Error [%]
Carbon	6	K-series	3195	60.16	66.79	8.2
Oxygen	8	K-series	1109	39.84	33.21	6.4
Total:				100.00	100.00	

Spectrum: Point

Element	AN	Series	Net unn. C [wt.%]	norm. C [wt.%]	Atom. C [at.%]	Error [%]
Carbon	6	K-series	7933	95.05	96.24	11.7
Oxygen	8	K-series	99	4.95	3.76	1.5
Total:				100.00	100.00	

Figure 4.3: Quantification of carbon and oxygen in a bare GCE from EDX image (size: 30 µm). Difference in the percentage of both elements in two locations, in and out of the particle observed.

4.2. Electrochemical characterization: roughness factor study

The electrochemical determination of the surface area of glassy carbon was executed using Hexacyanoferrate (Ferrocyanide) due to its surface sensitive property, which means it is sensitive to the state of the carbon surface and its redox reaction depends strongly on the presence of oxides on the surface [125].

Randles-Sevcik equation was used for determination of the electrochemically active surface area A^{ECSA} of the electrode as opposed to the geometrical surface area A^{geo}, and consequently the roughness factor (A^{ECSA}/ A^{geo}), through plotting the peak current vs. square root of the scan rate. A^{geo} is simply πr^2 where r is the electrode radius. Two methods were used for the purpose.

Redox reaction Ferri/Ferrocyanide:

$$Fe(CN)_6^{3-} + e^- \rightleftharpoons Fe(CN)_6^{4-} \qquad U^0(vs.SHE) = 0.361\,V \qquad Equation\ 4.1$$

- For a reversible system (at 25^0C):

$$i_p = (2.69 \times 10^5).n^{3/2}.A^{ECSA}.C_0(D.\upsilon)^{1/2} \qquad Equation\ 4.2$$

In Equation 4.2, i_p: peak current (A), n: number of electrons transferred, A^{ECSA}: electrochemical surface area (cm^2), C: concentration (mol/cm^3, υ: scan rate (V/s), D: diffusion coefficient cm^2/s.In Equation 4.2, i_p: peak current (A), n: number of electrons transferred, A^{ECSA}: electrochemical surface area (cm^2), C: concentration (mol/cm^3, υ : scan rate (V/s), D: diffusion coefficient cm^2/s.

4.2.1 Direct application of the Randles-Sevcik equation

The first set of experiments were carried out using 10 mM hexacyanoferrate (II) in 1M KCl(aq) as supporting electrolyte. The electrochemical experiment employed a three-electrode cell. The set of ten GCEs was used for this study to calculate the roughness factor. Cyclic voltammograms were taken accordingly at four different scan rates (25, 50, 75 and 100 mV/s) as it can be seen in Figure 4.4. Randles-Sevcik equation is applied to analyse the data.

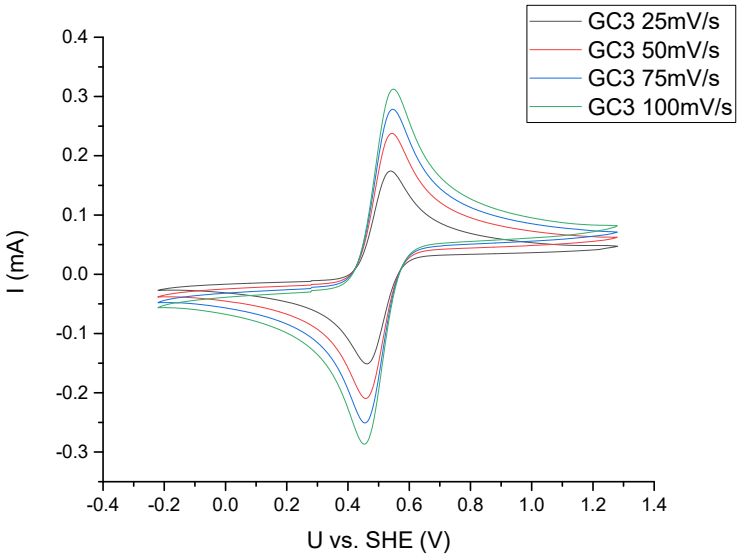

Figure 4.4: Cyclic voltammograms of the couple $FeCN_6^{3-/4-}$ in 1 M KCl(aq) at a glassy carbon disk electrode.

The graph i_p versus square root of the scan rate ($\upsilon^{1/2}$) exhibited a good linearity as shown in Figure 4.5. This linearity confirms that the process is diffusion controlled. The peak current increases with the scan rate due to the difference in slopes for concentration-distance profiles at x=0 for fast and slow scan rates [104]. For any given potential $(\partial C/\partial x)_{x=0}$ is larger for the faster scan. Consequently, the current is larger. As required in the literature, i_p versus $\upsilon^{1/2}$ has to be linear (Figure 4.5) with intercepts at the origin for a reversible couple.

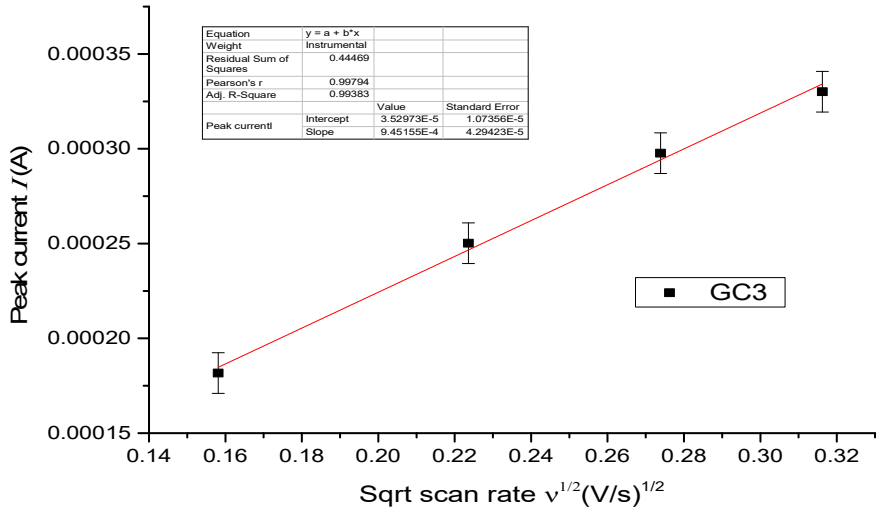

Figure 4.5: Plot Peak current vs. square root of the scan rate with GC3 as working electrode. The error bars represent the standard error of the intercept.

Values of A^{ECSA} were obtained from the slope of the Randles-Sevcik plot using the value of D = 7.26 x $10^{-6}cm^2s^{-1}$ [107] for the diffusion coefficient of couple $FeCN_6^{4-}$. However, as illustrated in Figure 4.6, all the electrodes provided a roughness factor below 1, having as average 0.7. Electrode GC9 exhibited a particularly low roughness factor of 0.5. Values below 1 indicate that not all of the electrode is active. This result may be due to the variation of oxygen functionalities across the surface. The presence of alumina from polishing, as observed by microscopy, cannot explain the data on its own because it is certainly not the case that 30% of the surface is covered by alumina particles. The low roughness factor may also be caused by the reaction occurring preferentially on the edges of the disk.

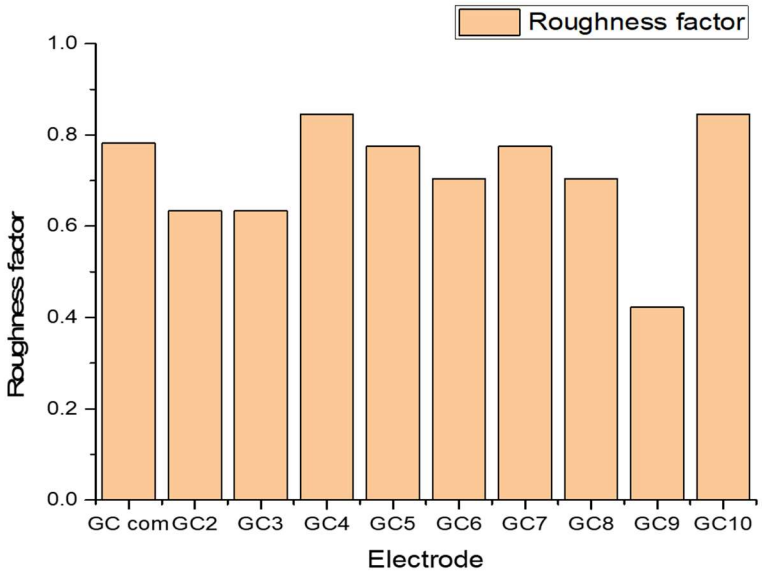

Figure 4.6: Results roughness factor A^{ECSA}/A^{geo} from direct use of the Randles Sevcik equation.

4.2.2. Recalibration technique

The second method used for the calculation of A^{ECSA} was a calibration technique, it was conceived using the concept of hydrogen adsorption desorption at a Pt electrode (Figure 4.7). Since the direct calculation of the roughness factor provided values below 1 using voltammetry of $FeCN_6^{4-}$, the recalibration technique was executed in order to check those results. The method has been applied in three steps: in the first step the electrochemically surface-active area for a Pt electrode was calculated from the hydrogen desorption peak. The peak is integrated to obtain $\mathbf{q_{ad}}$. After that, equation 4.3 below was used to calculate A^{ECSA}. The results are displayed in Table 4.1.

$$A^{ECSA} = \frac{q_{ad}}{q_m} \qquad Equation\ 4.3$$

where:

- q_{ad}: the adsorption charge associated with a known adsorbate on the electrode surface.
- q_m: the charge associated with a monolayer coverage of the said adsorbate. In this case, its value corresponds to 210 µC cm^{-2} [188].

Table 4.1: Parameters values obtained from Hydrogen adsorption-desorption of 1M H_2SO_4 in Pt disk electrode.

q_{ad} (µC)	14.04
q_m (µC/cm^2)	210
A^{ECSA} (cm^2)	0.067
d (cm) Pt disk	0.25
A^{GEO}(cm^2)	0.0491
R_f	1.36

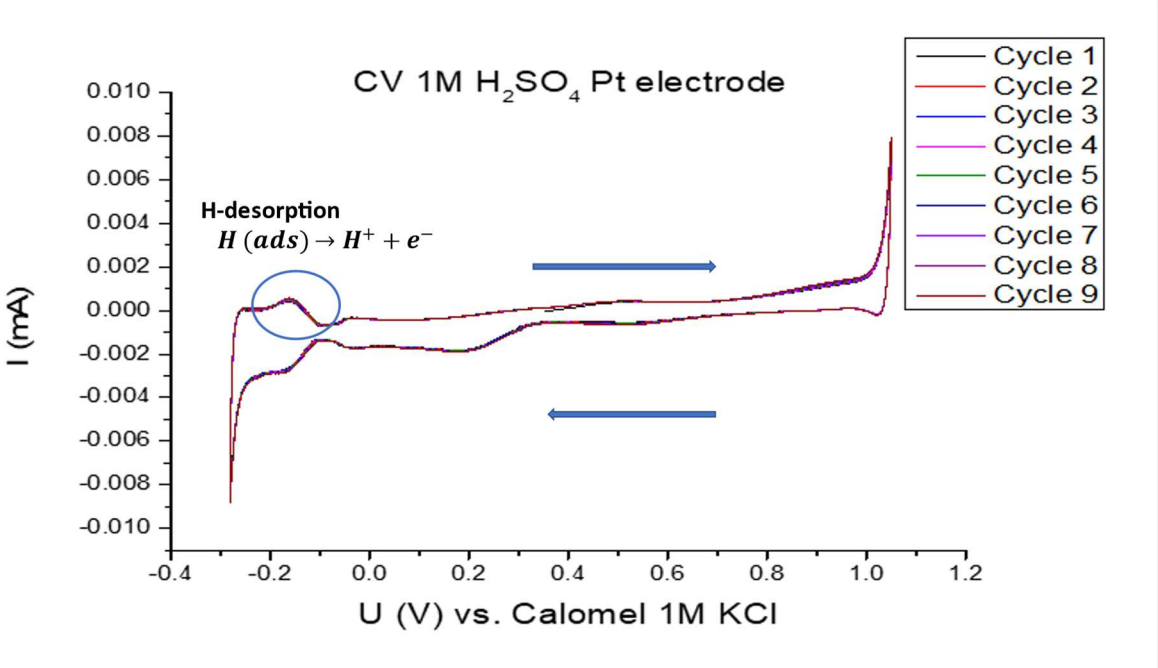

Figure 4.7: CV 1M H_2SO_4 using a Pt disk as the working electrode at 100 mV/s as scan rate.

The second step is the determination of the product "$D^{1/2}C$", which will eventually be used for the calculation of a new diffusion coefficient. In order to accomplish that, a CV was taken with 10 mM couple $FeCN_6^{4-}$ using the Pt disk as working electrode. The CV was produced from -0.2 V to 0.9 V vs. a calomel reference in 1M KCl, at four scan rates for the purpose of building a plot of i_p versus square root of the scan rate. Then, the Randles Sevcik equation is reused (equation 4.2), and consequently a new diffusion coefficient is obtained. The area used in this calculation was obtained in the first step. The results obtained are displayed in Table 4.2.

- The slope:

$$m = (2.69 \times 10^5).n^{3/2}.A.C.D^{1/2} \qquad Equation\ 4.4$$

- The product $CD^{1/2}$ is:

$$CD^{1/2} = \frac{m}{(2.69 \times 10^5).A.n^{3/2}} \qquad Equation\ 4.5$$

- And:

$$D = (\frac{m}{(2.69 \times 10^5).C.A.n^{3/2}})^2 \qquad Equation\ 4.6$$

Table 4.2: Parameters values for the new diffusion coefficient estimated.

m (slope)	2.00 x 10^{-3}
Intercept	5 x 10^{-7}
Concentration (mol/cm^3)	1.00 x 10^{-5}
A (cm^2)	0.0668
$CD^{1/2}$	1.11x 10^{-8}
$D^{1/2}$	1.11 x 10^{-3}
D (cm^2/s)	1.24 x 10^{-6}

The third step is the determination of the roughness factor for GC electrodes using the diffusion coefficient calculated previously in the second step. The methodology is the use of the same couple ferri/ferrocyanide, CVs are performed at four scan rates, the curve i_p vs. square root of the scan rate is generated. Randles-Sevcik equation is used as mentioned previously in the second step, however, the diffusion coefficient applied is the one obtained from the second step. As a result, the roughness factor achieved presents the values between 1.02 and 2.05 as may be seen in Figure 4.8.

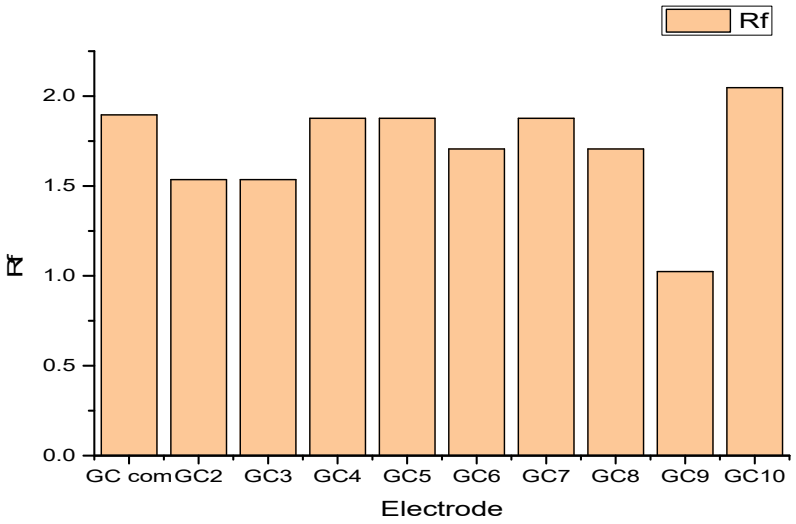

Figure 4.8: Results roughness factor from the recalibration technique.

4.3. Summary

The electrode used for this work is glassy carbon, its characterization was required in order to evaluate the electrode before using it for further experiments. Two techniques were used for this characterization: -Microscopic and electrochemical techniques. The microscopic characterization showed the scratches from AFM and optical microscopy and oxygen, aluminium and carbon from SEM and EDX. The scratches may have been probably generated during the cutting process of the electrodes; the electrodes used were specially ordered in order to fit in the AFM instrument. Polishing works done could not remove those scratches; on the contrary, more scratches which are smaller than the originals, are produced.

Furthermore, SEM and EDX results displayed the presence of oxygen and aluminium. The presence of these elements means there are some remains of the polishing solution used, although, the electrode was washed with ethanol and sonicated. On the other hand, the lack of uniformity in the proportion of oxygen and aluminium indicates that some oxygen may have been come from the air during the polishing process. These elements may constitute a block to the surface; consequently, it may affect the electrodeposition.

Concerning the electrochemical characterisation, two methods were used all of them based on the Randles Sevcik equation. In the first method the peak currents in cyclic voltammetry were used to estimate A^{ECSA} using a literature value of the diffusion coefficient. This surprising result led to roughness factors below 1 which suggests that not all the electrode surface is

active. A separate estimate of the diffusion coefficient was therefore made on a Pt electrode whose A^{ESCA} was determined from the known properties of the H-desorption peak in acidic medium. This value of diffusion coefficient was used in the Randles-Sevcik data for the GCE and produced roughness values A^{ECSA}/A^{geo} between 1.5 to 2.0. This range of values was considered more accurate and better reflects the surface roughness and active area of the GCEs studied.

Comparing results from both characterization microscopic and electrochemical, the first showed the presence of oxygen aluminium on the surface, this may affect at some extension the electrode activity. On the other hand, the electrochemical characterisation result obtained from the first method, which was described as a direct use of the Randles Sevcik equation; the roughness factor achieved was below 1, and the opposite was observed with the recalibration technique. Thus, the latter is more reliable for the determination of A^{ECSA}, consequently the roughness factor since the values obtained in this research are more within the range expected for an ideal GCE.

Chapter 5: Detection of Zn and Pb

5.1. Bi ex situ electrodeposition

Bi electrodes have been investigated as an alternative to mercury and that there is some evidence they are as good as mercury [102]. Since the latter have been banned due to mercury toxicity. In some works, the results obtained by these Bi modified electrodes can be comparable to ones achieved from Hg mercury electrodes [181,183].

Bismuth modified electrodes can be produced either in situ or ex situ. Ex situ deposition is when the Bi electrodeposition is performed before the analysis and in a different solution which does not contain the analyte while the in-situ deposition is when the electrodeposition is done simultaneously with the analyte and then stripped.

Initially in this research, ex situ bismuth electrodeposition was executed, which means the Bi is deposited on the surface before introducing analytes into the system. Afterwards, in-situ electrodeposition was introduced because it is less time consuming than the ex-situ methodology.

5.1.1. CA and CV electrodeposition

The formation of Bi modified electrodes requires the application of an electrochemical technique. In most cases, the techniques used for the purpose are chronoamperometry, cycling voltammetry and galvanostatic methods. In this work, two electrodeposition techniques are used initially: constant applied potential (chronoamperometry) and cycling potential (cycling voltammetry). As it is research, several reference electrodes were used as trial before selecting the most appropriate for the fulfilment of the purpose of this work. The first series of initial experiments were undertaken using MSE mercury (1 M H_2SO_4) as reference electrode. According to the literature which suggests the supporting electrolyte used is 0.1 M acetate buffer pH 4.5 to avoid hydrolysis [4] and 5 mM Bi(III) is prepared in that supporting electrolyte. This concentration of Bi is chosen considering it as a high concentration test for initial experiments.

The cycling potential ex situ electrodeposition was carried out applying a potential from -0.074 V to -0.526 V vs. SHE (-0.8 V to -1.2 V vs. MSE (1 M H_2SO_4)) in 10 cycles at a scan rate

of 25 mVs^{-1} as it is illustrated in the Figure 5.1. The range of this cycling potential was chosen considering the standard potential of Bi and based on some trials executed initially. At the beginning, it was necessary to estimate the equilibrium potential of Bi according to the concentration used (5 mM Bi); from the Nernst equation, it was obtained $U^0(Bi^{3+}/Bi)$ = -0.402 V vs MSE (1M H_2SO_4) [$U^0(Bi^{3+}/Bi)$ = -0.272 V vs. SHE]. The objective of using the cycling potential is to deposit effectively Bi on the surface for further metal detection. Initial attempt to produce an appropriate potential range required to disclose the cathodic and anodic peaks, then extending the range at nearly 0.0 V vs. MSE (0.674 V vs. SHE), has showed that the cathodic peak appears at -0.352 V vs. MSE (0.322 V vs. SHE); thus, the range to be chosen must be below this value in order to avoid reoxidation of Bi electrodeposited. On the other hand, the anodic peak was observed at roughly -0.7 V vs. MSE (-0.026 V vs. SHE), this means, the start of the potential range should slightly more negative; therefore, -0.8 V vs. MSE (0.074 V vs. SHE) was chosen as the start point for the CV. Moreover, the Hydrogen evolution region (HER) is also a concerning issue, the end point of the CV is set at -1.2 V vs. MSE (-0.526 V vs. SHE) to avoid reaching that region.

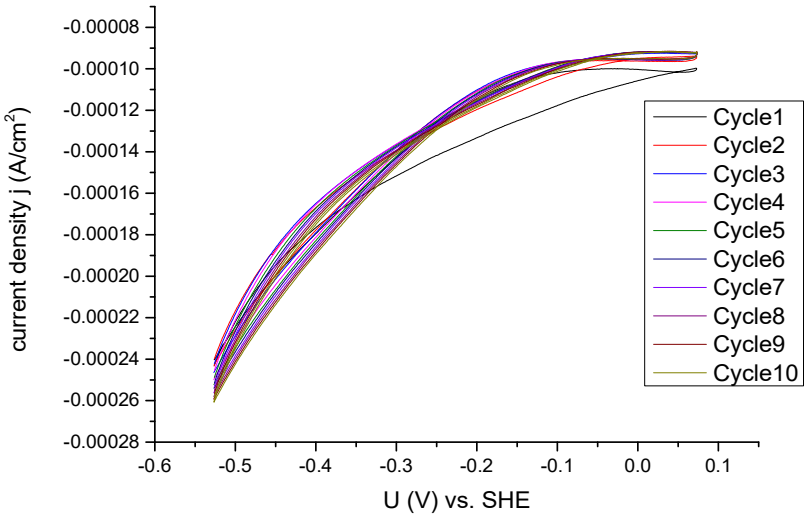

Figure 5.1: Electrodeposition 5 mM Bi(III) under conditions of potential cycling at 20 mVs^{-1} as scan rate, working electrode: glassy carbon electrode, counter electrode: Au wire, reference electrode: MSE (1 M H_2SO_4).

Another technique used for the electrodeposition is chronoamperometry, for which it is applied a potential of -0.126 V vs. SHE (-0.8 V vs. MSE (1 M H_2SO_4)) during 300 s. The Figure 5.2 and 5.3 depict the Chronoamperometry electrodeposition in the case of stirred and unstirred conditions. Figure 5.2 illustrates an example of chronoamperometry electrodeposition in stirred conditions where 250 ppm (1.2 mM) Bi(III) is used unlike the Figure 5.3 shows the one under unstirred with a concentration of 5 mM Bi(III).

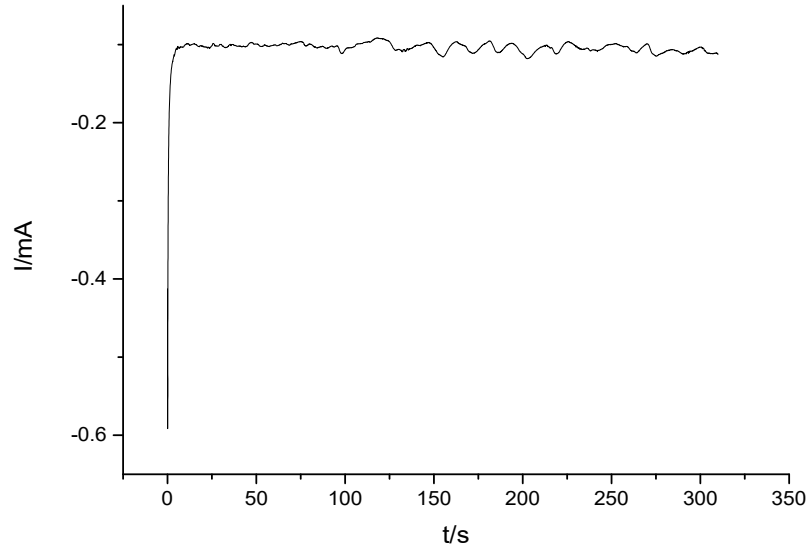

Figure 5.2: CA electrodeposition stirred conditions 250 ppm (1.2 mM) Bi(III) in 0.1 M acetate buffer pH 4.5, E_d (deposition potential): -0.8 V vs. MSE (1 M H_2SO_4), t_d (deposition potential): 300 s, working electrode: glassy carbon electrode, counter electrode: Au wire, reference electrode: MSE (1 M H_2SO_4), stirring rate: 50 rpm.

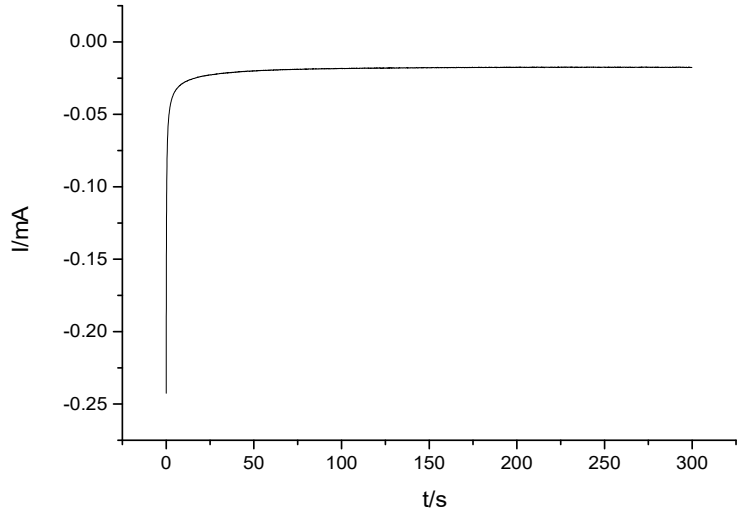

Figure 5.3: CA electrodeposition in unstirred conditions 5 mM Bi(III) in 0.1 M acetate buffer pH 4.5, t_d (deposition time): 300 s, E_d (deposition potential): -0.8 V vs. MSE (1 M H_2SO_4), working electrode: glassy carbon electrode, counter electrode: Au wire, reference electrode: MSE (1 M H_2SO_4).

The charges estimated for the stirred conditions was 32.4 mC (Figure 5.2) and unstirred conditions 5.80 mC (Figure 5.3) obtained through integration of the respective curves current versus time signal. Using Faraday's law of the electrolysis, represented by the equation 5.1 below:

$$Q = nFN \qquad Equation\ 5.1$$

where *Q* is the electrical charge (in Coulomb), n: the number of electrons transferred, in case of Bi n equals to 3, N corresponds to mols and F: the Faraday constant (96485 C/mol). From the equation 5.1, the mols of Bi can be estimated as below:

$$N = \frac{Q}{nF} \qquad Equation\ 5.2$$

Then, the mols of Bi(III) were estimated as 1.12×10^{-7} mol and 2.00×10^{-8} mol respectively from the equation 5.2, the mass of Bi is also calculated as in the equation 5.3 below:

$$N = \frac{m}{M} \quad \rightarrow \quad m(Bi) = N \times M(Bi) \qquad Equation\ 5.3$$

Where M(Bi) is the molar mass of Bi which corresponds to 208.98 g/mol. After that, from the relationship between the density and the volume is used to estimate *h*, the thickness of the

film. The equations 5.4 and 5.6 combined produce the equation 5.7 which corresponds to the estimation of *h*, the thickness of Bi-film:

$$V = \pi r^2 h \qquad Equation\ 5.4$$

From the equation 5.4, *h* is then isolated (Equation 5.5), ρ(Bi) the density of Bi is known and corresponds to 9.78 g/cm^3, taking also into account that the glassy carbon disk employed in this work has a diameter of 5.0 mm, thus, *r* (radius) corresponds to 2.5 mm (0.25 cm).

$$V = \pi r^2 h \qquad \rightarrow \qquad h = \frac{V}{\pi r^2} \qquad Equation\ 5.5$$

$$\rho = \frac{m}{V} \qquad \rightarrow \qquad V = \frac{m}{\rho} \qquad Equation\ 5.6$$

After that, the equation 5.6 substitutes the term *V* (volume) in equation 5.5, the resulting equation 5.7 is appropriate to estimate the thickness of Bi-film:

$$h = \frac{m}{\pi r^2 \rho} \qquad Equation\ 5.7$$

From this perspective, the equivalent thickness of Bi-film assumed to cover the substrate glassy carbon electrode uniformly would be 122 nm and 21.8 nm respectively as shown in Table C.1, Appendix C in the Appendix section.

5.1.2. Characterisation of Bi films (electrodeposited)

Following the electrodeposition process, the modified electrodes are required to be characterized. This work has focused on microscopic characterization using the following techniques: Optical Microscopy, AFM, SEM, EDX and XPS. The objective of using these techniques is to obtain information such as the extent of Bi in the surface, the state at which it is found electrodeposited, and which other elements are present on the surface.

Optical Microscopy and AFM

Optical microscopy and AFM have been used to characterize the surface of the electrode modified with Bi. From the Optical Microscopy images in the Figure 5.6 (alongside with EDX images), the surface becomes darker compared to the image of a bare Glassy carbon electrode. The black spots can be deduced to be Bi deposited on the surface. In the case of AFM, its micrographs showed clusters of Bi in some locations of the electrode surface. As it

can be seen in Figure 5.4 below, the height profile clearly shows the height of one of the Bi clusters in the image. It is clear from the image that Bi does not deposit as a uniform film under the conditions employed in stripping voltammetry.

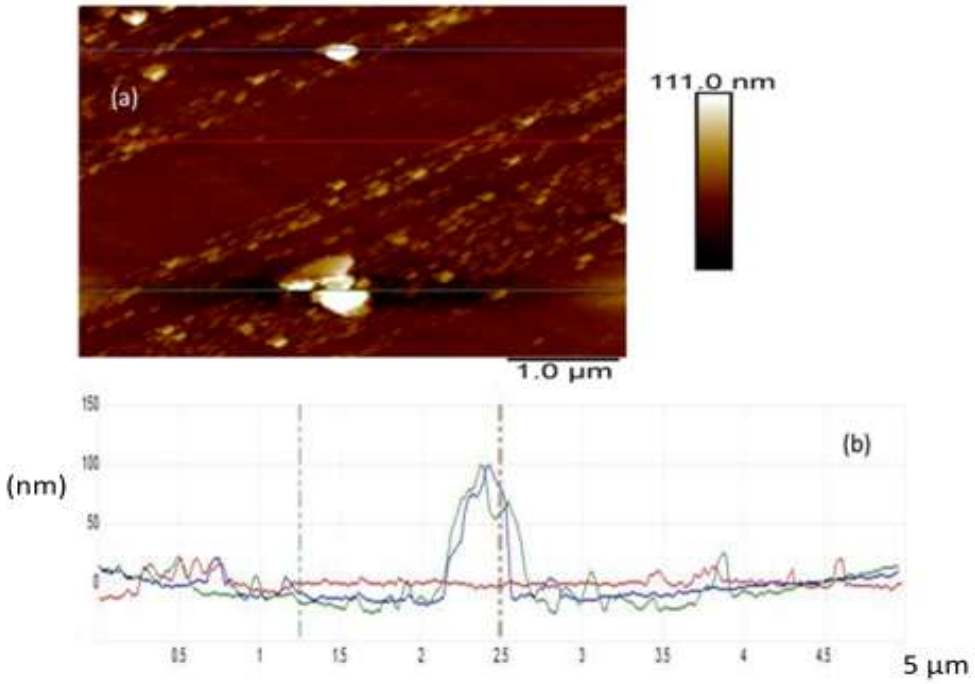

Figure 5.4: AFM micrograph and height profile of the GCE Bi modified, after its electrodeposition. (a) is the AFM micrograph where clusters of Bi are seen on the surface, and (b) is the height profiles of the deposition on the surface.

SEM and EDX

SEM and EDX are chosen to further the characterisation of the electrodeposited Bi on the surface. These techniques provide information regarding the quantification of Bi and all the elements predominant on the surface. Bi is electrodeposited by chronoamperometry, or potential cycling as described previously.

Not surprisingly both chronoamperometry and potential cycling techniques showed a non-uniform distribution of Bi on the surface. According to EDX quantification, it could be seen clearly that the percentage of Bi was variable in different locations on the surface from the micrographs below. The thickness of the film was estimated to be a few nanometres; however, remains of alumina (Al_2O_3) could also be observed on the surface through a considerable amount of Al and oxygen are found while identifying elements, although in some

locations oxygen alone was identified. Figure 5.5 and Table 5.1 present an example of a non-uniform distribution of Bi on the electrode surface. Since a substantial extent of oxygen is also detected, this information raised an awareness on the state of Bi on the surface.

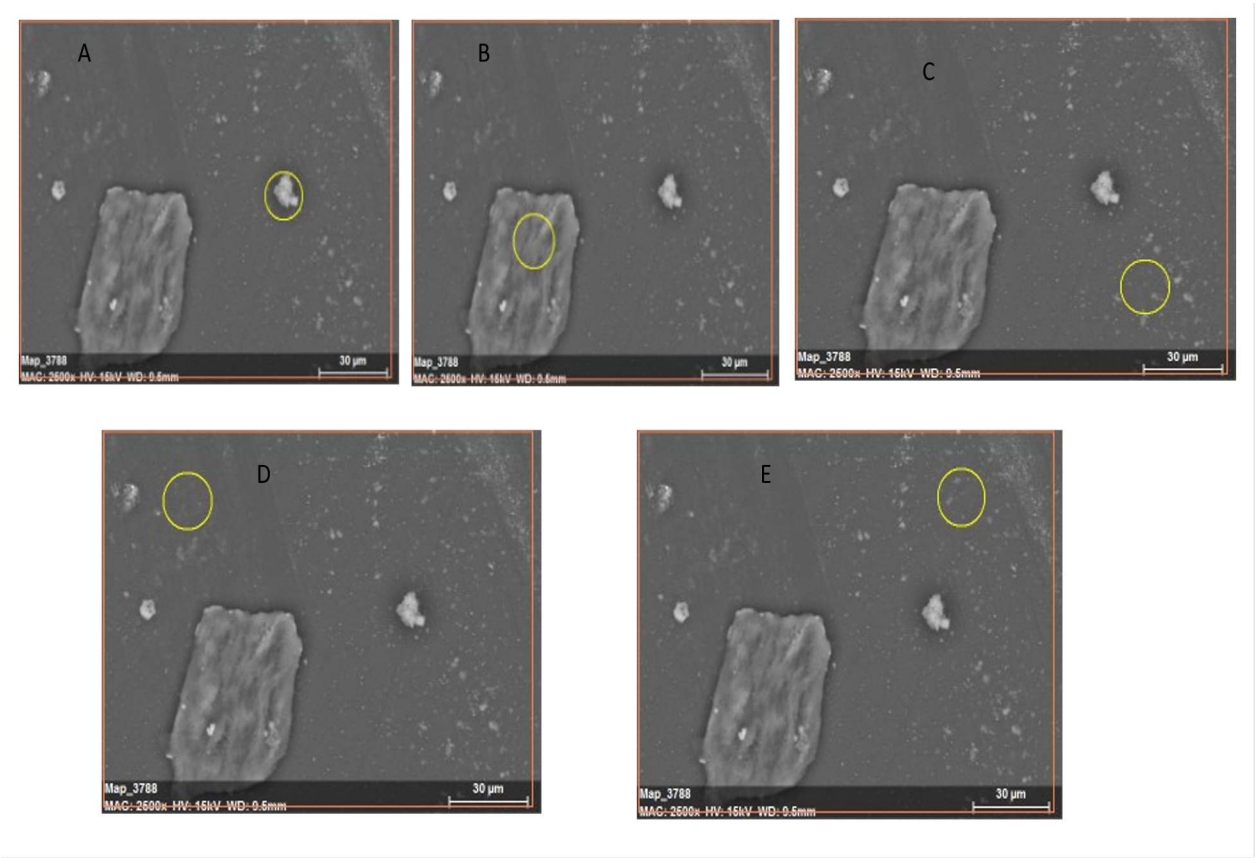

Figure 5.5: SEM images and EDX quantification showing the non-uniform distribution of Bi on the electrode surface. A, B, C, D and E images are showing the quantification in different locations on the surface to evaluate the distribution of Bi on the surface.

Table 5.1: EDX quantification details according to SEM images shown in the Figure 5.5. The values present the proportion of Bi on the in different locations of the surface.

Image	Element	AN	Series	Net	Unn. (wt. %)	C Norm. (wt. %)	C Atom. (at. %)	C error (%)
A	Carbon	6	K-series	1565	98.31	98.31	99.9	14.8
	Bismuth	83	M-series	18	1.69	1.69	0.10	0.1
	Total				100	100	100	
B	Carbon	6	K-series	1270	94.77	94.77	99.68	14.8
	Bismuth	83	M-series	48	5.23	5.23	0.32	0.2
	Total				100	100	100	
C	Carbon	6	K-series	2272	100.0	100.0	100.0	14.2
	Bismuth	83	M-series	0	0.0	0.0	0.0	0.0
	Total				100	100	100	
D	Carbon	6	K-series	2351	99.55	99.55	99.97	14.1
	Bismuth	83	M-series	7	0.45	0.45	0.03	0.0
	Total				100	100	100	
E	Carbon	6	K-series	2388	98.66	98.66	99.92	13.9
	Bismuth	83	M-series	22	1.34	1.34	0.08	0.1
	Total				100	100	100	

In agreement with the Figure 5.6, the difference between the stirred and unstirred electrodeposition conditions is remarkable. As reported earlier, the chronoamperometric technique is executed under both stirred and unstirred conditions. Observing the results, it could be seen that the coverage of Bi electrodeposited is more extensive in stirred conditions than unstirred. This result was predictable as stirring the solution when a potential is applied, increase the mass transport rate of the Bi(III) ions.

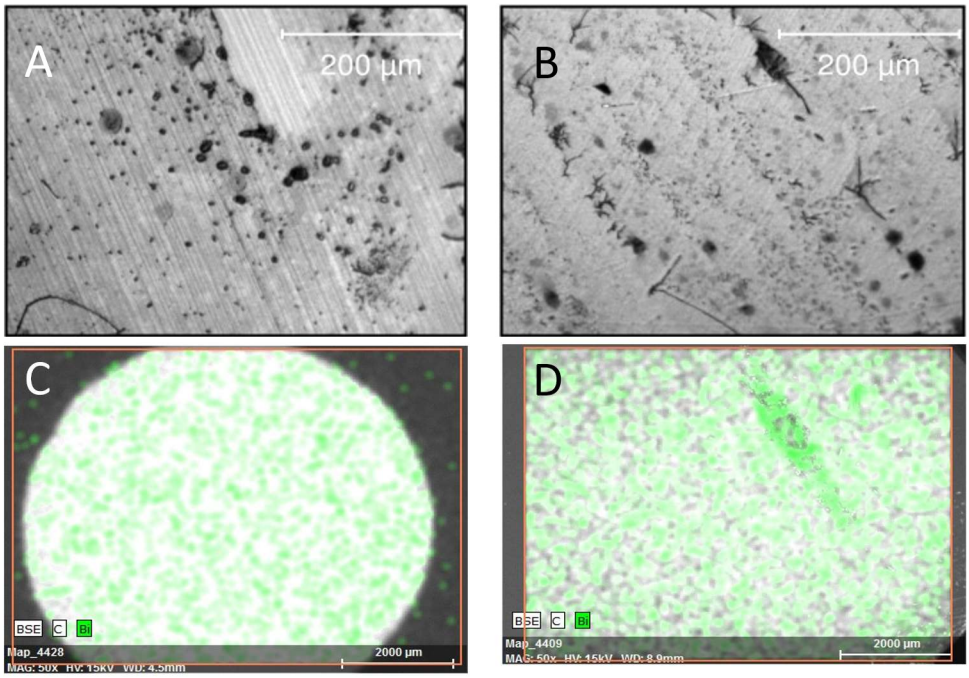

Figure 5.6: Optical microscopy and EDX micrographs (Quantax 70) for electrodeposition under stirred and unstirred conditions, deposition potential: -0.8 V vs. MSE (1 M H_2SO_4), deposition time: 300 s, stirring rate: 50 rpm, working electrode: glassy Carbon, Counter electrode: Au wire, supporting electrolyte: MSE (1 M H_2SO_4). Figures A and B are optical microscopy images in which black spots represent Bi deposition on glassy carbon electrodes, while C and D display EDX images of the same GC electrodes where green spots indicate the presence of Bi on the same surface.

XPS Characterisation

In the previous chapter, the characterisation of bare GC electrodes was reported. SEM micrographs and EDX information showed oxygen on the surface, which raised a concern about how Bi is bonded and in which state it is found on the surface. Hence, XPS measurements were introduced to clarify this situation. Some samples were prepared under in situ conditions which means Bi and Pb were electrodeposited simultaneously.

The results showed the presence of Bi on the surface as expected. However, as showed on Figure 5.7 below, according to the literature findings, Bi electrodeposited on the surface should be in its elemental state with a binding energy of 157 eV, however, XPS images display similar Bi 4f peaks at roughly 160 eV and 165 eV and according to the literature, the position of these peaks confirms the presence of bismuth oxide (Bi_2O_3). The oxygen bonded to Bi likely reflects the reactivity of finely divided Bi to oxygen and the strong Lewis-acid character of the element (Figure 5.6). Further, it is worth noting that XPS is surface sensitive (to a depth of 2-

3 nm typical) and therefore it is more sensitive to the surface of the electrodeposit, which is also more likely to be oxidised.

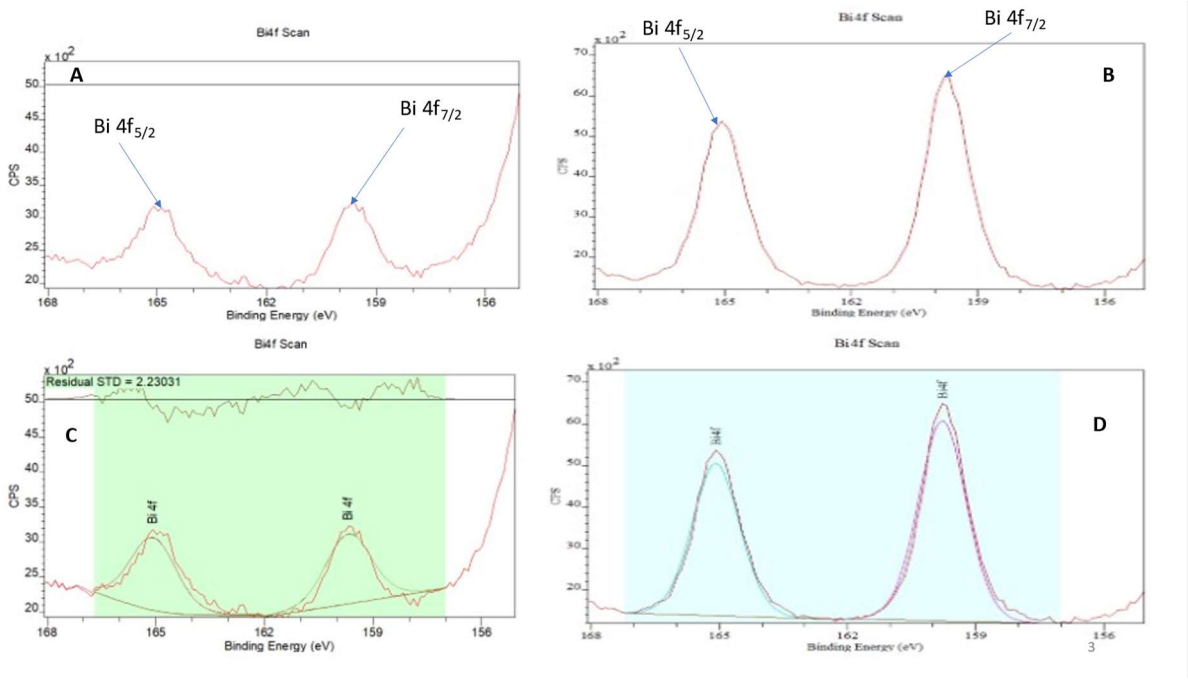

Figure 5.7: XPS characterisation results, two Bi modified electrodes measured using a K-Alpha Spectrometer, A and B are spectra of both modified electrodes in which the peaks identifying the presence of Bi on the surface, C and D represent the same peaks quantified to estimate the atoms counts to be used for normalization.

As the electrodeposition of Bi was performed simultaneously with the analyte, the influence of the latter needed to be investigated. Thus, a normalized graph was generated. The count of Bi over the count of carbon versus the image. The plot did not show a significant difference between the image of the electrode containing both the analyte and Bi. It could be said the presence of the analyte does not influence in the bismuth electrodeposition (Fig 5.8).

Three glassy carbon electrodes Bi modified were scanned and each one in three locations on its surface. in Figure 5.8, each point represents a location scanned on the electrode. That means three points represent an electrode, so in this case three electrodes were used in this study.

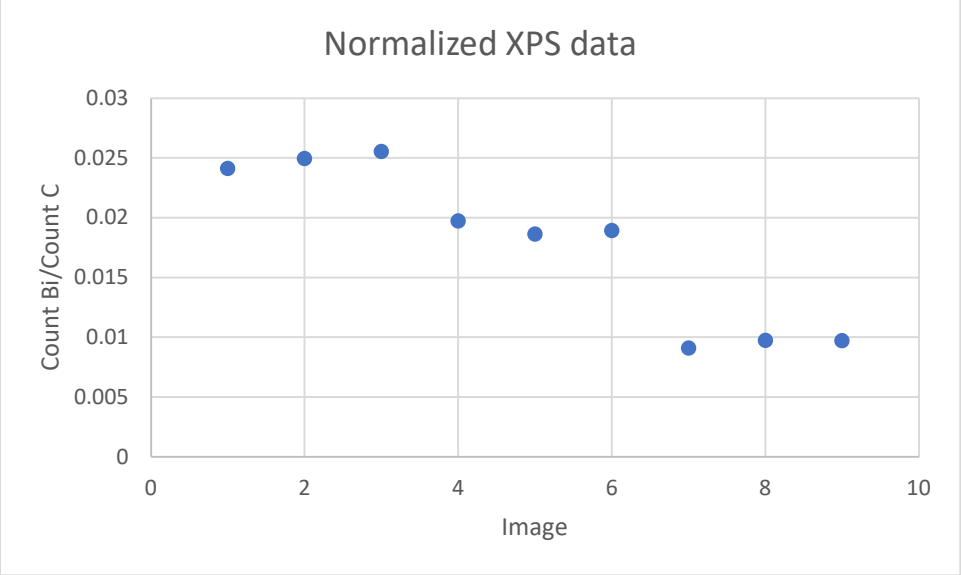

Figure 5.8: Normalized XPS data, the intensity (counts) of the Bi 4f signal over the intensity (counts) of the C 1s signal.

5.2. Stripping Analysis

5.2.1. Cyclic voltammetry of Zn (II) in 0.1 M acetate buffer pH 4.5

Before starting the stripping process for the purpose of detection and quantification, it was necessary to perform cyclic voltammetry to verify the oxidation and reduction process as well as identify at which potential these processes occur. The oxidation and reduction occur at roughly -1.2 V and -1.5 V respectively, while using MSE (1 M H_2SO_4) as reference electrode as illustrated in Figure 5.9. This information is important to enlighten about the deposition potential for Zn. The CV was executed using a solution of 10 mM Zn(II), the potential was swept from -0.5 V to -1.8 V vs. MSE (1 M H_2SO_4).

There is a nucleation loop at around U= -1.3 V vs. MSE (1 M H_2SO_4), this is good evidence of deposition of a new phase in which the deposited material adheres better to itself than to the underlying substrate (glassy carbon electrode).

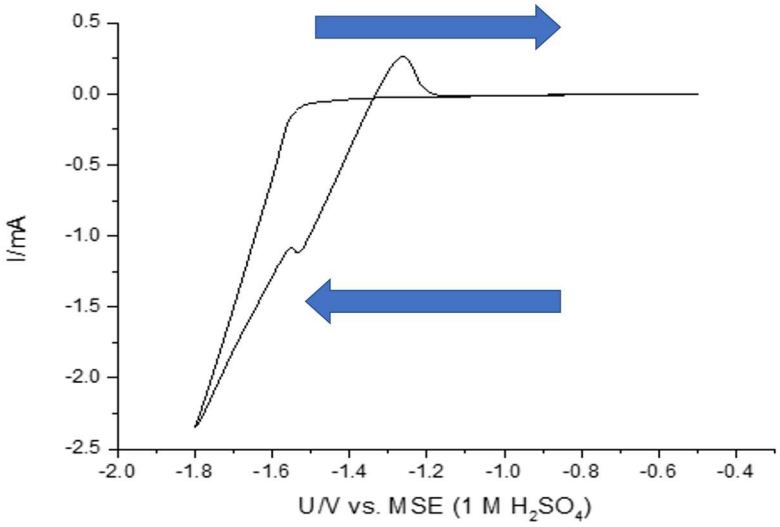

Figure 5.9: Cyclic Voltammetry 10 mM Zn (II) in 0.1 M acetate buffer pH 4.5 25 mV s^{-1} as scan rate, from -1.8 V to -0.4 V vs. MSE (1 M H_2SO_4), working electrode: glassy carbon electrode.

5.2.2. Detection of Zn

5.2.2.1. Stripping voltammetry of Zn (II) with Bi in acetate buffer

Initial attempts to study the stripping process were performed using an MSE (1 M H_2SO_4) as reference electrode. 1 mM Zn (II) solution was prepared in 0.1 M acetate buffer pH 4.5 [from the salt Zinc nitrate hexahydrate $Zn(NO_3)_2.6H_2O$; such a high concentration is suitable for initial attempt using as working electrodes glassy carbon bismuth ex situ deposited GC3 (ex situ constant applied potential electrodeposition) and GC5 (ex situ cycling potential electrodeposition).

These attempts are performed in order to confirm at which potential Zn is stripped. The electroanalytical technique DPV was chosen for the stripping as it is one of the most sensitive techniques which can reach limits of detection down to 10^{-10} M. After some literature findings [98], the following set up details have been chosen: E_d (deposition potential)= -1.6 V vs. MSE (-0.926 V vs. SHE), deposition time= 60 s; quiet time= 20 s, for the stripping step-differential pulse voltammetry: E_i= -1.6 V to Ev= -0.5 V, P_H (pulse height)= 50 mV, P_W (pulse width)= 50 ms, S_H (step height)= 2 mV, S_T (step time)= 200 ms, pulse duration= 300 s. At the end of the procedure, using all the parameters mentioned earlier, a sharp peak was obtained at -0.703 V vs. SHE (-1.4 V vs. MSE (1 M H_2SO_4)) while using substrates GC3 and GC5. Remembering that at this time, Bi solution used was prepared in 0.1 M acetate buffer pH 4.5, the Bi film was

electrodeposited in ex situ mode mentioned previously. Figure 5.10 illustrates the Zn stripping peak when using GC3 as substrate.

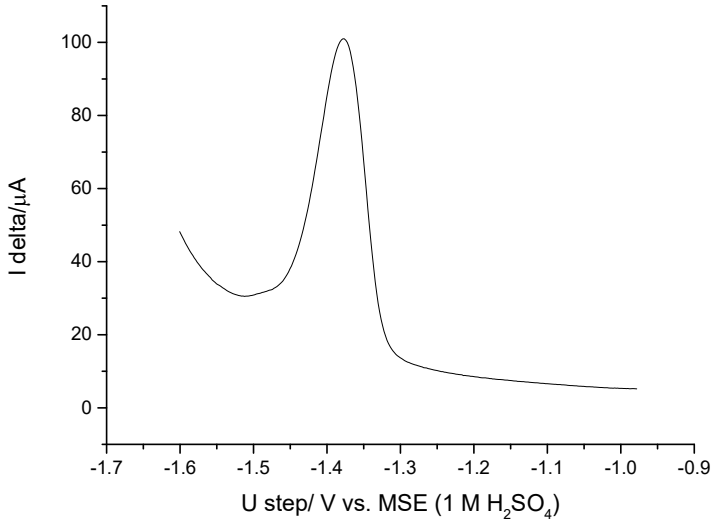

Figure 5.10: Anodic Stripping DPV 1 mM Zn(II), deposition potential: -1.6 V vs. MSE (1 M H_2SO_4), deposition time: 300 s, P_H (pulse height): 50 mV, P_W (pulse width): 50 ms, S_H (step height): 2 mV, S_T (step time): 200 ms.

The detection assignment started with the anodic stripping voltammetry specifically with the electroanalytical pulse technique DPV. Preliminary attempts were done using different concentrations Zn (II) and Pb (II) in 0.1 M acetate buffer pH 4.5. Since both metals Zn and Pb present different chemical properties for example the low solubility of $PbSO_4$, which can be formed due to interaction of Pb (II) ions and H_2SO_4; thus, it is essential to test both MSE (1 M H_2SO_4) and Calomel (1 M KCl) as reference electrodes. The trial was done separately for both Zn (II) and Pb (II). In order to evaluate the behaviour of each analyte before engaging into a simultaneous determination.

Moreover, after a thorough observation, it was noticed that there was a side reaction, the reduction Zn (II) occurred and metallic Zn deposited on the gold wire, which was used as counter electrode. Bubbles of hydrogen could be observed, which are produced during the reduction of Zn (II), as well as a change in the colour of the gold wire from yellow to brown. Therefore, the MSE (1 M H_2SO_4) cannot be used for the purpose because of the high proton concentration and the reference electrode needed to be replaced by MSE (K_2SO_4, sat'd).

5.2.2.1.1. Effect of the addition of an electrolyte on the stripping peak and reproducibility test

The performance of the stripping voltammetry is also influenced by the supporting electrolyte used. Therefore, a study of the effect of the electrolyte was performed. The base electrolyte chosen is 0.1 M acetate buffer pH 4.5 as it is the one suggested by the literature [102]. However, adding to it another electrolyte increases the ionic effect, consequently the performance of the technique will be enhanced. In this work, the influence of two electrolytes were studied: Na_2SO_4 and $NaClO_4$. Because the test with MSE (1 M H_2SO_4) as reference electrode failed, eventual electrochemical works are executed using MSE (K_2SO_4, sat'd) and calomel (1 M KCl) reference electrodes including the effect of addition of the electrolyte on the stripping peak.

a) Mixture of 0.1 M acetate Buffer pH 4.5 + 1 M Na_2SO_4

As part of the study of the influence the electrolyte in the metal detection Zn in this case, one of the electrolytes used for the purpose is Na_2SO_4 with a concentration of 1 M alongside with 0.1 M acetate buffer pH 4.5. A clear comparison was done while using Na_2SO_4 and the mixture prepared, the ionic strength including the protonation effect estimated for this mixture is nearly 3.05. The ex-situ Bi electrodeposition was chosen for this experiment. The preparation of the Bi film was as previously stated in 5.1.1. As mentioned earlier, the electroanalytical technique used was DPV (differential pulse voltammetry), the following set up details were used: E_d (deposition potential) = - 1.6 V vs. MSE, K_2SO4 sat. (-0.96 V vs. SHE), t_d (deposition time) = 300 s, stirring rate= 100 rpm. Quiet time= 30 s, E_i= -1.7 V to E_v= -0.3 V vs. MSE (K_2SO_4, sat'd). Pulse height= 50 mV, Pulse width= 50 ms, Step height= 2 ms, Step time= 200 ms. The equilibrium potential estimated for Zn under 1 mM conditions: U_{eq} Zn^{2+}/Zn = -0.85 V vs. SHE (-1.13 V vs. Calomel (1 M KCl) and -1.49 V vs. MSE (sat'd K_2SO_4).

In this case, the reference electrode used was MSE (K_2SO_4, sat'd). The proportion of the electrolyte mixture 1 M Na_2SO_4 + 0.1 M acetate buffer (pH 4.5) was 1:1. As it can be seen in the Figures 5.11 and 5.12, stripping voltammograms were performed using both Na_2SO_4 and the mixture Na_2SO_4 + acetate Buffer. Bi films were prepared under ex situ conditions in each case, CV and CA electrodeposition under stirred and unstirred conditions. In general, comparing both cases when 1 M Na_2SO_4 and the mixture 1 M Na_2SO_4 + 0.1 M acetate Buffer pH 4.5, sharp and well-defined peaks are obtained when used the mixture. However, GC3 CV

unstirred used as substrate showed a large peak although not very well defined which, after integration, produced a high value of estimated charge in the case of using 1 M Na_2SO_4.

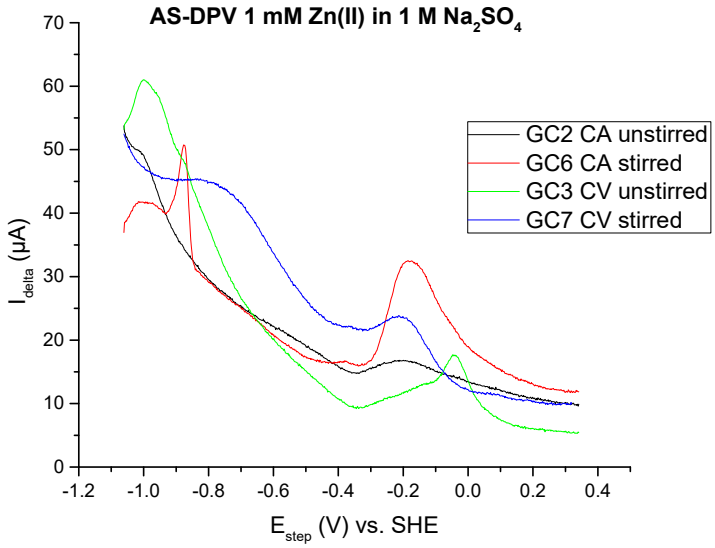

Figure 5.11: Stripping voltammogram 1 mM Zn (II) in 1 M Na_2SO_4 as supporting electrolyte. E_d (deposition potential) = -1.6 V vs. MSE, K_2SO_4 sat'd (-0.96V vs. SHE), t_d (deposition time): 300 s, stirring rate: 100 rpm, Quiet time: 30 s. P_H (pulse height): 50 mV, Pulse width: 50 ms, S_H (step height): 2 mV, S_T (step time): 200 ms., working electrode: glass carbon, counter electrode: Au wire, reference electrode: MSE (K_2SO_4, sat'd).

GC3 and GC8 substrates, both ex situ CV electrodeposited under stirred and unstirred conditions, have shown higher peaks (Figure 5.12) in the case of the mixture 1 M Na_2SO_4 + 0.1 M acetate Buffer pH 4.5.

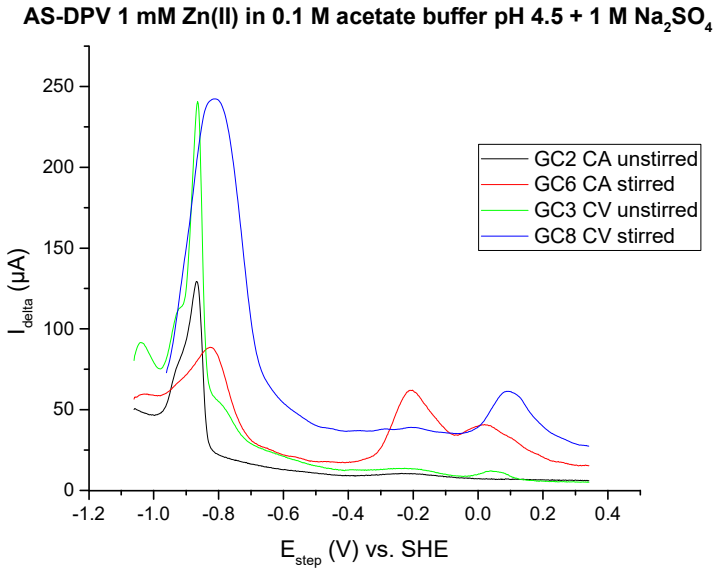

Figure 5.12: Stripping Voltammogram 1 mM Zn (II) in the mixture 1 M Na_2SO_4 + 0.1 M acetate Buffer pH 4.5. E_d (deposition potential): -1.6 V vs. MSE, K_2SO_4 sat'd (-0.96 V vs. SHE), t_d (deposition time): 300 s, stirring rate: 100 rpm. Quiet time: 30 s. P_H (pulse height: 50 mV, P_W (pulse width): 50 ms, S_H (step height): 2 ms, S_T (step time): 200 ms., working electrode: glassy carbon, counter electrode: Au wire, reference electrode: MSE (K_2SO_4, sat'd).

As it can be seen clearly, in all the previous figures (5.11 and 5.13) a peak appears near 0.2 V vs.SHE; this is actually a Bi stripping peak. In some experiments where Bi was not added to the system, this peak was not observed.

Bi^{3+} in aqueous solution can be found as a monomeric $Bi^{3+}(aq)$, which was characterized as $[Bi(H_2O)_9]^{3+}$ in a triflate salt $(Bi(O_3SCF_3)_3.9H_2O$, it displayed nine primary shell water molecules coordinated in a tricapped trigonal prismatic arrangement. Besides, the monomeric $Bi^{3+}(aq)$ specie estimated pKa value corresponds 1.09. On the other hand, two Bi_9 species, formally $[Bi_9(OH)_2O]^{7+}(aq)$ and $Bi_9(OH)_{22}^{5+}(aq)$, also emerge significantly in pH range above 3.0 from potentiometric data in the region of n between 2.0 and 2.5 [154].

The aquo specie for Zn^{2+} reported as $[Zn(H_2O)_6]^{2+}$ with a pKa ≈ 9 prevails in the majority of Zn salts with non-coordinating anions, despite the prospect of a hydration number of four (tetrahedral) is expected from solutions of $Zn(ClO_4)_2$ in aqueous $HClO_4$ because of the increase of the acid concentration. The rise of the temperature on aqueous $Zn(NO_3)_2$ solutions leads to a conversion to tetrahedral species $[Zn(H_2O)_4]^{2+}$. In addition to that, the presence of coordinating anions such as SO_4^{2-} and Cl- also results into a switch in the coordination (hydration) number due to the increase of the anion concentration [154].

b) Mixture of 0.1 M acetate Buffer pH 4.5 + 1 M $NaClO_4$

Another electrolyte used for the study of the effect of the addition of the electrolyte is $NaClO_4$, for this case Calomel (1 M KCl) is used as reference electrode. The choice of perchlorate ClO_4^- was motivated by the fact that it is a weakly-coordinating anion. The concentration used is the same as previously as well as the counter electrode which was the Au wire. This means 1 mM Zn(II) is prepared in two electrolytes 0.1 M acetate buffer pH 4.5 and the mixture 0.1 M acetate buffer + 1 M $NaClO_4$. As it is mentioned in the previous mixture, a similar proportion was also used for 0.1 M acetate buffer + 1 M $NaClO_4$, which means 1:1.

The ex-situ Bismuth film was produced by applying cycling potential under stirred and unstirred conditions as in the case of Na_2SO_4 as electrolyte. The set up details were the followings while using 0.1 M Acetate buffer as electrolyte: deposition potential: -1.4 V vs. Calomel (1 M KCl) , deposition time: 300 s, quiet time: 20 s; DPV parameters: E_i= -1.4 V vs.to E_v= -0.5 V vs. Calomel (1 M KCl), P_H (pulse height): 50 mV, P_W (pulse width): 50 ms, Step height (S_H): 2 ms and Step time (S_T): 200 ms.

The procedure is similar to that for the previous mixture and two experiments were done in two phases. First, the metal ion Zn(II) was analysed in acetate buffer only and then in the mixture 0.1 M acetate buffer pH 4.5 + 1 M $NaClO_4$.

In the case of acetate buffer as supporting electrolyte, the peak was sharp and appeared at roughly -1.15 V vs. Calomel (1 M KCl). On the other hand, Using the mixture 0.1 M acetate buffer + 1 M $NaClO_4$ produced a peak at -1.34 V vs. Calomel (1 M KCl); the reason for such shift may be attributed to the increase of the ionic strength by adding $NaClO_4$.

A test on successive stripping was done to investigate any change on the behaviour. Surprisingly, at the same conditions the second stripping analysis was performed using the same Bi-modified electrode, it was observed another small shift, the peak appeared at -1.42 V and a reduction in the peak current from 79.0 µA to 52.3 µA as it can be seen in Fig 5.13.

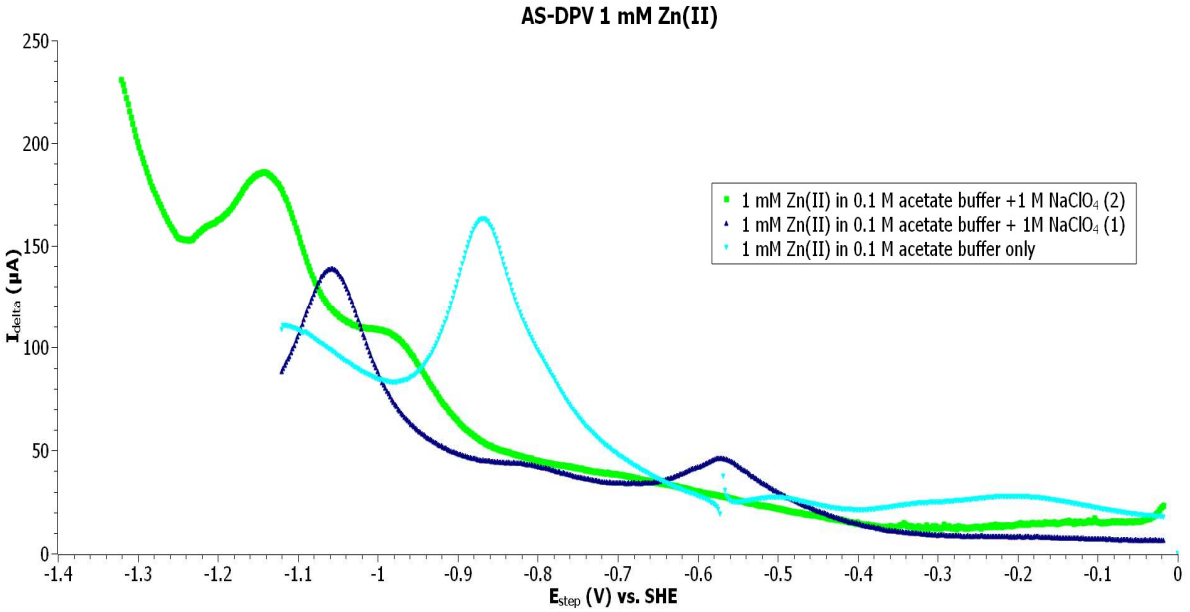

Figure 5.13: AS-DPV 1 mM Zn(II) with GC Bi-modified in 0.1 M acetate buffer and the mixture 1 M $NaClO_4$ + 0.1 M acetate Buffer, E_d (deposition potential): -1.4 V vs. Calomel (1 M KCl) , t_d (deposition time): 300 s, quiet time: 20s; DPV parameters: E_i= -1.4 V vs. Calomel (1 M KCl) to E_v= -0.5 V vs. Calomel (1M KCl), P_H (pulse height): 50 mV, P_W (pulse width): 50 ms, Step height (S_H): 2 ms and Step time (S_T): 200 ms.

The equilibrium potential estimated for 1 mM Zn, $U^0_{Zn^{2+}/Zn} = -0.851\ \text{V}\ vs.\ SHE$ (-1.13 V vs. Calomel (1 M KCl)). As mentioned earlier, the Bi film was produced via an ex-situ method. Using the CV (Cycling potential) electrodeposition and also in different glassy carbon electrodes GC3 and GC7. GC3 (CV unstirred) and GC7 (CV stirred), the stirring is expected to increase the particle migration; therefore, the stripping performance was better than in unstirred conditions, which means higher peaks are observed when GC7 is used. Since the peak height is proportional to the concentration; hence, both the concentration of Bi and the analyte Zn on the surface seemed to be at a considerable amount as observed in Figure 5.14.

Note that the glassy carbon electrodes used in this research were modified under ex situ electrodeposition using cycling voltammetry.

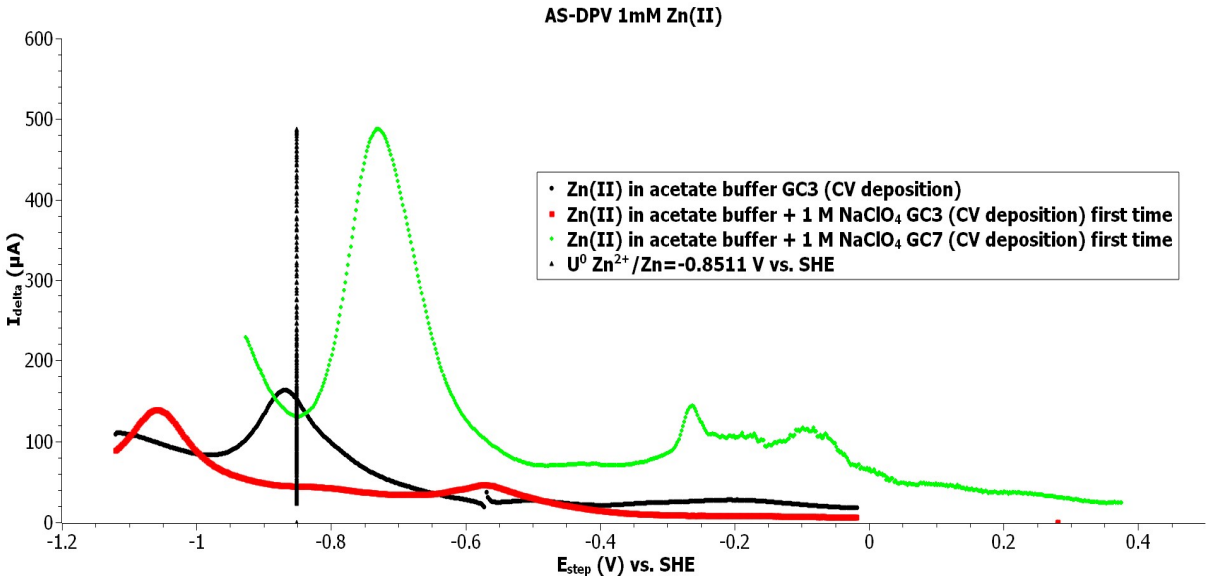

Figure 5.14: Stripping 1 mM Zn(II) in the mixture 0.1 M acetate buffer pH 4.5 + 0.1 M $NaClO_4$ in different stirring conditions, deposition potential: -1.4 V vs. Calomel (1 M KCl) , deposition time: 300 s, quiet time: 20 s, stirring rate: 100 rpm; DPV parameters: E_i= -1.4 V to E_v= -0.5 V vs. Calomel (1M KCl), P_H (pulse height): 50 mV, P_W (pulse width): 50 ms, Step height (S_H): 2 ms and Step time (S_T): 200 ms.

As referred earlier GC3 Bismuth films was produced under unstirred conditions, repeated stripping keeping the same conditions and set up, has produced a surprising behaviour. It can be noticed that while the stripping is being repeated the peak potential shifted and decreased in height, as a consequence, it is a signal of a decrease in sensitivity, since the apparent concentration of the metal detected would be reduced.

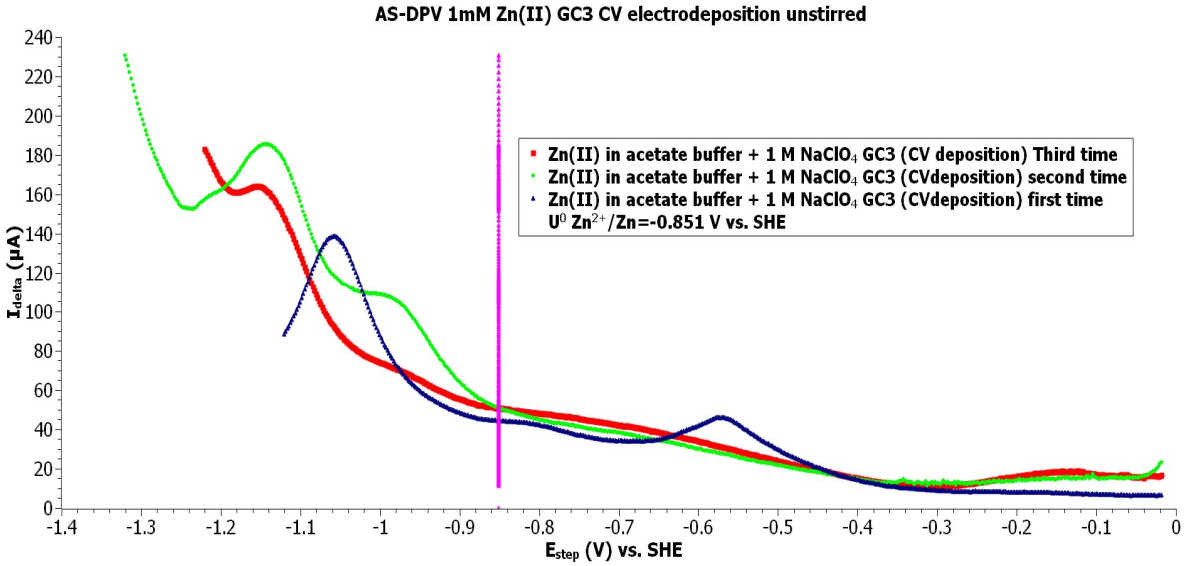

Figure 5.15: Behaviour of repeated stripping Zn(II) in the mixture 0.1 M acetate buffer pH 4.5 + 1 M $NaClO_4$ with GC3, deposition potential= -1.4 V vs. Calomel (1 M KCl) , deposition time: 300 s, quiet time: 20 s; DPV parameters: E_i= -1.4 V to E_v= -0.5 V vs. Calomel (1 M KCl), P_H (pulse height): 50 mV, P_W (pulse width): 50 ms, Step height (S_H): 2 ms and Step time (S_T): 200 ms.

Similar behaviour has been reported as well with GC7 (Fig 5.16 and Table 5.2), although the values for peak height are higher than for GC3. GC7 which was produced through ex situ electrodeposition applying cycling potential under stirred conditions, reported similar behaviour to GC3. Peaks shifts were small and not significant compared to GC3 behaviour. However, the decrease in peaks heights is still observed, that indicates the loss of analytical sensitivity.

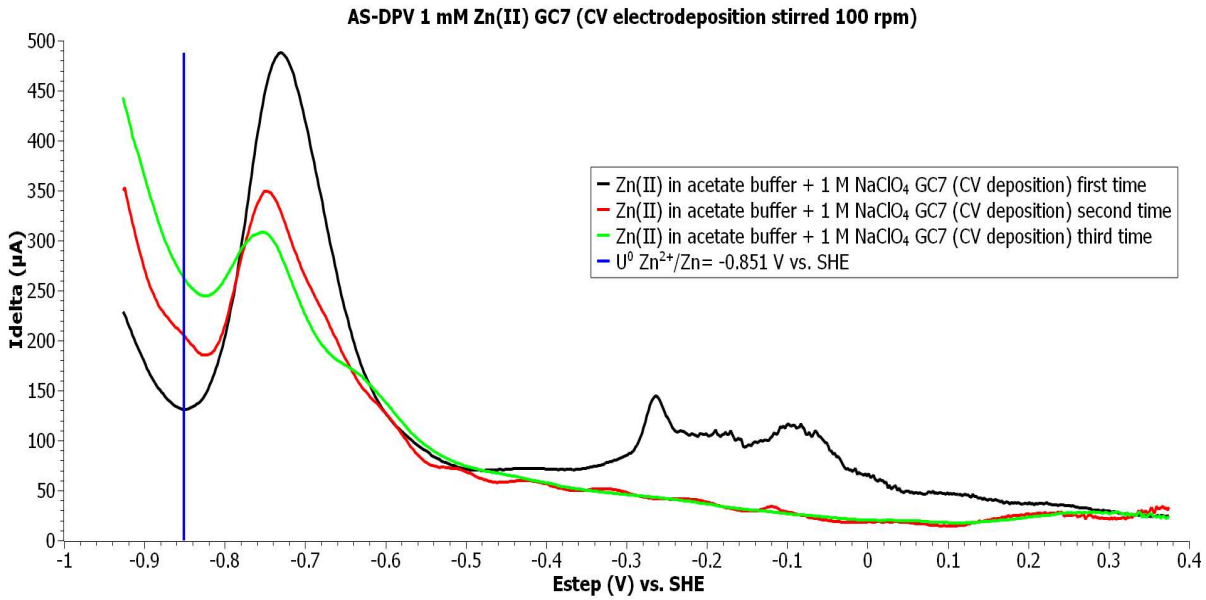

Figure 5.16: Behaviour of repeated stripping Zn(II) in the mixture 0.1 M acetate buffer pH 4.5 + 1 M $NaClO_4$ with GC7, deposition potential: -1.4 V vs. Calomel (1 M KCl) , deposition time: 300 s, quiet time: 20 s; DPV parameters: E_i= -1.4 V to E_v= -0.5 V vs. Calomel (1M KCl), P_H (pulse height): 50 mV, P_W (pulse width): 50 ms, S_H (step height): 2 ms and S_T (step time): 200 ms

Summarily, the increase of the ionic strength by adding $NaClO_4$ caused shifts in the peak potential in stirred and unstirred situations as well as changes in the peak height. The peak in case of the use of a GC CV deposited showed a higher peak current which may be due to the stirring that increased the mass transport of Bi(III) and Zn(II) ions and, lead to a film thicker than in unstirred cases.

The peak current decreased when the Bi-modified GCE was used repeatedly, from the first to the third time. Further, the stripping voltammogram changed; another peak which appears after the Zn (II) peak, vanished when the electrode was used for the second time. It may be due to Bi oxidation on the surface, forming of Bi_2O_3 which is not as active as Bi in metallic state, which may constitute certain instability in the deposit and being lost throughout experiments. Another explanation, it may be due to the complete loss of Bi on the surface since the stripping potential reached also de the reoxidation region of Bi.

Table 5.2: Comparison of Zn stripping peak heights according to the supporting electrolyte and stirring conditions.

	AS-DPV 1mM Zn(II) GC3 CV deposition unstirred.	**AS-DPV 1mM Zn(II) GC7 CV deposition stirred (100 rpm).**			**AS-DPV 1mM Zn(II) GC3 CV deposition unstirred.**		
Supporting electrolyte	**0.1 M Acetate buffer**	**0.1 M Acetate buffer + 1 M $NaClO_4$**			**0.1 M Acetate buffer + 1 M $NaClO_4$**		
		1^{st}	2^{nd}	3^{rd}	1^{st}	2^{nd}	3^{rd}
Potential peak (V)	-1.15	-1.40	-1.42	-1.42	-1.34	-1.42	-1.42
Peak height (μA)	96.96	379.6	196.2	93.2	78.99	52.3	24.7

c) Comparison between the use of $NaClO_4$ and Na_2SO_4

Overall, two electrolytes were used for the purpose of a study of the electrolyte effect on the stripping peak and performance. Both have shown different performances.

First, it could be observed that a shift in the peak position although not significant, in all the conditions of the ex-situ Bi film formation. However, the stripping peak is higher when GC electrode Bi modified CV electrodeposited is used, especially under stirred conditions, this indicates a large amount of Zn has been deposited on the surface.

Table 5.3: Comparison of Zn stripping peak heights according to stirring conditions

	AS-DPV 1mM Zn (II) GC3 CV deposition unstirred.	**AS-DPV 1mM Zn (II) CV deposition stirred (100 rpm).**		**AS-DPV 1mM Zn (II) CV deposition unstirred.**	
Supporting electrolyte	**0.1 M Acetate buffer**	**0.1 M Acetate buffer + 1 M $NaClO_4$**	**0.1 M Acetate buffer + 1 M Na_2SO_4**	**0.1 M Acetate buffer + 1 M $NaClO_4$**	**0.1 M Acetate buffer + 1 M Na_2SO_4**
Potential peak (V)	-1.15	-1.40	-1.45	-1.34	-1.51
Peak height (μA)	96.96	379.6	191.4	78.99	176.8

Comparing both mixtures used to improve the performance of the stripping analysis for Zn detection, as demonstrated in Table 5.3 above, the mixture acetate buffer + $NaClO_4$ displayed a higher peak height while the Bi modified electrode is produced by using a CV electrodeposition under stirred conditions while the mixture acetate buffer + Na_2SO_4 yields comparable results in both stirred and unstirred condition, providing higher peaks than in the case of using acetate buffer only as supporting electrolyte. Though, the mixture 0.1 M acetate buffer pH 4.5 + 1 M $NaClO_4$ presents a Zn stripping peak current that is greater when the electrode used is CV electrodeposited under stirring conditions as confirms Table 5.3. Thus, Since the use of these electrolytes is to improve the performance of Zn detection using GCE Bi modified (applying constant or cycling potential), Na_2SO_4 fulfilled better this purpose than $NaClO_4$ in both cases stirred and unstirred conditions, since its mixture showed this enhancement.

5.2.2.1.2. Test of repeatability (Electrode Cleaning)

The cleanliness of the surface is fundamental for a successful production of a Bi modified electrode as well as its analytical performance.

In order to ensure that a residual heavy metal previously deposited does not interfere in future results, an electrochemical cleaning protocol is introduced after each stripping process.

Remembering that a mechanical cleaning is mandatory before each experiment, it is worth to combine both types of cleaning.

Bismuth solutions used for the electrode plating remained as 5 mM Bi (III) and electrodeposition was carried out chronoamperometrically. The electrode cleaning protocol consisted of the application of a positive potential for 10 minutes. Four different cleaning potentials were tested: 250 mV, 500 mV, 750 mV and 1.0 V vs. MSE (K_2SO_4, sat'd); the values of Zn peak charge for all the potentials applied are reported in Table 5.4 and Figure 5.18. The test was realized at room temperature and different cleaning potentials were applied immediately after the stripping step.

Procedure: Electrodeposition 5 mM Bi(III) on GC (chronoamperometry), U= -0.126 V vs. SHE (-0.766 V vs. MSE(K_2SO_4, sat'd)) during 5 min. Deposition 1 mM Zn at U= -0.96 V vs. SHE (-1.6 V vs. MSE(K_2SO_4, sat'd), Stripping Zn, DPV conditions have been kept unchanged since the beginning. Cleaning of the electrode at variable potential during 10 min (U= 250 mV, 500 mV, 750 mV and 250 mV rep. vs. MSE (K_2SO_4, sat'd)). Rinse the surface of the electrode. Cleaning at 500 mV vs. MSE (K_2SO_4, sat'd) showed a good reproducibility compared to others as demonstrated in Figure 5.19.

Table 5.4: The reproducibility of the electrochemical cleaning results.

Cleaning potential	**Run**	**Charge (mC) electrodeposition (chronoamperometry graph)**		**Charge (µC) Zn peak (stripping graph)**	
			Standard Deviation		Standard Deviation
250 mV	First run	94.03	4.92	31.94	64.19
	Second run	102.06		91.11	
	Third run	93.13		69.51	
500 mV	First run	95.65	1.29	29.17	2.61
	Second run	98.18		24.99	
	Third run	97.35		29.80	
750 mV	First run	78.93	13.06	35.10	7.80
	Second run	95.07		24.07	
	Third run	69.22		12.82	
250 mV (2)	First run	85.88	10.35	35.10	13.50
	Second run	67.15		16.003	
	Third run	68.87		18.001	

The electrodeposition chronoamperometric signal is also integrated to obtain the charge that was passed in the stripping step as it may be seen in Table 5.4 and Figure 5.17. Once again, the charge electrodeposited is reproducible when 500 mV is used as cleaning potential without repeating the mechanical cleaning. A closer look to their standard deviations, when at 500 mV, 1.29 is reported. In other words, applying lower potential, the electrode cannot be cleaned, too high potential causes unwanted changes to the underlying carbon. Thus, this potential was selected for electrochemical cleaning.

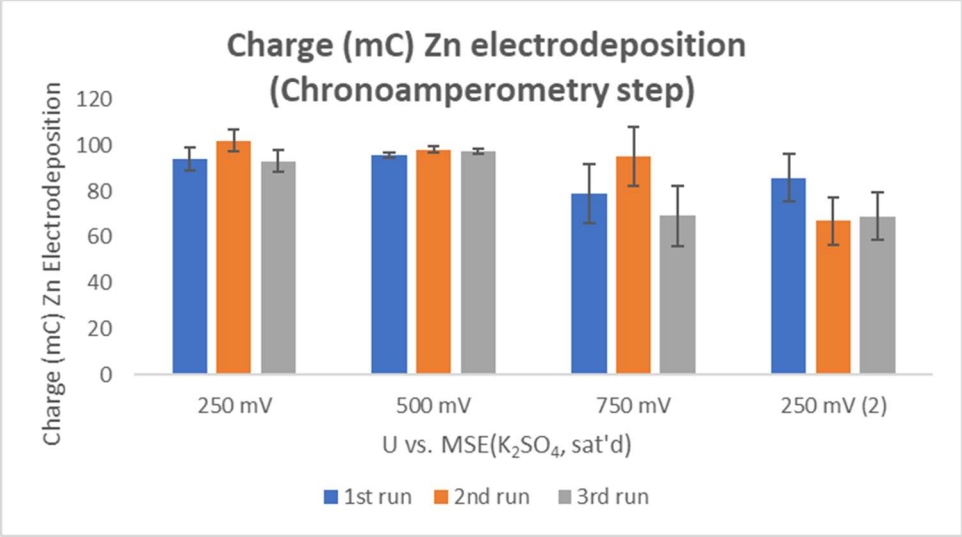

Figure 5.17: Electrodeposition charge from chronoamperometry (deposition step). Deposition potential: -1.6 V vs. MSE (K_2SO_4, sat'd), deposition time: 300 s. The error bars represent the standard deviation of the charges registered.

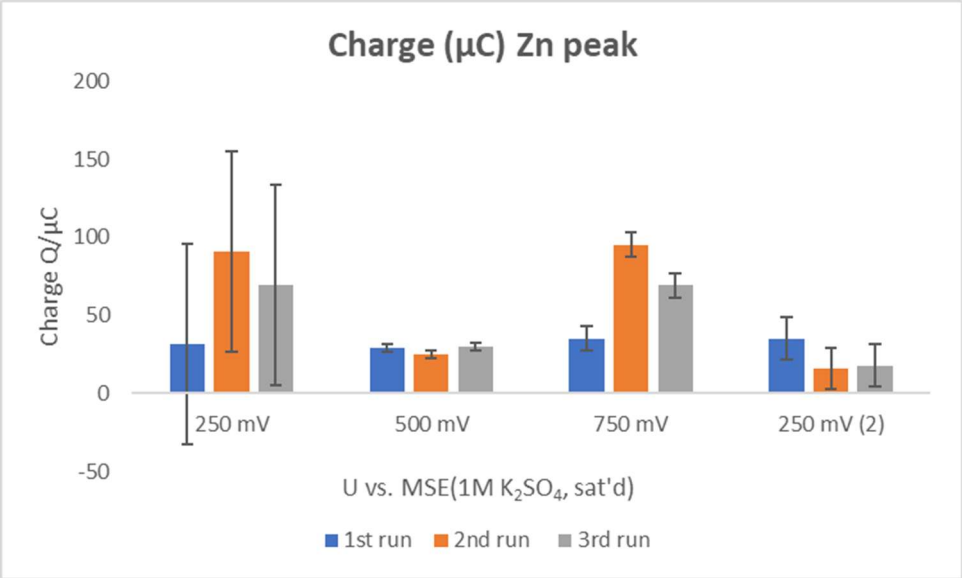

Figure 5.18: Zn peak charge from the stripping voltammogram, DPV details: E_i= -1.6 V to E_v= -0.3 V, Pulse height= 50 mV, Pulse width=50 ms, Step height= 2 ms, Step time= 200 ms., working electrode: glassy carbon, counter electrode: Au wire, reference electrode: MSE (K_2SO_4 sat'd). The error bars represent the standard deviation of the charges registered.

As it may be observed from Table 5.4, the potential U= 500 mV vs. MSE (K_2SO_4, sat'd) showed an acceptable reproducibility, however, the other potentials, though occasionally producing higher detection signals, displayed irreproducible behaviour. Therefore, this potential is then chosen as cleaning potential. Figure 5.19, presents a set of three stripping results at which this potential was applied for the cleaning step. Thus, this potential will be used for eventual

stripping experiments, however, it is subject to be changed according to the behaviour of the electrode in future experiments as it may no longer be effective to provide a cleaner surface and reproducible results afterward.

The electrodeposition step and Zn peak charges from 1 mM Zn(II) solution were determined as illustrated in Figures 5.17 and 5.18 taking into account the cleaning potentials selected throughout this work. Unexpectedly, the charge registered for the electrodeposition figures in the range of mC (milli coulomb) while Zn stripping peaks in µC (micro-Coulomb) range. It may be because the electrodeposition process includes current due to protons reduction (reminding that the deposition current employed was -1.6 V vs. MSE (K_2SO_4, sat'd) as in the caption of Figure 5.17 for example, which is near the HER region), note that nitrogen was purged throughout the experiment which could minimise the effect of oxygen. Another possibility, during the electrodeposition step, the redox species in the solution used may go through reduction/oxidation process along with the deposition on the surface, so this may have resulted in the observation of a higher electrodeposition charge.

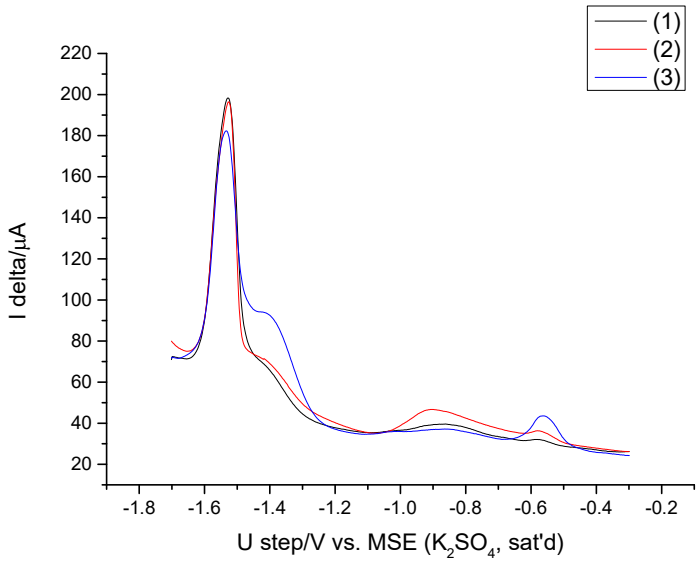

Figure 5.19: Reproducibility of Zn peak while using a cleaning potential of 500 mV vs. (K_2SO_4, sat'd) as in Fig. 5.18, DPV details: E_d (deposition potential) = -1.6 V vs. MSE, K_2SO_4 sat'd (-0.96 V vs. SHE), t_d (deposition time)= 300 s, stirring rate= 300 rpm, quiet time= 30 s, P_H (pulse height)= 50 mV, P_W (pulse width)= 50 ms, S_H (step height)= 2 ms, S_T (step time)= 200 ms., working electrode: glassy carbon, counter electrode: Au wire, reference electrode: MSE (K_2SO_4 sat'd).

5.2.2.2. Stripping voltammetry of Zn(II) with Bi in 0.1M HNO_3

5.2.2.2.1. Calibration curve

The detection of Zn using Bi modified electrode is not the only purpose for this research, it is aimed to also quantify the metal. This task can be done by using analytical quantifications techniques such as calibration curve, standard addition and internal standards. In this work, calibration is chosen for the purpose due to its simplicity.

The calibration curve is a general method of determining the concentration of a substance in an unknown sample by comparing the unknown to a set of standards, the samples contain unknown concentration of the specie in study.

The calibration curve is a plot of how the instrumental response, the analytical signal, changes with the concentration of the analyte (the substance to be measured). A series of standards is prepared across a range of concentrations near the expected concentration of the analyte in the unknown. The concentration of the standard must lie within the working range of the technique used. Analysing each of these standards using the chosen technique will produce a series of measurements. For most analyses, a plot of the instrument response versus concentration will show a linear relationship. Then, the response of the unknown can be measured, and using the calibration curve through interpolation the concentration of the analyte can be found.

The calibration curve prepared for the quantification of Zn was prepared for the range of 1-6 µM. Each stripping of the analyte was followed by a blank stripping (0.1 M acetate buffer pH 4.5) as another way of clearing residual metal in the cell and the electrode.

The Bi film was produced in situ alongside with deposition of the analyte. The Bi(III) solution employed for the production of the in-situ film, was prepared in 0.1 M HNO_3, unlike studies previously reported where the ex-situ Bi film was prepared in 0.1 M acetate buffer pH 4.5.

A turbidity is observed when Bi is prepared in the pH 4.5 acetate buffer, which means an incomplete dissolution of Bi salt, therefore, the concentration of Bi could be lower than expected. This is more crucial for the in-situ Bi electrodeposition because it may affect the co-deposited metal analytes. For this reason, a second option was taken into account, in this case 0.1 M HNO_3 is selected as the electrolyte to prepare Bi(III) solutions. Since Bi film formation

requires a pH between 4 and 6, the pH in the solution transferred in the cell for ASV measurement after the addition of Bi(III)/HNO_3 (Bi prepared in 0.1 M HNO_3) was verified. The solution in the cell can be either the analyte standard solution prepared in acetate buffer pH 4.5 or the sample buffered. It was found that there is a slight reduction in the pH, the one recorded is 4.40 instead of 4.5. This slight decrease does not significantly affect the production of the Bi film nor the detection of the metal. A clear explanation on the record of a pH 4.4 while using a strong acid as HNO_3, Bi stock and working solutions were prepared in 0.1 M HNO_3, while the metal of interest (Zn or Pb) solutions are prepared in 0.1 M Acetate Buffer pH 4.5. The measurement cited earlier, refers to the addition of 500 µL Bi (1 mM Bi) into the cell containing 50 mL of the analyte (Zn or Pb). Therefore, it was selected for eventual experiments especially for the quantitative purpose for both Zn and Pb, 1 mM Bi (III) stock solution was prepared in 0.1 M HNO_3, from which 500 µL are taken and added into a cell of roughly 100 mL capacity. Thus, 10 µmol/L Bi is the concentration in the cell.

In the cell, 50 mL of the solution containing the analyte (Zn or Pb) was added. Reminding that the metal solutions are prepared in acetate buffer pH 4.5. A concentration range of 1-6 µM was chosen to prepare the calibration curve for quantitation. All the DPV parameters were unchanged as for the previous reported experiments, the stirring rate used was 300 rpm. From each analyte solutions, 50 mL were taken and submitted to the stripping process.

The results showed as stripping peaks (voltammograms) and afterward, the charges obtained through their integration are used to build a calibration graph. The instrument signal used to generate the plot is charge versus concentration (Figure 5.20).

First calibration curve

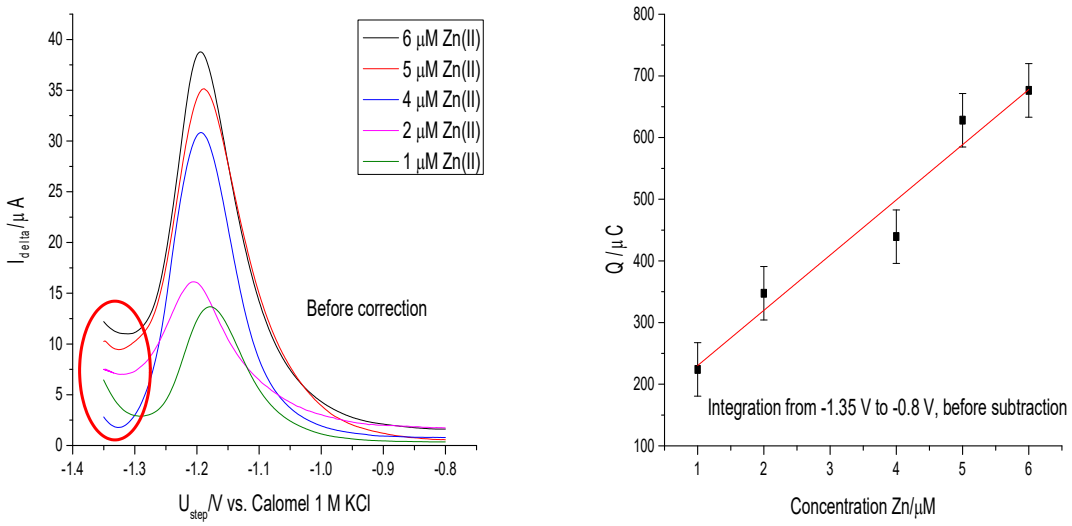

Figure 5.20: First Zn calibration curve (right) and stripping voltammetry peaks (left), deposition potential= -1.4 V vs. Calomel (1M KCl), deposition time: 10 min, quiet time: 20 s; DPV parameters: E_i= -1.4 V to E_v= -0.5 V vs. Calomel (1 M KCl), P_H (pulse height): 50 mV, P_W (pulse width): 50 ms, S_H (step height): 2 ms and S_T (step time): 200 ms. The error bars refer to the standard error of the intercept.

Table 5.5: Regression analysis of the first Zn calibration curve seen in Figure 5.20, integration range -1.35 V to -0.8 V vs. Calomel (1 M KCl).

Equation	y=a+bx integration range -1.35 V to -0.8 V vs. Calomel (1 M KCl)	
Residual sum of squares	5932.88	
Pearson's r	0.979	
Adj. R-Square	0.945	
	Value	Standard Error
Intercept	140.7	43.42
Slope	89.55	10.72

Figure 5.20 presents the result of the stripping peak and the calibration curve generated, while Table 5.5 exhibits the regression analysis of the referred curve. It was observed that the peaks do not start at the same potential, this may be due to the consistent change in the behaviour of the electrode observed after each cleaning step (mechanical and

electrochemical). As a result of that, some treatments are necessary to improve the reliability of the curve obtained. First, it is necessary to subtract the peaks by a common background as seen in Figure 5.21, which means, the signal voltammograms of the concentration range chosen (1-6 µM Zn(II)) have showed different background, a correction to uniformise the background is essential, therefore, one of the background is selected for the correction, in this case, the background of 4 µM Zn(II) was found adequate since it is the lowest as seen in Figure 5.20. This background is subtracted to all the remaining voltammograms.; second, the curve obtained from the first step has a residual current which may be due to the fact of applying a current at the most negative potential reduction of protons as illustrated in Table 5.6. Therefore, a subtraction of the residual charge was also executed to obtain a final version of the calibration curve which can be used for sample determination.

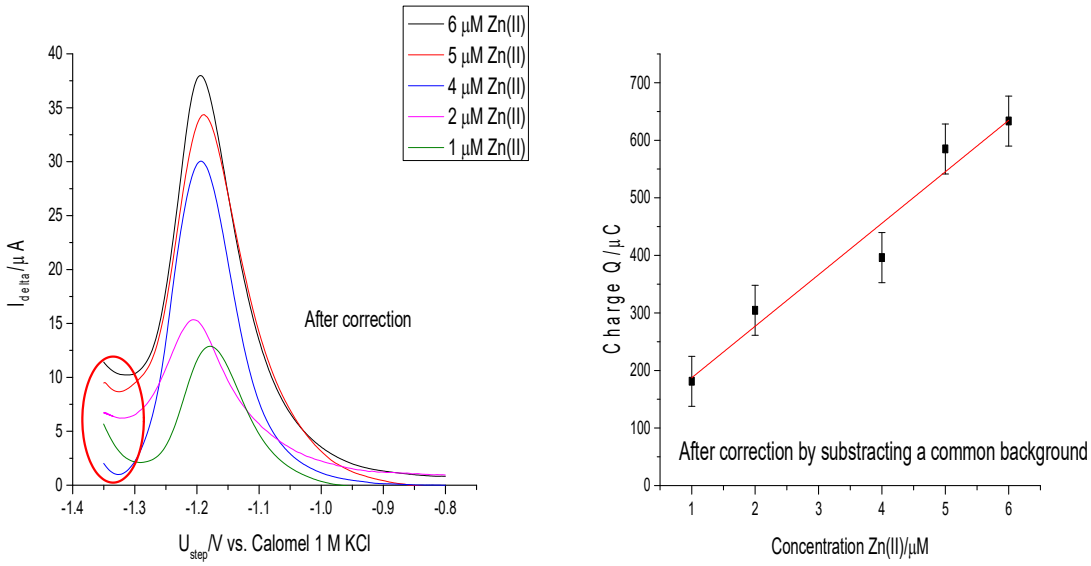

Figure 5.21: Zn stripping peaks and first calibration curve after subtracting to a common background. deposition potential= -1.4 V vs. Calomel (1M KCl), deposition time: 10 min, quiet time: 20 s; DPV parameters: E_i= -1.4 V to E_v= -0.5 V vs. Calomel (1 M KCl), P_H (pulse height): 50 mV, P_W (pulse width): 50.0ms, S_H (step height): 2.0ms and S_T (step time): 200 ms. The error bars represent the standard error of the intercept.

The regression data in Table 5.6 shows a residual current through the intercept value which is significantly different to zero.

Table 5.6: Regression analysis first Zn calibration curve after a common background subtraction as in Figure 5.21, integrated range -1.35 V to -0.8 V vs. Calomel (1 M KCl).

Equation	y=a+bx (integrated range -1.35 V to -0.8 V vs. Calomel (1 M KCl))	
Residual sum of squares	5944.24	
Pearson's r	0.979	
Adj. R-Square	0.945	
	Value	Standard Error
Intercept	97.93	43.46
Slope	89.47	10.73

The curve obtained has showed a good correlation r= 0.979 and its intercept is close to the origin as shown in Table 5.7. According to the requirements for a calibration curve, this correlation is acceptable. After all the treatments, the final curve found will be used for sample calculation as seen in Figure 5.22.

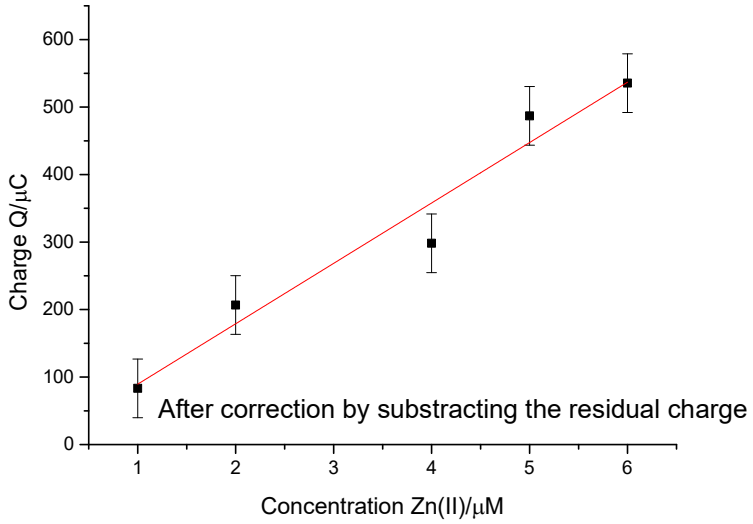

Figure 5.22: Final version of the first Zn calibration curve after all the treatments. The error bars represent the standard error of the intercept.

Table 5.7: Regression data of the first Zn calibration curve final version seen in Figure 5.22.

Equation	y=a+bx (integrated range -1.35 V to -0.8 V vs. Calomel (1 M KCl))	
Residual sum of squares	5944.24	
Pearson's r	0.979	
Adj. R-Square	0.945	
	Value	Standard Error
Intercept	0.0079	43.46
Slope	89.47	10.73

Second and average calibration curve

A single calibration curve may compromise the reliability of the results obtained; thus, it is important to produce multiple curves. A second calibration curve was produced for the same selected range of concentration keeping the same conditions. However, a lower sensitivity was recorded, and a drop in the correlation was observed. As a result of this behaviour, an average curve needed to be created to be used for sample determination.

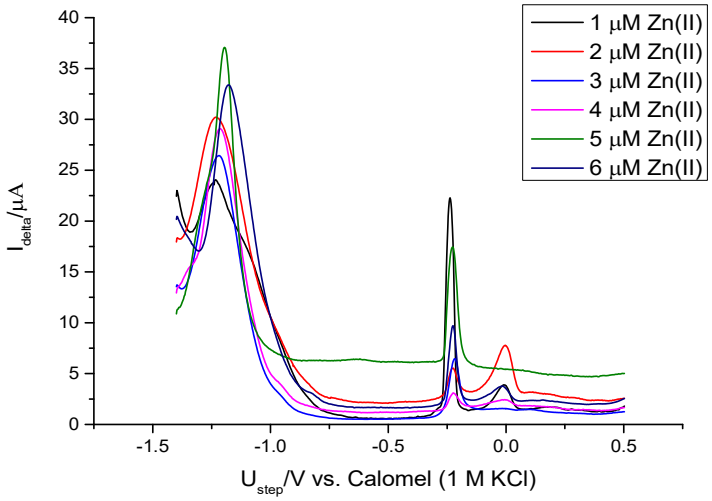

Figure 5.23: The stripping voltammograms for the second Zn calibration curve, deposition potential= -1.4 V vs. Calomel (1M KCl), deposition time: 10 min, quiet time: 20s; DPV parameters: E_i= -1.5 V to E_v= -0.5 V vs. Calomel (1 M KCl), P_H (pulse height): 50 mV, P_W (pulse width): 50.0ms, S_H (step heigh): 2 ms and S_T (step time): 200 ms.

The second curve is produced in similar conditions as the first as well as the data obtained have been treated the same way. Figures 5.24 presents Zn stripping peaks before and after common background correction.

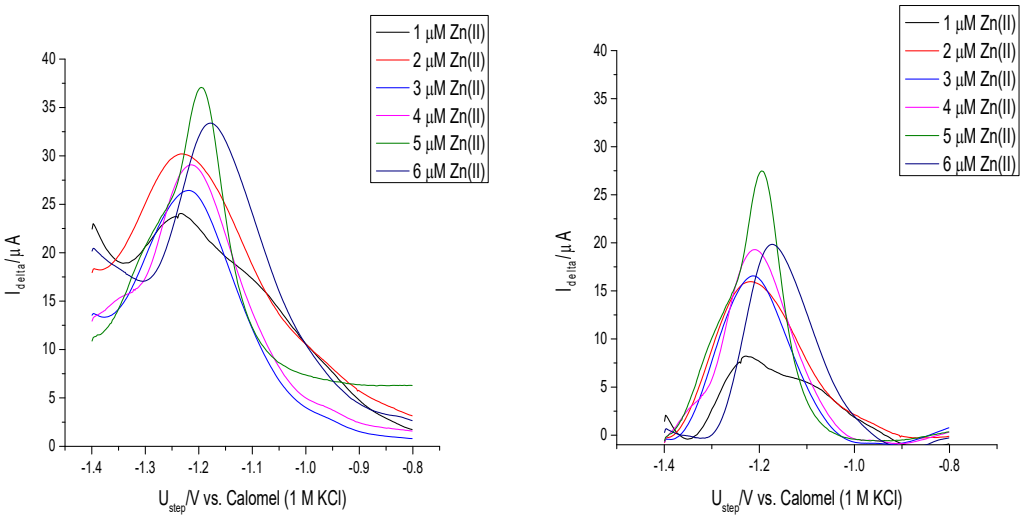

Figure 5.24: Zn stripping peaks for the second calibration curve before and after background correction. Deposition potential= -1.4 V vs. Calomel (1 M KCl), deposition time: 10 min, quiet time: 20 s; DPV parameters: E_i=-1.4 V to E_v=-0.5V vs Calomel (1 M KCl), P_H (pulse height): 50 mV, P_W (pulse width): 50 ms, S_H (step height): 2 ms and S_T (step time): 200 ms.

The voltammogram of 1 µM Zn(II) in Figure 5.23 and 5.24 showed some overlapping peaks, which may be due to the formation of different species on the surface. It also could be observed some shifts in the peaks which may be related to concentration variation. On the other hand, consistent change of the electrode behaviour during repeated use may also have contributed to the emergence of peak shifts.

At the end of the treatments, the curve generated showed a low correlation coefficient (Pearson's r) about 0.886 as observed in Table 5.8. Thus, this curve does not fulfil the requirements to be used individually for sample quantification. A loss of sensitivity has been reported through the curve in Figure 5.25.

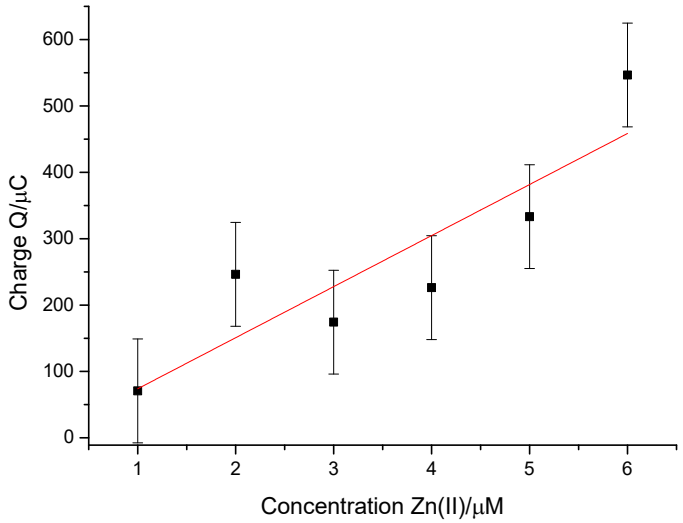

Figure 5.25: Final version of the second Zn calibration curve. The error bars represent the large standard error of the intercept observed.

Table 5.8: Regression data Zn second calibration curve from Figure 5.25.

Equation	y=a+bx (Integration range -1.4 V to -0.8 V vs. Calomel (1 M KCl))	
Residual sum of squares	28225	
Pearson's r	0.886	
Adj. R-Square	0.732	
	Value	Standard Error
Intercept	-3.0	78.20
Slope	76.9	20.1

Average calibration curve

Since the second calibration curve is unsuitable for individual use, generating an average curve could add more value in comparing the results. The average curve was generated from the first and second calibration curve data.

The average curve produced have shown an acceptable sensitivity although it is lower than the first curve. The average curve was offered the same treatment as it was done for the first curve as illustrated in Figure 5.26.

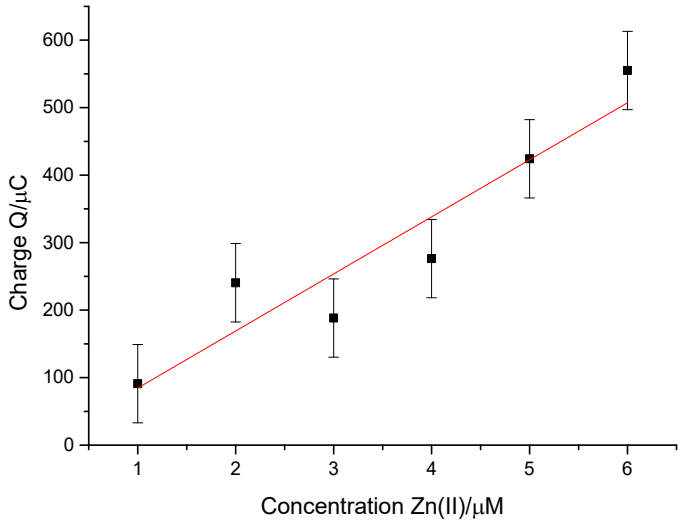

Figure 5.26: Average Zn(II) calibration curve. The error bars represent high standard error of the intercept estimated.

The regression analysis shown in Table 5.9. A correlation coefficient r = 0.943 was obtained and the intercept was near zero. Owing to the origin of this average curve (the curve generated from the first and second calibration curve data, reminding that the second calibration curve exhibited a very large standard error), a large standard error is also observed in the Table 5.9 below.

Table 5.9: Regression data average Zn calibration curve shown Figure 5.26.

Equation	y=a+bx	
Residual sum of squares	15529.41	
Pearson's r	0.943	
Adj. R-Square	0.862	
	Value	Standard Error
Intercept	0.00001	58.0
Slope	84.5	14.9

5.2.3. Detection of Pb

5.2.3.1. Cyclic Voltammetry of Pb (II) in 0.1M acetate buffer pH 4.5

The detection of Pb constitutes one of the milestones of this research due to its cancerous properties to humans and wildlife. It is also a bio accumulative element, which cannot be easily removed from the organism. Before engaging into the most important step, which is the electrochemical detection, it is essential to identify the reduction and oxidation potential for Pb. In order to accomplish that purpose, it was essential to perform a CV. Remembering that $U^0_{Pb2+/Pb}$= -0.126 V vs. SHE (U^0= -0.376 V vs. Calomel 1 M KCl). Then, 10 mM Pb(II) in 0.1 M acetate buffer pH 4.5 was prepared to produce a cyclic voltammogram which was performed by sweeping the potential from -1.0 V to +0.2 V vs. Calomel (1M KCl) at a scan rate of 25 mVs^{-1}. Under these conditions, the oxidation of Pb to Pb(II) occurs at -0.2 V (the cathodic peak) and the reduction of Pb(II) to Pb at nearly -0.8 V (the anodic peak) vs. Calomel (1 M KCl) as illustrated in Figure 5.27.

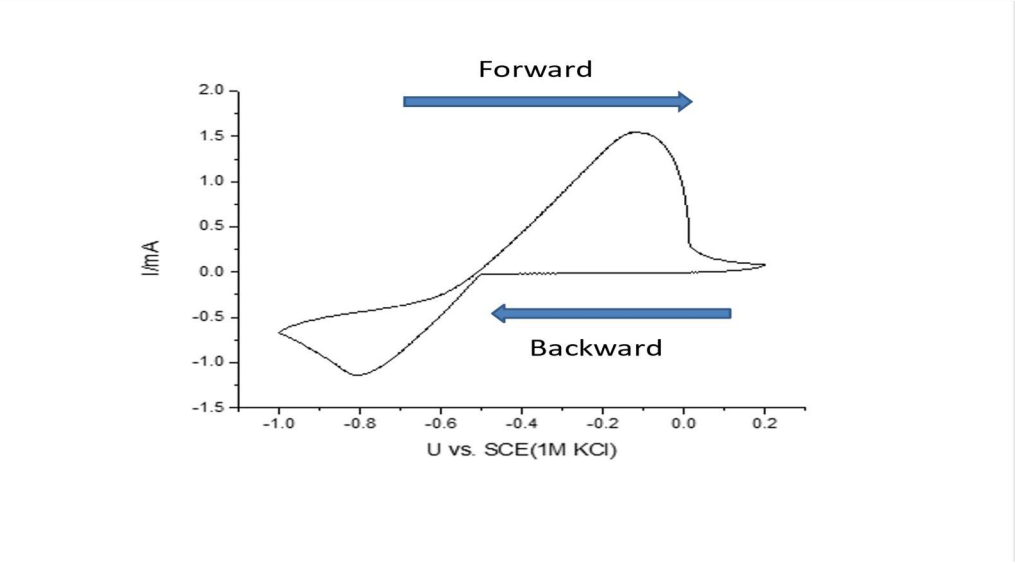

Figure 5.27: Cyclic Voltammetry 10 mM Pb(II) in 0.1 M acetate buffer pH 4.5, scan rate: 25 mV/s. Reference electrode: Calomel (1 M KCl), working electrode: glassy carbon electrode, counter electrode: Au wire.

The potential values provided by the CV are relevant for the stripping analysis protocol. In other words, it provides a clear idea on the deposition potential and the initial potential for the stripping step.

5.2.3.2. Pb electrodeposition and stripping analysis

Bismuth modified electrodes are produced either via in-situ or ex-situ electrodeposition as mentioned throughout this research. Due to the length of time that the ex-situ electrodeposition task took to complete, trials with Pb detection were carried out using in situ electrodeposition as in the case of Zn(II).

Bi electrodeposition on the surface is executed under stirring conditions of 300 rpm, and throughout the experiment the system was purged with N_2 to eliminate oxygen in the system.

During in situ deposition, by definition, the coverage of Bi on the surface electrode occurs simultaneously with the metal electrodeposition, which in this case is Pb. In short, it is a codeposition of Bi and the metal of interest forming the alloy at the surface. After the simultaneous Bi and metal electrodeposition, the modified electrode is taken to the next step which is the stripping. The latter was performed using the electroanalytical technique DPV (differential pulse voltammetry).

At first instance, several deposition potentials were trialled from -0.5 V to -0.8 V vs. Calomel (1 M KCl), there was no significant change in the stripping peak for Pb; thus, it was thought to keep -0.6 V as deposition potential, in order to explore the behaviour of the Bi-film when applying a less negative deposition potential, note that Pb peak may shift to less negative potential at lower concentrations [144]. The metal electrodeposition occurs at -0.6 V vs. Calomel (1 M KCl) during 5minutes followed by 30s as a rest period and the stripping process is executed using the set-up details: Ei= -0.6 V to Ev= +0.1 V vs. Calomel (1M KCl). the conditions mentioned are used for higher concentration from 1 mM and above.

At lower concentrations, five minutes electrodeposition time is insufficient; thus, the necessity to increase it to 10 minutes. These new conditions make possible the observation of low concentrations peaks such as 1 µM Pb(II).

At the beginning of the process, the position of the peak for higher concentration is at roughly -0.5 V vs. SCE (1 M KCl) as seen in the Figure 27. However, lowering the concentration of Pb, multiple peaks are observed instead of a unique peak; consequently, some shifts are observed and the detection of Pb at lower concentrations became difficult. These multiple peaks show shifts to nearly -0.2 V vs. Calomel (1M KCl) comparing to the single peak obtained at -0.5 V vs.

Calomel (1 M KCl) for higher concentrations. These shifts may be because fact that the peak current and the potential vary with the concentration of the metal in study in this case Pb [144].

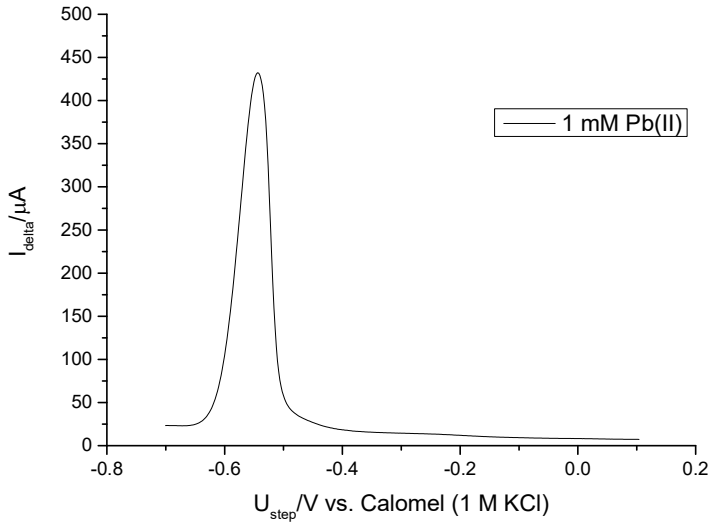

Figure 5.28: Stripping peak for 1 mM Pb(II) in 0.1 M acetate buffer pH 4.5, deposition potential= -0.6 V vs. Calomel (1 M KCl), deposition time: 5 min, quiet time: 20 s; DPV parameters: E_i= -1.4 V to E_v= -0.5 V vs. Calomel (1 M KCl), P_H (pulse height): 50 mV, P_W (pulse width): 50 ms, S_H (step height): 2 ms and S_T (step time): 200 ms.

5.2.3.2.1. Bi solution in 0.1 M acetate buffer pH 4.5 and 0.1 M HNO_3

First attempts for the bismuth electrodeposition on the surface were executed in different conditions such as the way the bismuth solution was prepared. At the beginning of the research, Bi solutions were prepared in acetate buffer pH 4.5 and then in 0.1 M HNO_3. Each supporting electrolyte behaved differently. It was important to use and evaluate both, uncover the difference in using each one and what the difference of pH can make to the stripping peak. In order to obtain that a number of trials have been made to find a considerable bismuth quantity or concentration that can provide accurate results (near to the exact quantity).

Since Bi film is produced under in-situ conditions, a consideration of the amount of Bi added in order to obtain consistent peak heights was made. Trials were made to roughly 800 µL (1 mM Bi(III)) increment of Bi in the cell already containing 50 mL of Pb solution. The detection peak increases upon increasing Bi concentration, but there was no significant change in the

peak height above additions of 500 µL. Therefore, 500 µL was chosen as the volume added to the cell for the production of the in situ electrodeposited Bi. Though, 500 µL (from 1 mM Bi (III) stock solution) is added into the cell, in terms of quantity (mols), 0.05 µmol is spiked into the cell.

In order to clarify the impact of using Bi in the improvement of the peak height and consequently the electric charge, Figure 5.29 presents the difference between a stripping peak with and without Bi in the system. A remarkable increase in sensitivity is observed when Bi is used, the peak height has increased by a factor of nearly two. This voltammogram confirms that Bi introduced to produce the alloy with the metal enhances the analytical sensitivity.

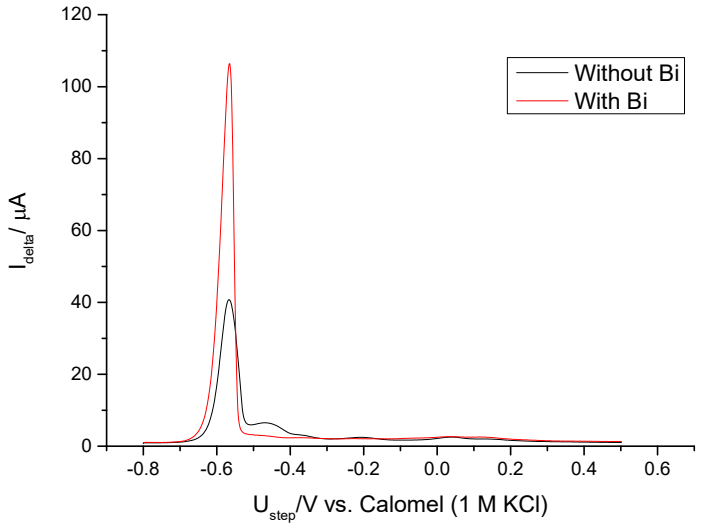

Figure 5.29: Stripping voltammograms 6 µM Pb(II) in 0.1 M acetate buffer pH 4.5, deposition potential= -0.6 V vs. Calomel (1 M KCl), deposition time: 10 min, quiet time: 20 s; DPV parameters: E_i=-0.8 V to E_v= -0.5 V vs. Calomel (1 M KCl), P_H (pulse height): 50 mV, P_W (pulse width): 50 ms, S_H (step height): 2 ms and S_T (step time): 200 ms.

a) Bi solution in acetate buffer

Bi salts from $Bi(NO_3)_3.5H_2O$, 10 and 100 mM Stock solutions were prepared with 0.1 M acetate buffer pH 4.5. However, the solution appeared turbid, which means, the solid does not dissolve completely in the buffer. Nonetheless, despite this solubility issue, there is a need to continue to use the solution and observe the behaviour in this case.

During the process of the detection of Pb, which includes Bi and Pb electrodeposition and consequently Pb stripping, the Bi peak is also stripped, and its charge is evaluated as can be seen in Figure 5.31 in order to understand its variation and implications in Pb quantification.

Figure 5.30 illustrates the stripping voltammogram of 8 µM Pb(II) in 0.1 M acetate buffer pH 4.5. As it can be seen, multiple peaks are observed instead of a single peak as observed in the case of 1 mM or 10 mM Pb(II) stripping peaks. Peaks appeared from roughly -0.5 V to nearly 0.0 V vs. Calomel (1 M KCl). The peaks that appear near zero, could also be spotted in the blank (acetate buffer + bismuth) stripping voltammogram, that means they may be treated as Bi peaks. Conversely, the series of peaks that are seen from -0.5 V to -0.2 V vs. Calomel (1 M KCl) may be considered as Pb peaks. The behaviour of multiple peaks was observed for lower concentrations. Kefala, et al in reference [102] has studied glassy carbon bismuth film modified electrodes for Pb detection simultaneously with Zn under similar conditions to this work, however, the deposition potential was established at -1.4 V vs. Ag/AgCl and SWV was selected as the voltammetric technique for the stripping step. A thorough study of the parameters affecting the performance of Bi film electrodes in the simultaneous determination of Zn and Pb in human hair and tap water using both in-situ and ex-situ electrodeposition mode was made. They observed a shift of the hydrogen evolution overpotential due to higher surface coverage of Bi, the peaks potentials shifted to the anodic direction when the frequency of the square wave (or step increment) was increased. This was presumably an effect of the decrease in reversibility of the oxidation of the metals at higher frequencies (range of the frequency studied was from 12.5 to 200 Hz and the step increment was between 1 and 16 mV). When the effect of the SW pulse height was studied in the range from 10 to 80 mV, the peak potential shifted to the cathodic direction and the peak heights increased upon the increase of pulse heights, yet, the background deteriorated, and the peak widths increased at higher pulse heights. Nonetheless, a lower relative standard deviation was attained (below 5%) in four ranges of concentrations used for the calibration curve. In the following year Kefala, et al in reference [101] investigated Nafion - coated bismuth film electrodes (NCBFEs) for the determination of trace metals by ASV. SWV was also chosen as the stripping technique, however, the deposition time was 180 s. The investigation was based upon the thickness of the film on a Nafion-coated electrode, the deposition time varied from 60 to 300s and, the Nafion coating was categorised as low, medium and high thickness. It

demonstrated that the amount of Bi deposited on an uncoated glassy carbon was lower than that on a coated glassy carbon, besides NCBFEs produced are stable (long term stability films). The Nafion coating improved the sensitivity to Pb by a factor of 2.5 or 3 compared to bare BFE, while Zn sensitivity was similar in both electrodes. The study based in three groups of NCBFEs showed a non-uniform distribution of Bi on the surface similarly to the finding of this research showed in section 5.1.2. Though, NCBFEs have also observed the potential peak shifts due to coulombic interaction between the cation exchanging Nafion film and the accumulated metals that affect the redox potential. Krolicka, et al in reference [110] also investigated carbon paste modified electrode with Bi_2O_3. The study revealed that the electrode modified described as a thicker film was generated externally, showed stability and reproducibility, and exhibited better analytical performance (a more favourable baseline) compared to that of metallic films deposited in-situ. Both in-situ and ex-situ electrodeposition modes were used with DPV as the stripping technique (deposition time: 60s, deposition potential: -1.2 V vs. Ag/AgCl). In addition to that, Hwang, et al in reference [94] investigated carbon nanotube Bi modified for simultaneous determination of Zn, Cd and Pb using SWV as stripping technique (deposition time: 300 s, deposition potential: -1.4 V vs. SCE). CNT's limitation for Zn detection is due to a more positive HER (it also exhibits higher background current); this was overcome when plated with Bi). Bi-CNTs showed much more sensitivity than other electrodes such as glassy carbon and produced the sharpest peaks and highest peak currents. Stripping responses were higher for separate measurements than in simultaneous measurements. These findings mentioned earlier have not reported the multiple-peak behaviour.

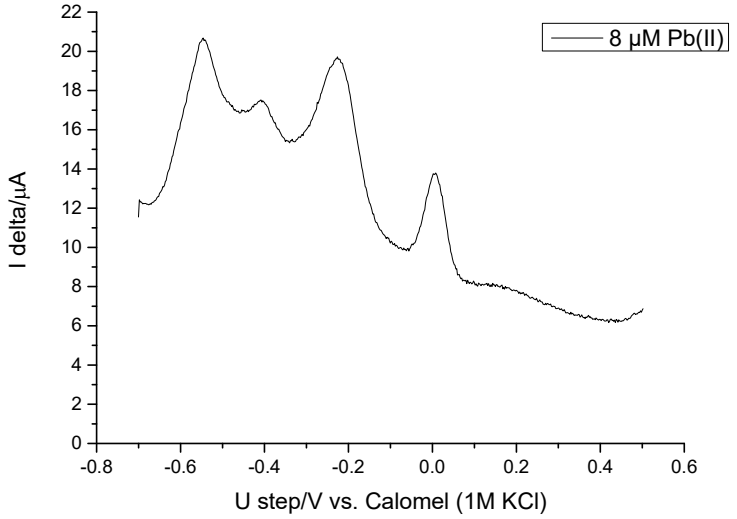

Figure 5.30: Stripping voltammetry 8 µM Pb(II) in 0.1 M acetate buffer pH 4.5, deposition potential= -0.6 V vs. Calomel (1 M KCl), deposition time: 10 min, quiet time: 20 s; DPV parameters: E_i= -0.8 V to E_v= -0.5 V vs. Calomel (1 M KCl), P_H (pulse height): 50 mV, P_W (pulse width): 50 ms, S_H (step height): 2 ms and S_T (step time): 200 ms.

The blank peak which appeared near zero, were then integrated, and its charges evaluated to explain its variation. From Figure 5.31, the range of the charges registered varies between 6-32 µC. The amount of Bi stripped varied after each experiment. That also proves Bi deposited very differently after each experiment, there is no clear trend in the variation since it occurred randomly. This variation determines the alteration of Bi deposition during each experiment, for some reason this also confirm that Bi amount deposited is variable even though the amount spiked and the concentration of Bi in the electrochemical cell is the same in every experiment. This may be estimated as one the sources of irreproducibility of the analyte peaks and consequently, reduces the precision of the results. This may be due to the state of the electrode, especially the lack of uniformity of the deposition, the presence of residual polishing solution used, alumina and oxygen reported in chapter 4, Section 4.1.2.

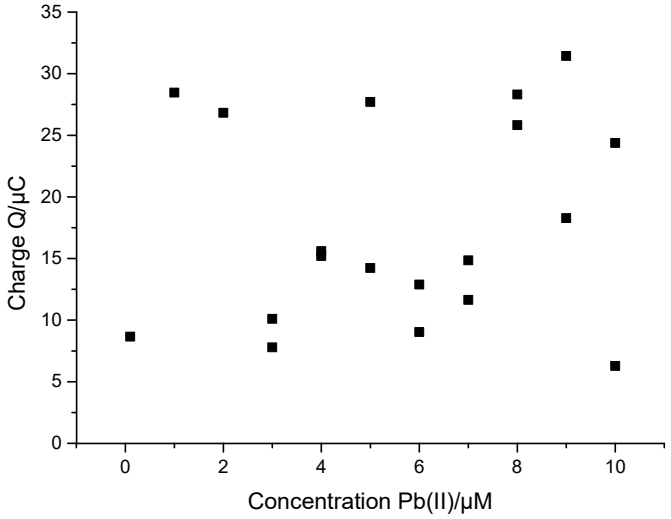

Figure 5.31: Blank peaks (Bi stripping peak) charges variation versus concentration of Pb (II).

Besides, previously irreproducibility problems were reported due to the change on the behaviour of the glassy carbon electrode.

Pb solutions are prepared from 1-10 µM, all the solutions are submitted to measurements. In more details, at first instance, the range chosen for the construction of a calibration curve is from 1-10 µM. However, the deposition time needed to be improved as 5 minutes was insufficient to detect lower concentrations below 1 mM. The conditions for the stripping step remained unchanged. Therefore, it was necessary to extend the deposition time to 10 minutes after several trials.

Since the objective of this work is the detection and quantification of metals such as Pb, it is necessary to produce a calibration curve. Pb peaks observed as multiple have been integrated to generate the charge which, was used to yield the graph charge versus concentration (calibration curve). Yet, this graph has produced a non-linear curve.

Initially, the results were not satisfactory as a linear trend could not be reached which may be due to the irreproducibility issue reported earlier. To minimise its effect, the data has been normalised, that means the charge of Pb peak normalised to Bi peak charge. As a result of this normalisation, a linear trend was observed in the range from 1-6 µM, then after 6 µM to 10 µM a linear decrease was observed as illustrated in Figure 5.32.

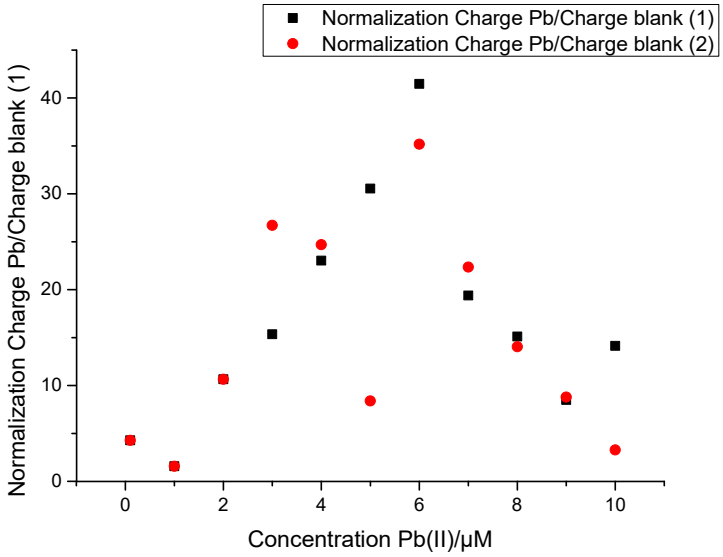

Figure 5.32: Normalized charges versus concentration of Pb(II).

After this finding, a calibration curve was built in accordance with the charge normalized estimated for the range 1-6 µM Pb(II). However, this curve does not pass through the origin and the intercept is negative as seen in Figure 5.33. On the other hand, a good correlation is obtained as pictured in Table 5.10. Hence, this result is not reliable for sample quantification, then it should not be used.

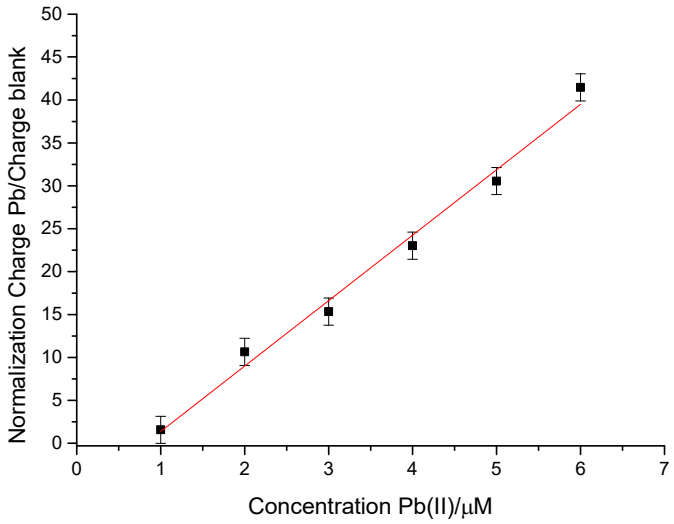

Figure 5.33: Calibration curve normalized charge versus concentration Pb(II). The error bars represent the standard error of the intercept.

Table 5.10: Regression data of Pb calibration curve normalized from Figure 5.33

Equation	y=a+bx	
Residual sum of squares	11.53	
Pearson's r	0.994	
Adj. R-Square	0.986	
	Value	Standard Error
Intercept	-6.25	1.58
Slope	7.63	0.406

The multiple behaviour has raised an issue. A closer look at the curve obtained some doubts to be used for samples determination. Therefore, the concern to improve this result has been raised. The reason for such result has not been clearly detected. It may be due to the state of the electrode, a poor cleanliness of the electrode. On the other hand, Bi solution used in these experiments was prepared in acetate buffer. However, it was observed that Bi did not completely dissolve in 0.1 M Acetate Buffer pH 4.5 as the solution was turbid. Besides, it can also be considered that the variability of the amount of Bi electrodeposited on the surface may also have influenced in the results. A lower amount of Bi electrodeposited may lead to a lower quantity of Pb detected and determined.

b) Bi solution in 0.1 M HNO_3

After evaluating the results from the Bi solution prepared in 0.1 M acetate buffer pH 4.5; problems such as multiple peaks, quality of the calibration curve raised concern about its application on samples. Therefore, as suggested by some literature for example [199], stock solutions of Bi(III) were prepared in 0.1 M HNO_3. Initially, multiple peaks behaviour was still being observed.

- Electrode cleaning and difficulties

As reported in the previous paragraph, the multiple peaks are constituting an issue for a successful calibration curve. Therefore, attempts are made to supress this obstacle. It was necessary to increase the length of the time for the cleaning process. During the initial procedure, after each stripping process, the electrode was submitted to a 10 minutes cleaning

at a potential of (0.7 V or 0.5 V vs. Calomel (1 M KCl)), unfortunately, this period showed to be ineffective to completely remove any residual metal or Bi on the surface. As a result of that, the cleaning time needed to be increase and verified every time.

Other attempts were made with a higher potential, some of them to at least 1.0 V vs. Calomel (1 M KCl). However, multiple peaks behaviour was still being observed.

Moreover, electrode was submitted to an extensive cleaning both mechanical and electrochemical. The first one was executed using alumina 0.05 µm, diamond and velvet pad. The electrochemical cleaning was performed by applying a potential of (0.7 V or 1.0 V vs. Calomel (1M KCl)), the duration of the process was extensive varying from 30 minutes to an hour, at some point it was done several times until a stripping voltammogram free of any peak is obtained. Consequently, a single peak was obtained and with a higher current comparing to the one obtained in the previous case (when Bi was prepared in 0.1 M acetate buffer pH 4.5).

The objective of the extensive cleaning is to eliminate any residual metal or impurities that prevent a clear detection of the analyte as they may constitute a blockade on the surface. After each cleaning step, the stripping voltammetry is necessary to ensure that all the impurities have been removed on the surface in order to allow the detection of the metal in a single peak instead of multiple ones.

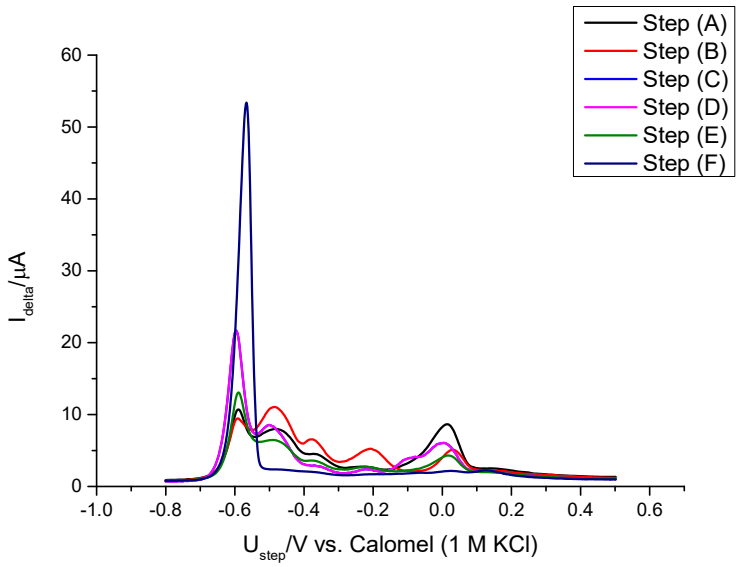

Figure 5.34: Cleaning steps results for 4 µM Pb(II) in 0.1 M acetate buffer pH 4.5, deposition potential= -0.6 V vs. Calomel (1 M KCl), deposition time: 10 min, quiet time: 20 s; DPV parameters: E_i= -0.8 V to E_v= -0.5 V vs. Calomel (1 M KCl), P_H (pulse height): 50 mV, P_W (pulse width): 50 ms, S_H (step height): 2 ms and S_T (step time): 200 ms. From A to F are stages of improvement of the analytical signal (Pb peak), after intensive electrochemical combined with mechanical cleaning.

The Figure 5.34 above illustrates several steps of cleaning. The impact of combining electrochemical and mechanical cleaning several times results in the improvement of the Pb peak. It can be seen clearly that, the first set of cleaning provided multiple peaks, stripping voltammograms A to E in Figure 5.34. As long as the amount of cleaning was increasing, the electrode surface became cleaner and consequently instead of having multiple peaks, a single peak was obtained, step E in the stripping voltammogram in Figure 5.34.

This constitutes a lengthy process that can take hours, that is a disadvantage for this technique as the cleanliness must be verified all the time to obtain a single peak. This step is time consuming, however, it was necessary to provide reliable results.

5.2.3.3. Calibration curve

Since a single peak is achieved as a result of an extensive cleaning, conditions are prepared to build a calibration curve for detection of samples. As per the definition of the calibration curve procedure, standard solutions of Bi(III) were prepared. In the case of acetate buffer being used as electrolyte for Bi solution preparation. The results needed to be normalized as referred in the previous point 5.2.1.1.

Due to the fact that a linear trend was obtained in the concentration range 1-6 µM Pb in the previous case as showed in Figure 5.35. Thus, the same range is used in the case when Bi solution is prepared in 0.1 M HNO_3. Bi stock solution prepared in 0.1 M HNO_3, showed a complete dissolution of the salt unlike in the case of acetate buffer as supporting electrolyte. Figure 5.35 depicts stripping voltammograms of Pb standards solution from 1-6 µM Pb(II), expected to produce calibration curve.

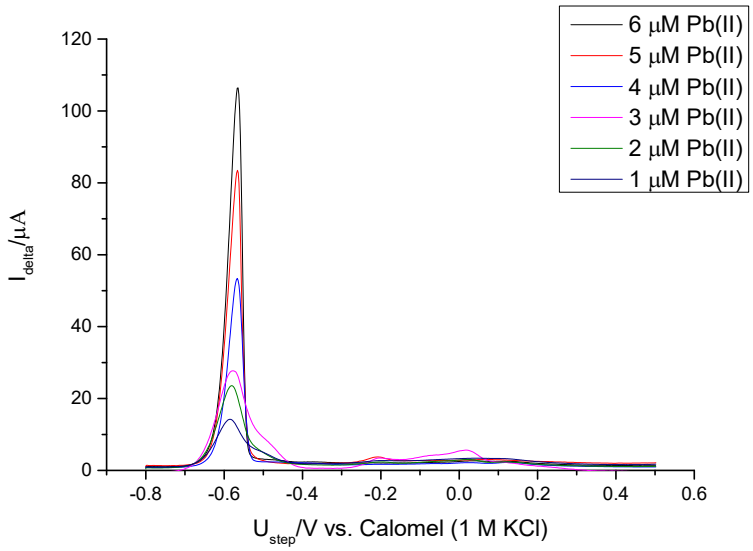

Figure 5.35: Stripping voltammograms 1-6 µM Pb(II) in 0.1 M acetate buffer pH 4.5, deposition potential= -0.6 V vs. Calomel (1 M KCl), deposition time: 10 min, quiet time: 20 s; DPV parameters: E_i= -0.8 V to E_v= -0.5 V vs. Calomel (1 M KCl), P_H (pulse height): 50 mV, P_W (pulse width): 50 ms, S_H (step height): 2 ms and S_T (step time): 200 ms.

As a result of the cleaning process, all the peaks are single meaning that multiple peaks issue was addressed. The peaks obtained were integrated in order to obtain the charge. A plot charge versus concentration is generated and using the least square regression method. The equation of the best straight line obtained, is used to calculate the concentration for unknown samples.

Comparing the current height and charges already obtained after all the treatment, it could be observed that the current recorded when Bi solution prepared in 0.1 M HNO_3 is used and after a prolonged cleaning are higher than when Bi solution prepared in 0.1 M acetate Buffer pH=4.5 is used. That explains the retention of Bi on the surface is higher than in the case of acetate buffer; as a result, a considerable quantity of Pb will be detected and quantified

compared to the previous case in which the supporting electrolyte Bi(III) solution was prepared in acetate buffer pH 4.5.

In order to obtain reliable results, the peaks are integrated using different range of potentials. The criteria for a good correlation are needed to select which curve obtained through integration is trustworthy. The slope and the intercept must fulfil some requirements such as the intercept is required to be positive and its value near zero.

Analyte peaks, in this case Pb peaks are integrated and the charge obtained. However, integrations are done using different ranges from -0.72 V to approximately -0.45 V vs. Calomel (1 M KCl). Some of them have provided poor correlation and intercept values extremely different from zero.

Several attempts have been made in order to provide a calibration curve that meets all the requirements. Some of these attempts include the integration of Pb peaks in the range -0.72 V to -0.50 V vs. Calomel (1 M KCl). As it can be seen in the Figures 5.36 and 5.37, first the curve obtained from this range provided a negative intercept although the correlation is acceptable.

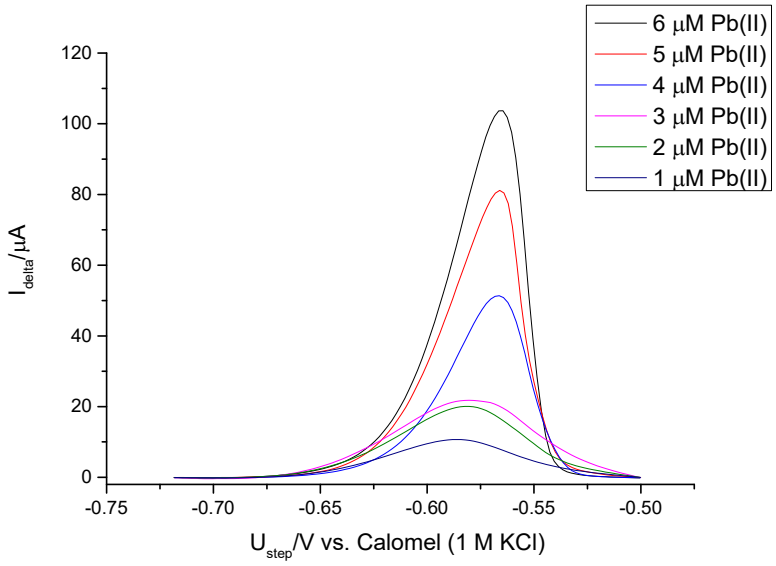

Figure 5.36: Stripping Voltammograms Pb(II) potential range -0.72 V to -0.50 V vs. Calomel (1 M KCl), deposition potential= -0.6 V vs. Calomel (1 M KCl), deposition time: 10 min, quiet time: 20 s; DPV parameters: E_i= -0.8 V vs. to E_v= -0.5 V vs. Calomel (1 M KCl), P_H (pulse height): 50 mV, P_W (pulse width): 50 ms, S_H (step height): 2 ms and S_T (step time): 200 ms.

The data have been treated as follow, the subtraction to the common background and to the residual current which could be found to the intercept.

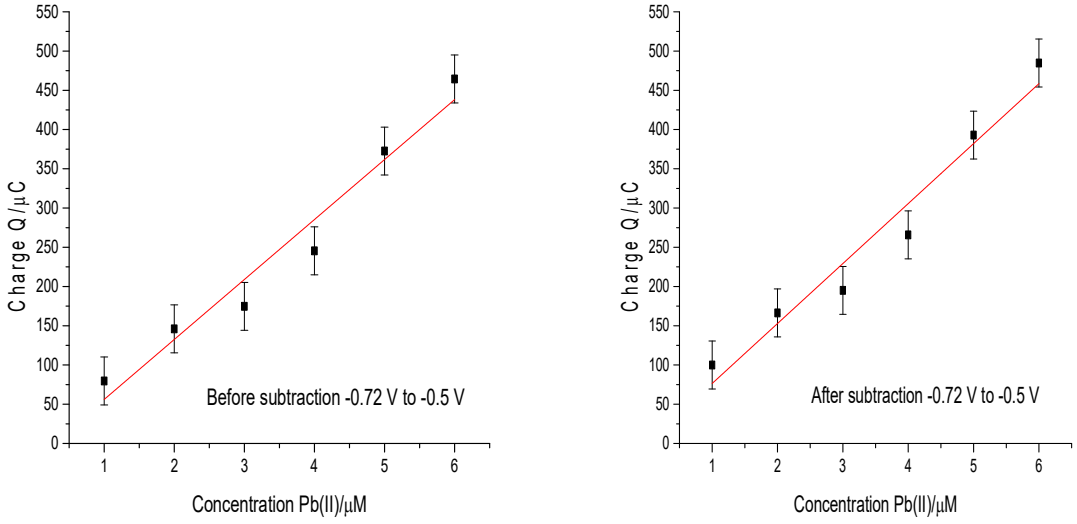

Figure 5.37: Calibration curve Pb(II) before (at the left) and after (at the right) subtraction by a common background. The potential range integrated to obtain the charge was -0.72 V to -0.5 V vs. calomel (1 M KCl). The error bars refer to the standard error of the intercept.

After all these treatments, the resulting curve continues to present a slightly negative intercept which is too significant as illustrated in Table 5.11.

Table 5.11: Regression analysis of Pb calibration curve, potential range integrated -0.72 V to -0.5 V vs. Calomel (1 M KCl) as in Figure 5.37.

Equation	Y=a+bx (Integration range -0.72 V to -0.5 V vs. Calomel (1 M KCl))			
	Before subtraction		After subtraction	
Residual Sum of squares	4311.52		4311.52	
Pearson's r	0.979		0.979	
Adj. R-Squares	0.949		0.949	
	Value	Standard Error	Value	Standard Error
Intercept	-20.33	30.56	-0.005	30.56
Slope	76.42	7.85	76.42	7.85

Another attempt to obtain a reliable calibration curve, was to change the integration range to -0.72 V to -0.52 V vs. calomel (1 M KCl). This range has also produced a curve that cannot be used for samples determination directly. As it can be seen in Figures 5.38 and 5.39, the data of the curve are treated as done to the previous ones, that means, the subtraction to the background and the residual current.

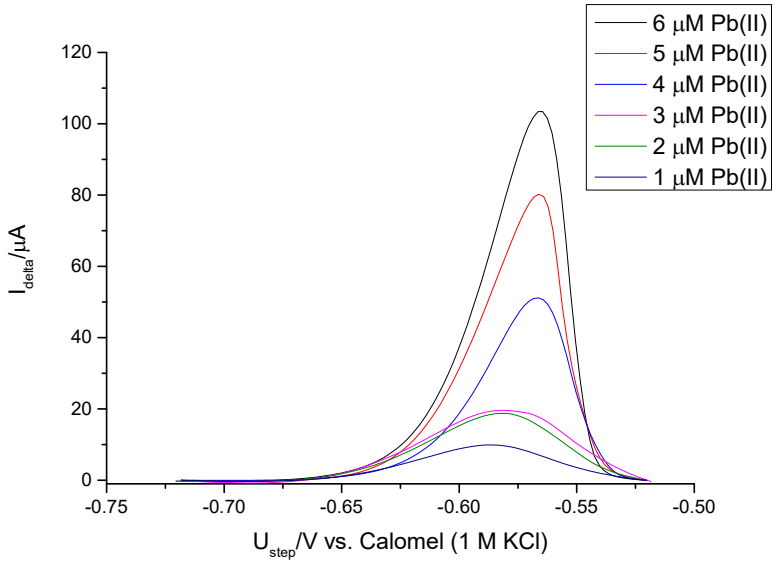

Figure 5.38: Stripping Voltammograms Pb(II) potential range -0.72 V to -0.52 V vs. Calomel(1 M KCl), deposition potential= -0.6 V vs. Calomel (1 M KCl), deposition time: 10 min, quiet time: 20 s; DPV parameters: E_i=-0.8 V to E_v= -0.5 V vs. Calomel (1 M KCl), P_H (pulse height): 50 mV, P_W (pulse width): 50 ms, S_H (step height): 2 ms and S_T (step time): 200 ms.

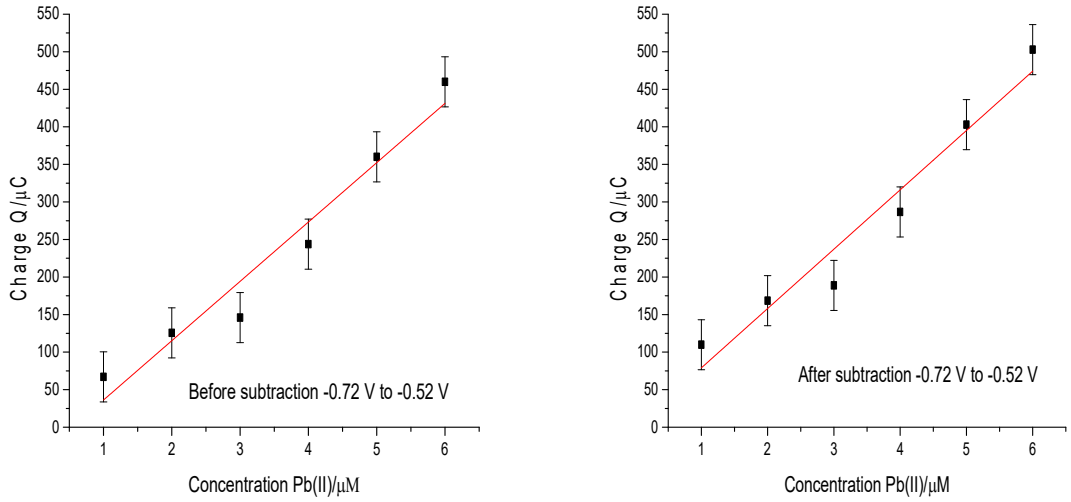

Figure 5.39: Calibration curve Pb(II) before (at the left) and after (at the right) subtraction by a common background, potential range integrated -0.72V to -0.52V vs. Calomel (1M KCl). The error bars refer to the standard error of the intercept.

The final curve has a slight negative intercept which is not significant as illustrated in the regression data in Table 5.12.

Table 5.12: Regression analysis Pb calibration curve (Integration range -0.72 V to -0.52 V vs. Calomel (1 M KCl)) from Figure 5.39.

Equation	Y=a+bx (Integration range -0.72 V to -0.52 V vs. Calomel (1 M KCl))			
	Before subtraction		After subtraction	
Residual Sum of squares	5128.64		5128.64	
Pearson's r	0.977		0.977	
Adj. R-Squares	0.944		0.944	
	Value	Standard Error	Value	Standard Error
Intercept	-42.86	33.33	-0.005	33.33
Slope	79.03	8.56	79.03	8.56

Following several trials, the last range integrated -0.72 V to -0.45 V vs. Calomel (1 M KCl) was also chosen to be evaluated in order to obtain a credible calibration curve. The peaks integrated within the range mentioned, have provided a curve which after all the treatments showed a positive intercept as demonstrated in Figure 5.40.

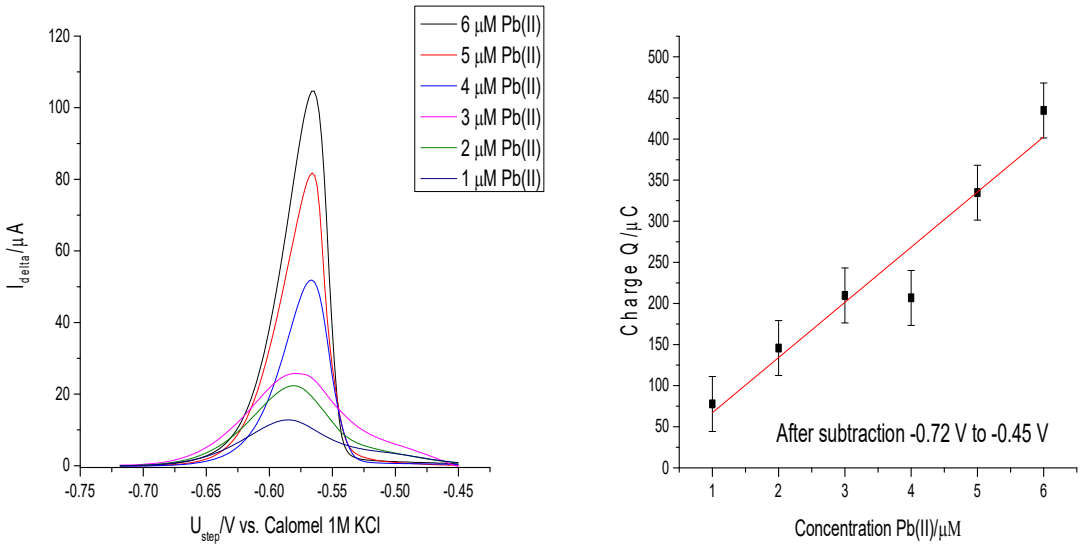

Figure 5.40: Stripping voltammograms (at the left) and Calibration curve (at the right) Pb(II), potential range integrated -0.72V to -0.45V vs. Calomel (1 M KCl). The error bars represent the standard error of the intercept.

The correlation obtained is 0.969, this is an acceptable figure for a calibration curve. Since this curve meets the requirements as confirmed in Table 5.13. Thus, it is retained as the one to be used for sample analysis. Therefore, this calibration curve is selected to be used for samples quantification.

Table 5.13: Regression data Pb calibration curve as in Figure 5.40, potential range integrated -0.72 V to -0.45 V vs. Calomel (1 M KCl).

Equation	y=a+bx (Range integrated: -0.72 V to -0.45V vs. Calomel (1 M KCl))	
Residual sum of squares	5153.10	
Pearson's r	0.969	
Adj. R-Square	0.923	
	Value	Standard Error
Intercept	6.67E-4	33.41
Slope	67.11	8.58

5.3. Summary

The detection of Pb and Zn as heavy metals using a simple procedure that can be used in countries with low income, is the main objective of this work. As mentioned at the beginning of the chapter and in the literature review, Bi films are produced either by in situ or ex situ conditions. The thickness of the film is greater when the film is produced using potential cycling rather than chronoamperometric electrodeposition under stirred and unstirred conditions. It could also be observed that the amount of Bi electrodeposited is higher when it is performed under stirring.

Bi electrodeposited when characterized microscopically by SEM, EDX, AFM, Optical Microscopy and XPS presented a larger amount of Bi under conditions of stirred solution than in the case of unstirred. The distribution of Bi deposition on the surface was not uniform and a large presence of oxygen on the same surface was also observed, this may have come from alumina or from the air in the laboratory despite the process being executed in N_2 atmosphere (N_2 purging)

The addition of an electrolyte normally increases the stripping peak height due to the increment of the ionic strength. Two electrolytes used for this study have confirmed that mixing acetate buffer and an electrolyte improve the sensitivity of the anodic stripping voltammetry. Both Na_2SO_4 and $NaClO_4$ were used, both cases have been examined with only Zn (II). However, limitations due to insoluble salts of Pb(II) produced with these electrolytes have made impossible to carry out the same electrolyte effect study with Pb as done with Zn. Therefore, these electrolytes have not been used for the simultaneous determination of Pb and Zn. The mixture of acetate buffer with Na_2SO_4 provided consistent enhancement in Zn stripping peak height using GC Bi-modified under stirring and unstirring conditions.

Since the electrode cleanliness is fundamental for the performance of the Bi film, a cleaning potential requires to be introduced right after each analyte stripping. At the beginning of the research, a potential of 500 mV vs. MSE (K_2SO_4, sat'd) was set up according to the working conditions used. However, this reference electrode was found unsuitable for Pb determination, the shift to Calomel (1 M KCl) electrode was essential. Because of the changes in circumstances, some conditions needed to be changed. The cleaning potential also suffered an alteration and was extended from 30 minutes to roughly an hour applying 0.7 V or 1.0 V

versus Calomel (1 M KCl). The prolonged electrochemical cleanliness was important in the detection of Pb peaks as it has addressed the multiple peaks problem observed in the conditions applied in this work.

The ex-situ Bi electrodeposition is more time consuming than the in-situ. Therefore, the in-situ electrodeposition is recommended in this work for calibration curve in this research. Another issue reported is the preparation of Bi solutions, the comparison between Bi solution prepared in 0.1 M acetate buffer pH 4.5 and 0.1 M HNO_3. The first case, Bi prepared in 0.1 M acetate buffer pH 4.5 have provided low peaks height and multiple peaks especially with Pb, as well as irreproducibility problems were considerably noticed. On the other hand, in the second case when Bi solution is prepared by dissolution in 0.1 M HNO_3 before addition to the acetate buffer, the sensitivity has improved since peaks heights and charges have grown considerably. Besides, singles peaks are obtained as a result of an extensive electrochemical cleaning. Since the use of 1 M HNO_3 has provided better results on the stripping results, it may be concluded that the use of acetate buffer to prepare Bi solutions may not be recommended in the conditions of this work. It is worth to note that, Bi(III) did not completely dissolve in 0.1 M acetate buffer pH 4.5 alone as the final solution was turbid.

Calibration curves generated for either Zn(II) or Pb(II) required treatment in order to fulfil requirements for an acceptable curve. When Bi is prepared in Acetate buffer, the linear trend is only observed in the concentration range of 1-6 µM Pb(II). This led to the introduction of the concept of normalization in order to minimise the effect of irreproducibility. Various integration ranges are necessary to obtain a reliable calibration curve. The integration should provide a curve containing a positive and near zero intercept and an acceptable correlation. The calibration curve for Zn(II) has been submitted to treatments, the range integrated from -1.35 V to -0.8 V vs. Calomel (1 M KCl) provided a positive intercept and near zero which is 0.00079 and the correlation coefficient of 0.979. Afterward, a loss of sensitivity has been reported when a second calibration curve was produced. The second Zn(II) calibration curve presented a correlation below 0.900 and a slight negative intercept of -2.9997, which is basically similar to zero within uncertainty. However, its correlation coefficient is extremely low (0.886) and a very large standard error is also observed. This indicates that there is a lack of consistency in the data, this may be due to the irreproducibility problem, and changes in the electrode behaviour

Again, in the case of Pb, when Bi(II) solutions are prepared in 0.1 M HNO_3, the improvement in sensitivity is remarkable by looking at the stripping peak heights and charges. Among ranges integrated, the range -0.72 V to -0.45 V vs. Calomel (1 M KCl) have produced curve with an intercept of 0.00067 and a correlation of 0.969. The electrochemical cleaning has made possible to attain a calibration curve for lower concentration (in this case 1-6 µM Pb(II)) applying a less negative deposition potential.

Chapter 6: Sample Analysis

6.1. Introduction

One of the ambitions of this research is to analyse real samples using the Bi modified electrode under room temperature conditions and a simple procedure. For the purpose, the sample used to undergo this evaluation is water; natural and tap water are chosen. Tap water samples were collected at two points: Stanton Street and Morpeth Street (Newcastle upon Tyne); for the natural water, three collecting points were used: Wylam, Blaydon bridge and Blaydon Burn.

6.2. Sample treatment

As a requirement to produce a successful bismuth modified electrode, the pH has to be maintained at the range 4-6. In order to reach this objective, the samples demand a pre-treatment. Thus, a solution of 0.1 M acetate buffer pH 4.5 as suggested by Wang, et al in reference [183] is used to adjust to the required pH. Each 50 mL of the water sample required 40-50 mL of the buffer in order to reach the pH 4.5 (Taking into account that 500 mL of the sample is diluted when adjusting the pH with acetate Buffer pH 4.5). Apart from the pH adjustment, the sample water was filtered using a Merck Millipore glass vacuum holder of 47 mm diameter and a membrane of 0.45 µm pore size.

The aliquot of 50 mL was used for all the samples both natural and tap water, buffered at pH=4.5. This aliquot transferred to the cell is then used for both calibration curve and standard addition. In the cell, apart from the sample itself it was added 500 µL Bi (1 mM), that means the concentration of Bi in the cell is estimated as 10 µM and the mols of Bi is 0.5 µmol.

Due certain problems with contamination observed throughout this work whose origin are unknown, the resulted stripping peaks are affected. After each stripping experiment with the sample, a complementary cleaning was required in order to avoid a further recontamination and remove any residual analyte on the surface. This step is performed in the supporting electrolyte in use 0.1 M acetate buffer pH 4.5 only applying the chronoamperometric technique (roughly 10 min at 1.0 V vs. Calomel 1 M KCl) followed by a differential pulse

voltammogram (DPV) in order to evaluate the cleanliness. If the surface is cleaned, the stripping graph will not show any peak as shown in the figure 6.1.

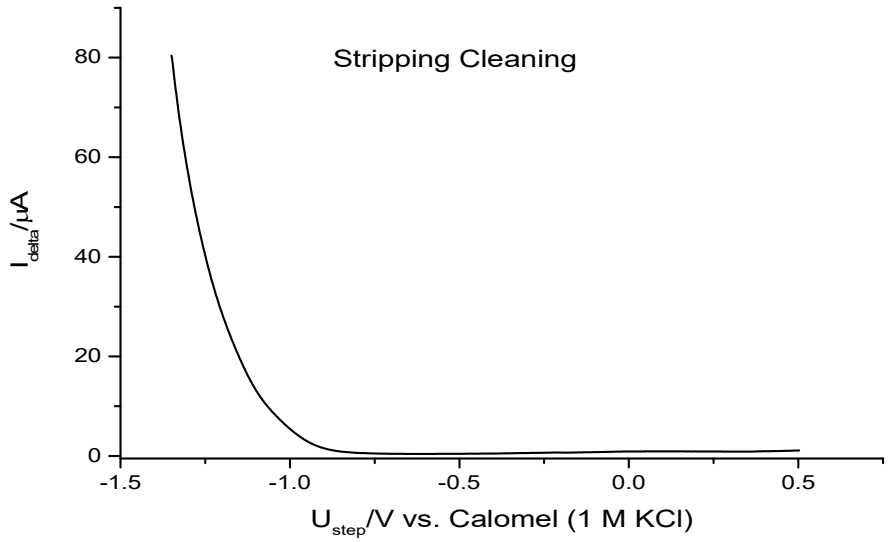

Figure 6.1: Stripping voltammetry of a clean electrode surface, DPV parameters: E_i= -1.4 V vs. Calomel (1 M KCl) to E_v= -0.5 V vs. Calomel (1 M KCl), P_H (pulse height): 50 mV, P_W (pulse width): 50 ms, S_H (step height): 2 ms and S_T (step time): 200 ms.

The assignment was the detection and quantification of both Zn and Pb in the various samples. The deposition potential used for these samples is -1.4 V vs. Calomel (1 M KCl) as it was for Zn, since its standard potential as well as the equilibrium potential is more negative than Pb in the chronoamperometry step. Moreover, DPV details are maintained the same as those for preparation of the calibration curve referred in chapter 5, section 5.2.2.2.

6.3. Tap and natural water results

As reported earlier two types of samples were used to evaluate the approach developed in this research: natural and tap water. The choice of both type of samples was done according to the complexity of the matrixes. As it is well-known, tap water is treated before distribution to households, consequently, its matrix is less complex than natural water. The aim is to evaluate the quantity of Zn and Pb in these samples and the impact of the quantity found in human health and environment.

The collection points for tap water were mentioned in the previous points and they were chosen randomly according to accessibility.

6.3.1. Tap Water

The tap water was collected in two sites Stanton Street and Morpeth Street. Two analytes were investigated namely Zn and Pb. At first, as it was suspected, No Pb peak was observed, which means, the approach developed throughout this work for Pb is not suitable for detection of this metal in this type of sample and matrix. Besides, the tap water is treated and expected to be potable since at some point, it is taken as drinking water as well. Therefore, considerable amount of Pb is fatal and risky for human health. These samples have been used to investigate the quality of the tap water consumed.

As mentioned earlier in the case of Zn in the previous chapter, two calibration curves were generated. The second curve was created as an average curve, that means, it was produced from several curves in this case, they were two. Both curves were used to estimate the concentration of the analytes in the samples. The metal Zn was detected and quantified unlike Pb. Either natural or tap water samples have been pretreated with acetate buffer and filtration following earlier treatment procedure stated in the section 6.2.

a) Stanton Street Tap Water

Stanton street is located in Arthur's Hill in the Newcastle NE4 area. The sampling process constitutes into a collection from the tap of a residence through 1 L bottles. Following the earlier step, the bottles labelled are taken to the laboratory where they are treated according to the pretreatment process mentioned earlier. After that, 50 mL aliquot is taken and transferred into the cell for stripping analysis alongside with the volume of B(III). This volume of the aliquot is maintained for all the experiments with the sample.

Five experiments were executed with the sample from this collection point. At the end of the stripping step, the results showed Zn peaks varying from -1.3 V to -1.4 V versus calomel (1 M KCl). As it can be seen in Figure 6.3 below, Zn peaks experienced some shifts and differences in peak heights; besides, it could also be seen that peaks start at different potentials. Another remark is the behaviour of Bi peaks, which varies in height and in terms of shape as some peaks are single and other multiples as illustrated in Figure 6.2. This could influence in the amount of Zn retained and stripped from the surface for further detection and quantification. However, Pb peaks were not detected as anticipated.

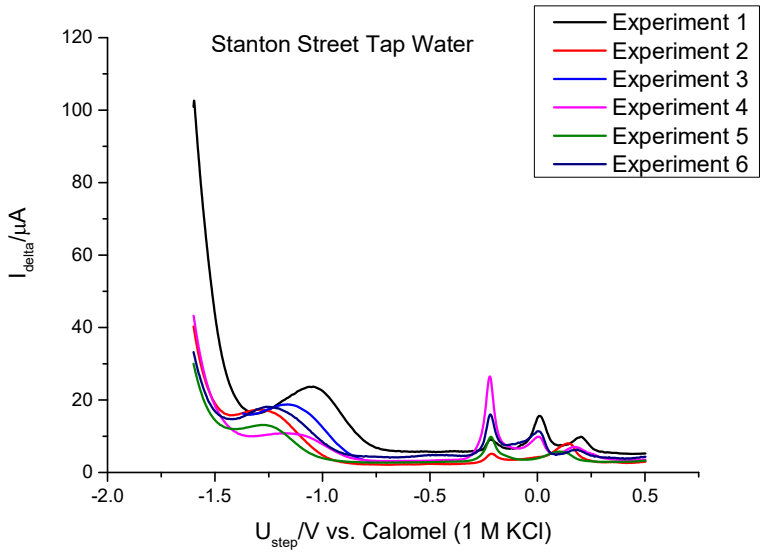

Figure 6.2: Stripping voltammograms of Stanton Street tap water, deposition potential: -1.4 V vs. Calomel (1 M KCl), deposition time: 10 min, quiet time: 20 s; DPV parameters: E_i= -1.6 V to E_v=-0.5V vs. Calomel (1 M KCl), P_H (pulse height): 50mV, P_W (pulse width): 50 ms, S_H (step height): 2 ms and S_T (step time): 200 ms.

The series of peaks that are thought to be related to Bi oxidation processes can be observed from roughly -0.25 V to +0.25 V versus Calomel (1 M KCl).

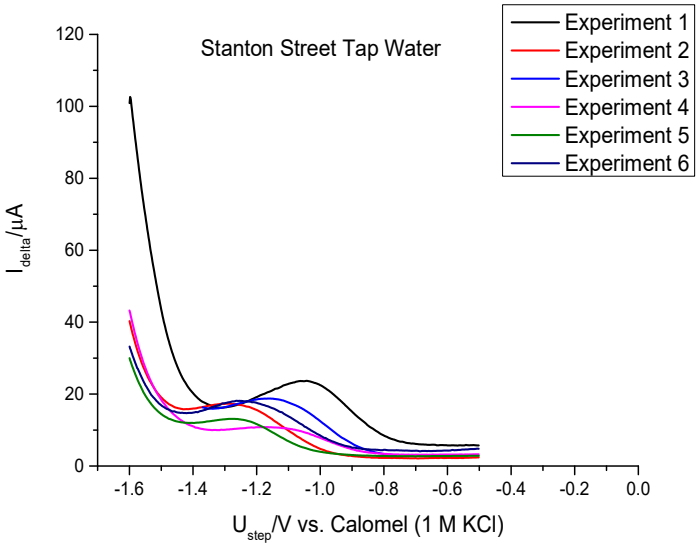

Figure 6.3: Stripping Zn peaks Stanton Street samples, deposition potential: -1.4 V vs. Calomel (1 M KCl), deposition time: 10 min, quiet time: 20 s; DPV parameters: E_i= -1.6 V to E_v= -0.5 V vs. Calomel (1 M KCl), P_H (pulse height): 50 mV, P_W (pulse width): 50 ms, S_H (step height): 2 ms and S_T (step time): 200 ms.

As reported earlier, five experiments were done with this sample from Stanton Street collecting point which generated the same number of large peaks. Each one of these peaks is integrated and the charges taken. According to the Figure 6.4, the charge varies from 90 µC to 330 µC. As it can be seen, it is a random variation and there are no specific trends. The experiment number 2 showed a high value of charge corresponding to 330 µC unlike the experiment number 1 which presented the lowest. The situation may be caused by some residual analytes may have remained on the surface, the second experiment has increased the amount of the analyte on the surface, even though the electrode was cleaned. Another probable explanation may be because of the variation between different samples used as its quality may vary. Besides, during each experiment, the electrodeposition of Bi is variable, thus, it affects the amount of the analyte as well, the lack of uniformity in Zn retained in the surface and then stripped.

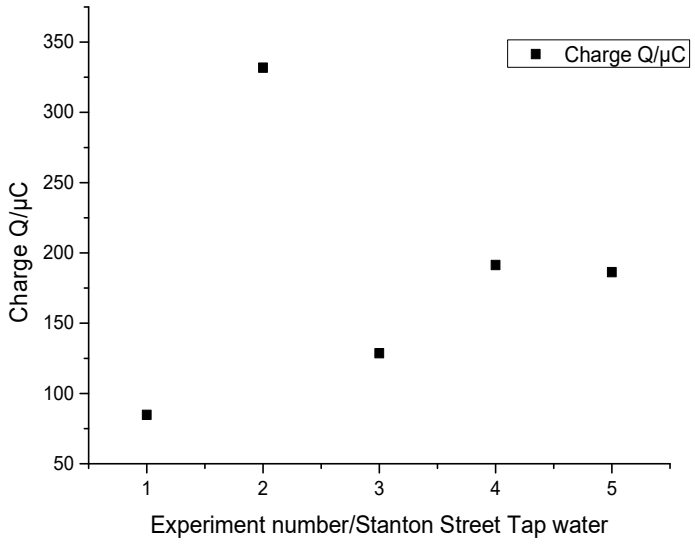

Figure 6.4: Estimated electric charges of Zn stripping peaks according to the experiment number, collection point: Stanton Street.

From the relationship between the charge and the current, there is a direct proportionality between the charge and the concentration. Hence, the calibration curves produced in terms of charge shown in the previous chapter is used to estimate the concentration of the metal detected, in this case Zn in the sample.

The concentration was primarily calculated in terms of the unit μM (μmol/L) and then in terms of μg/L (ppb). The lowest concentration was recorded for experiment number 1 while the highest was experiment number 2, similar to the charge graph behaviour shown earlier, and are 0.095 and 0.371 μM respectively based on the first calibration curve and 0.100 and 0.393 μM based on the average calibration curve. These values refer to the concentration of the analyte in the original sample and they are also illustrated in the Figure 6.5 and 6.6.

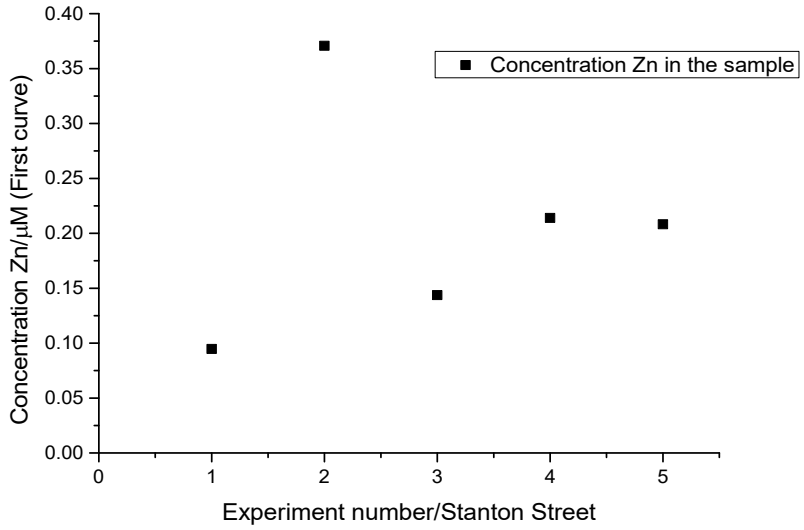

Figure 6.5: Concentration Zn (μM) in the original sample based on the first calibration curve. Variation of the concentration per experiment based on Zn first calibration curve Stanton Street tap water.

The variation of the concentration in the original sample estimated, follows the same trend as in the case of the charge against the experiment number.

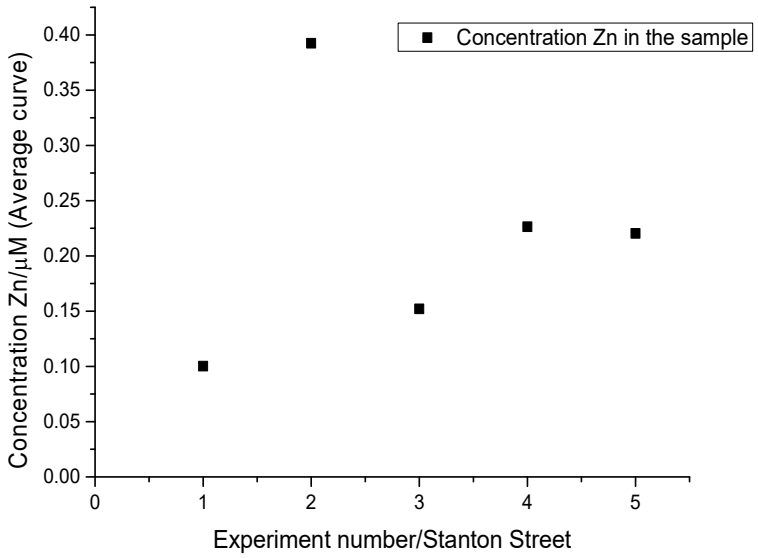

Figure 6.6: Concentration Zn (μM) in the original sample based on the average calibration curve. Variation of the concentration per experiment based on Zn average calibration curve Stanton Street tap water.

The final results of the concentration of the analyte in the original sample in terms of μg/L is illustrated in the Figure 6.7 below. The concentration of Zn in the sample is estimated between 6.2 and 24.2 μg/L for the calculation based in the first calibration curve (Figure 6.7) and between 6.5 and 25.6 μg/L for the average calibration curve estimation (Figure 6.8). Though, the same trend is reported as in the previous graphs.

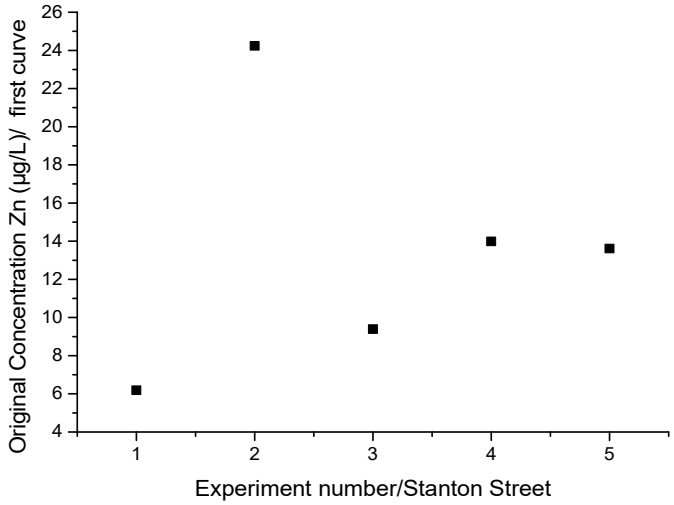

Figure 6.7: Concentration (µg/L) of Zn in the original Stanton Street sample based on the first calibration curve. Variation of the original Concentration (µg/L) per experiment based on Zn first calibration curve Stanton Street Tap Water.

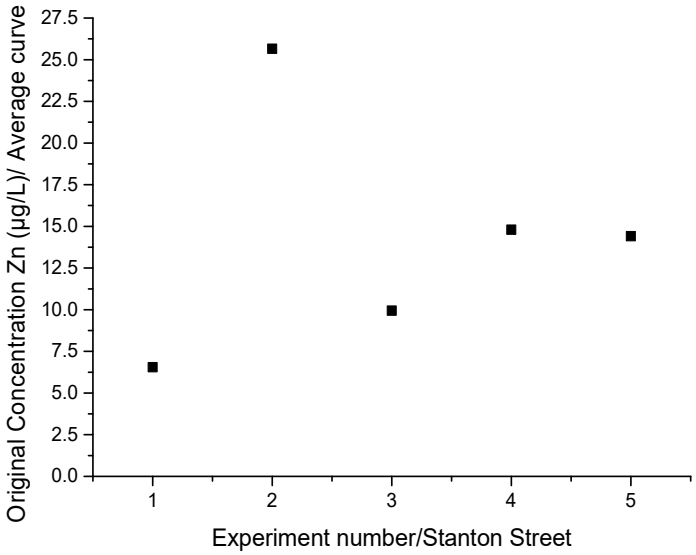

Figure 6.8: Concentration (µg/L) of Zn in the original sample Stanton Street based on the average calibration curve. Variation of the Original Concentration (µg/L) per experiment based on the Zn average calibration curve Stanton Street tap Water.

As stated in the previous chapter, two calibration curves were generated for Zn. The graphs generated charge versus experiment number and concentration versus experiment number have shown the same trend, in agreement with to the calibration curve used.

b) Morpeth Street Tap Water

Morpeth Street is located in Spital Tongues in Newcastle upon Tyne, NE2 4AS area. The collection procedure is similar to the one executed for the previous collection point Stanton Street. The sample was collected from a tap water of a residence, filtered, and pre-treated with the buffer. The stripping analysis for this sample was done under the same conditions as Stanton Street, in either the chronoamperometric step or the stripping one. The increase of the number of experiments for this sample was possible due to its accessibility. Fifteen (15) experiments were executed. From these experiments fifteen large Zn peaks were generated, some of them are illustrated in the Figures 9 and 10. Peaks shifts are observed from -1.4 V to -1.1 V vs. Calomel (1 M KCl) and Bi peaks have shown a variation in the size and shapes (multiples and singles), similar behaviour was observed in the Stanton Street sample.

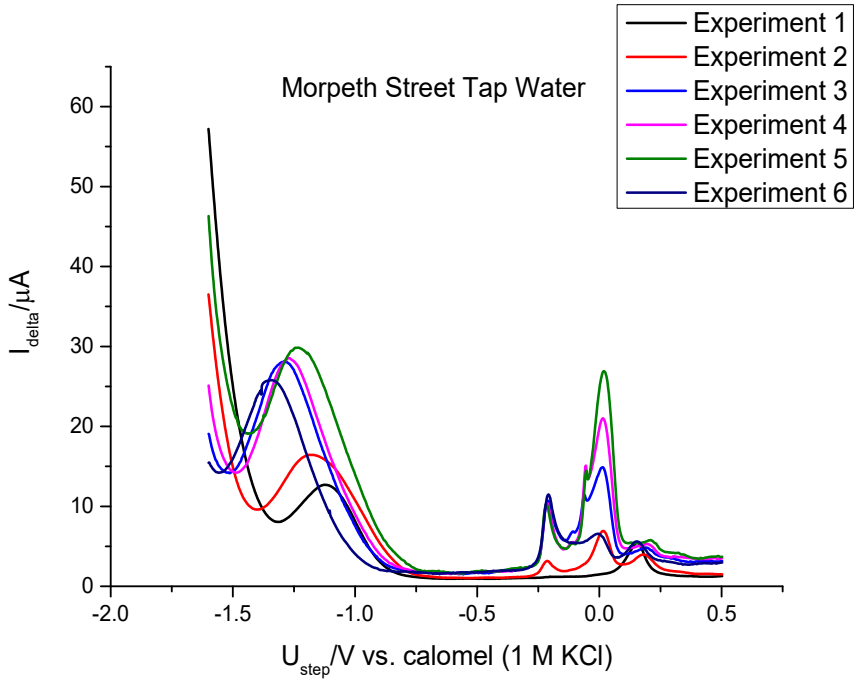

Figure 6.9: Stripping voltammograms Morpeth Street tap water, deposition potential= -1.4 V vs. Calomel (1 M KCl), deposition time: 10 min, quiet time: 20 s; DPV parameters: E_i= -1.6 V to E_v= -0.5 V vs. Calomel (1 M KCl), P_H (pulse height): 50 mV, P_W (pulse width): 50 ms, S_H (step height): 2 ms and S_T (step time): 200 ms.

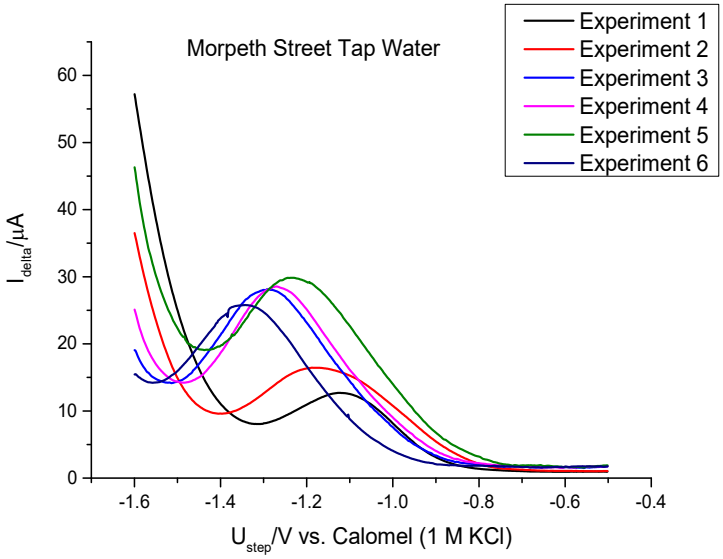

Figure 6.10: Stripping Zn peaks Morpeth Street samples, deposition potential= -1.4 V vs. Calomel (1 M KCl), deposition time: 10 min, quiet time: 20 s; DPV parameters: E_i= -1.6 V to E_v= -0.5V vs. Calomel (1 M KCl), P_H (pulse height): 50 mV, P_W (pulse width): 50 ms, S_H (step height): 2 ms and S_T (step time): 200 ms.

Each Zn peak is then integrated to obtain the charge which afterward produce a graph of the charge against the experiment number. As it can be observed from the Figure 6.11, the lowest charge recorded was 171.2 µC for the experiment number 2 and the highest 523.1 µC for the experiment number 3. There is not a strict trend in the variation of the values, fluctuations are observed, not in a certain order. The difference between the highest and the lowest charge is significant as it is roughly 350 µC.

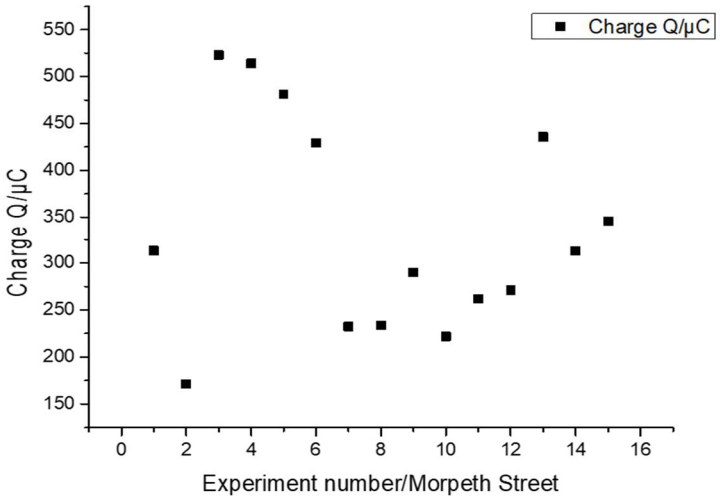

Figure 6.11: Estimated electric charge according to the experiment number for Morpeth Street samples.

From the charges estimated through integration of the stripping peaks and using calibrations curves generated in the previous chapter, the concentration of Zn is calculated. This concentration of Zn in the original sample is estimated and ranges between 0.191 µM and 0.584 µM based on the first calibration curve whereas with the average calibration curve figures between 0.203 µM and 0.619 µM. Figures 6.12 and 6.13 show these values in terms of graphs of the concentration versus experiment number. The same random tendency is still being observed.

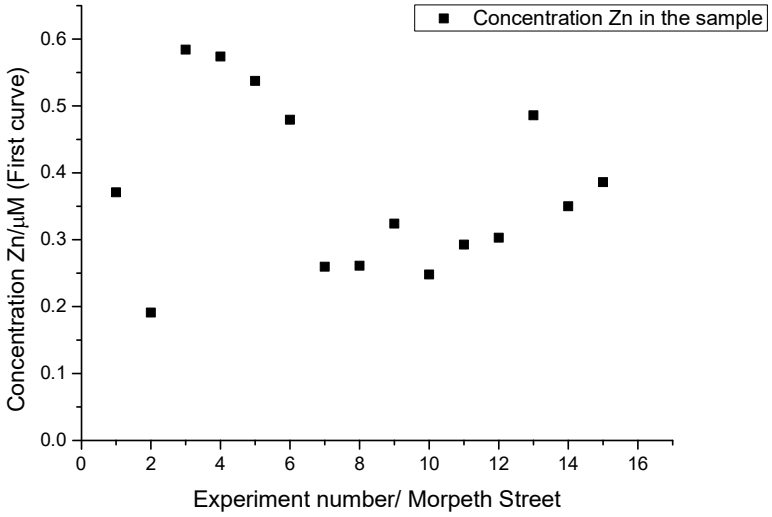

Figure 6.12: Concentration Zn (µM) in the original Morpeth Street sample based on the first calibration curve. Variation of the concentration per experiment based on the Zn first calibration curve Morpeth Street tap Water.

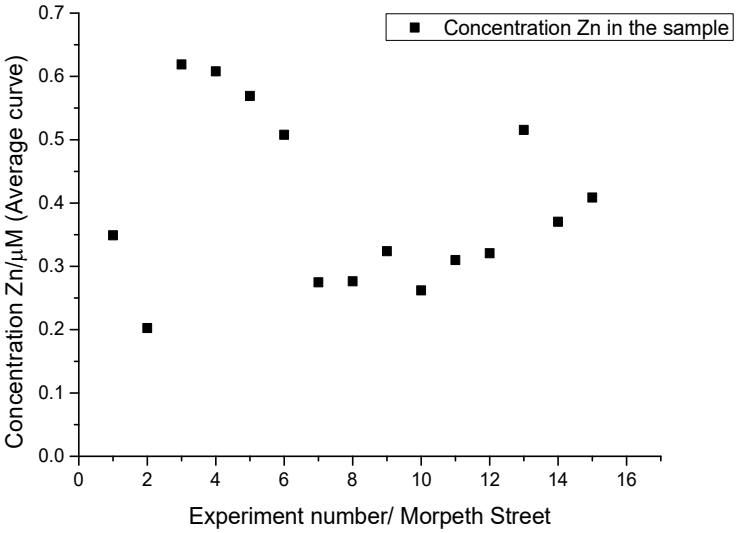

Figure 6.13: Concentration Zn (µM) in the original Morpeth Street sample based on the average calibration curve. Variation of the concentration per experiment based on the Zn average calibration curve Morpeth Street Tap Water.

The original concentration of Zn in terms of µg/L in this sample was also determined by using both calibration curve. Estimated concentration achieved with the first calibration curve is situated between 12.5 µg/L and 38.2 µg/L while with the average calibration curve 13.2 µg/L and 40.5 µg/L for the experiments number 2 and 3 respectively. Figures 6.14 and 6.15

represent the variation of the concentration in the original sample according to the experiment.

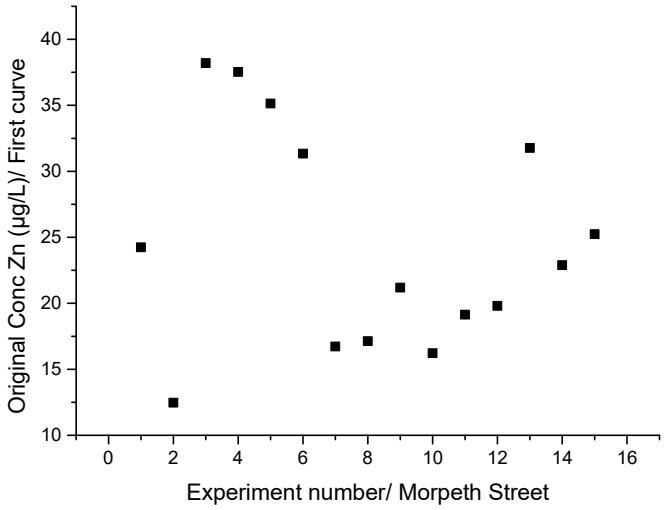

Figure 6.14: Concentration (µg/L) of Zn in the original Morpeth Street sample based on the first calibration curve. Variation of the original concentration (µg/L) per experiment based on Zn first calibration curve Morpeth Street tap Water.

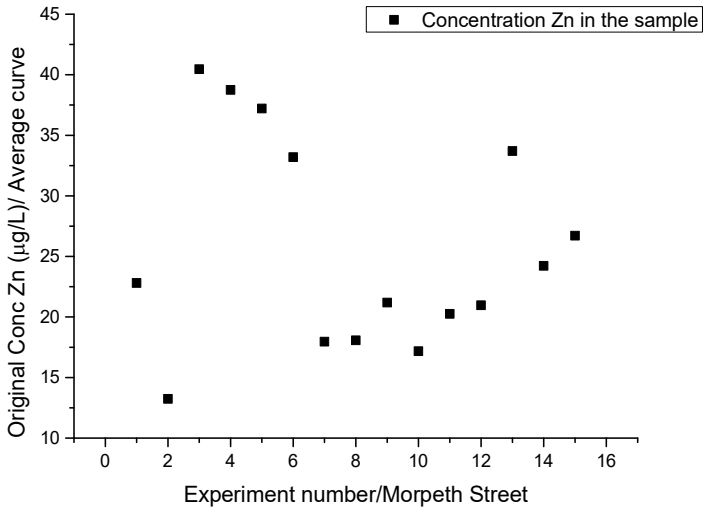

Figure 6.15: Concentration (µg/L) of Zn in the original Morpeth Street sample based on the average calibration curve. Variation of the original concentration (µg/L) per experiment based on the Zn average calibration Morpeth Street tap Water.

c) Full result tap water

According to previous statements and results, Zn is the only analyte detected in tap water for both collection points. The average result is then calculated alongside with the standard deviation. Comparing both results, although they are tap water, there is a large difference between them. It can be seen that the samples from Morpeth Street have showed a higher amount of Zn than the one from Stanton Street (As reported in Table 6.1). On the other hand, looking at the standard deviation values, it can be understood that the precision of the measurements is low – relative standard deviations of 30-50% are observed. It may be understable since the concentration at micromolar level are difficult to be measured reproducibly with higher precision. Table 6.1 presents a summary of the concentration of Zn in tap water.

Table 6.1: Summary of Zn concentration in tap water samples

Tap Water Sample		**Concentration Zn in the original sample**	
Collection point	Number of experiments	First calibration curve (µg/L)	Average calibration curve (µg/L)
Stanton Street	5	13.5±6.8	14.3±7.2
Morpeth Street	15	24.6±8.3	25.7±8.7

The frequency at which the highest and lowest points (charges) are observed raised some suspicion of a probable accumulation of the analyte on the surface or the residual analyte have not been completely removed from the electrode surface or the cell. On the other hand, it may be due to constant changes in the behaviour of the electrode.

6.3.2. Natural Water

Following the evaluation of tap water, the natural water was also collected for analysis purpose. Initially, three collection points were selected for the purpose: Blaydon Bridge, Blaydon Burn and Wylan. Stream water was collected and treated as done to the tap water samples.

However, due to insufficient result for statistical treatment, two of them have been found irrelevant namely Blaydon Bridge and Wylan.

a) Blaydon Burn

Blaydon Burn (54.963438, -1.729336) – Local stream, high flow due to rainfall. Historically, the adjacent road was used as a major transport route for coal. Also, collection site is downstream from two landfill sites, one of which is currently active.

Figure 6.16: Blaydon Burn collection point.

This sample was pre-treated as was the tap water, that means, filtered and pH adjusted with acetate buffer pH=4.5. The aliquot taken to the cell was still 50 mL. However, in this case peaks shifts are not accentuated as in the case of tap water (-1.4V to -1.2V vs. Calomel (1M KCl)) as seen in Figures 6.17 and 6.18 below.

Nine experiments were realized with this sample, multiple Bi peaks are again present as observed for the tap water (Figure 6.17 and 6.18).

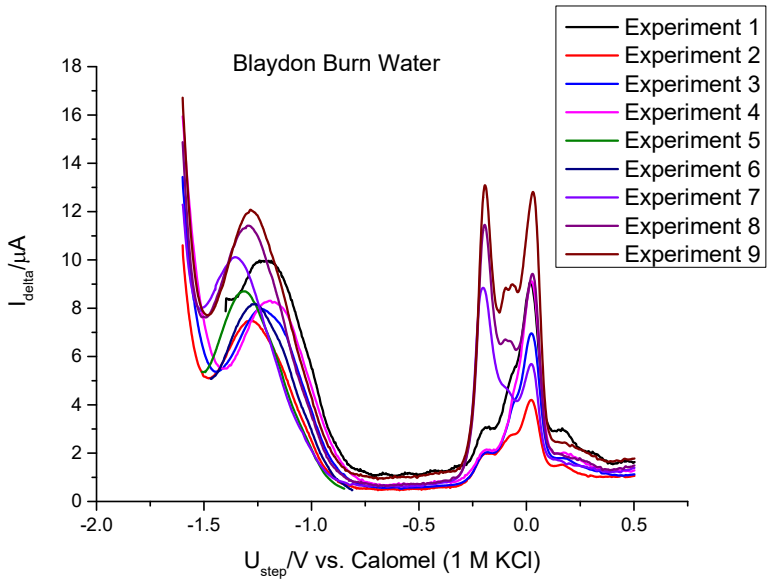

Figure 6.17: Stripping voltammetry Blaydon Burn sample, deposition potential= -1.4 V vs. Calomel (1 M KCl), deposition time: 10 min, quiet time: 20 s; DPV parameters: E_i= -1.6 V to E_v= -0.5 V vs. Calomel (1 M KCl), P_H (pulse height): 50 mV, P_W (pulse width): 50 ms, S_H (step height): 2 ms and S_T (step time): 200 ms.

It can be observed that, Zn peaks (near -1.3 V) are shifted although not accentuated as in the case of tap water. Moreover, all the peaks start at different potentials and The Bi peaks also are not uniform as they have different heights and positions.

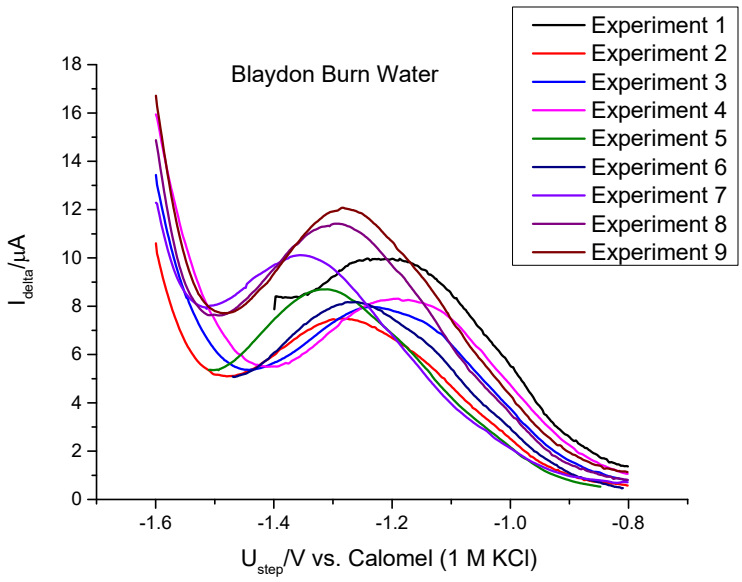

Figure 6.18: Stripping Zn peaks from Blaydon Burn sample, deposition potential= -1.4 V vs. Calomel (1 M KCl), deposition time: 10 min, quiet time: 20 s; DPV parameters: E_i= -1.6 V to E_v= -0.5 V vs. Calomel (1 M KCl), P_H (pulse height): 50 mV, P_W (pulse width): 50 ms, S_H (step height): 2 ms and S_T (step time): 200 ms.

Nine experiments were executed with this sample, looking at the Figure 6.19 (charge vs experiment number) which depicts the variation of the charge against experiment number, it can be seen that it varies from 107 µC to 194 µC. The variation between the highest and the lowest value of the charge, is much smaller than in the case of the tap water. This may indicate the proximity among values; thus, a higher precision. There is not a defined trend on the variation as it was the case for the tap water samples. The Figure 6.19 (charge vs. experiment number) illustrates this behaviour as a fluctuation variation.

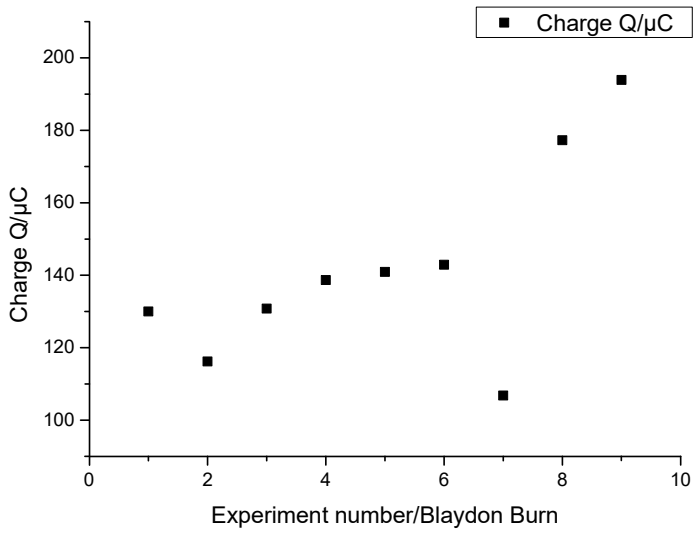

Figure 6.19: Estimated electric charge according to the experiment number for Blaydon Burn sample.

The Figures 6.20 and 6.21 present the variation of the concentration according to the experiment number according to the use of both calibration curves, showing a low difference among the values. The estimated concentration of Zn in the original sample while using the first calibration curve, the lowest value corresponds to 0.119 µM and the highest to 0.217 µM; based in the average calibration curve 0.126 µM and 0.229 µM are estimated for the lowest and the highest respectively. The concentration estimated for this sample is represented in the Figures 6.20 and 6.21 (concentration vs. experiment number) using both the first and average calibration curve.

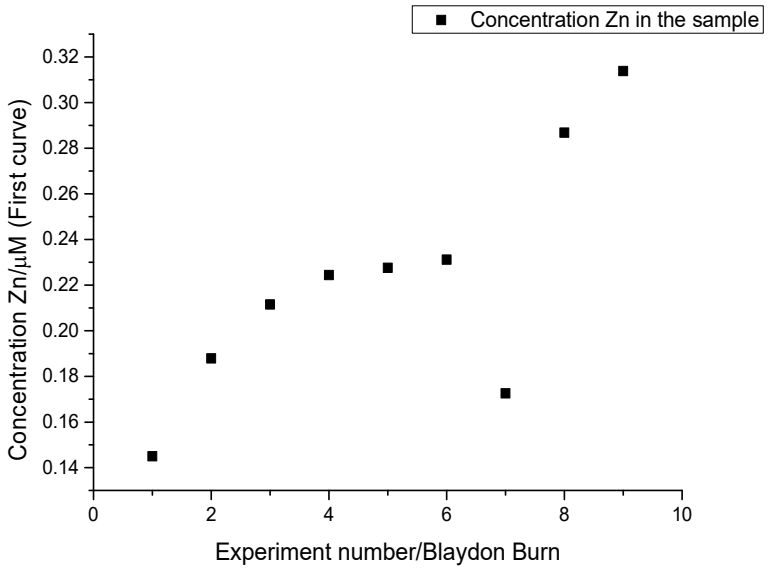

Figure 6.20: Concentration Zn (μM) in the original Blaydon Burn sample based on the first calibration curve. Variation of the concentration per experiment based on the Zn first calibration curve Blaydon Burn Water.

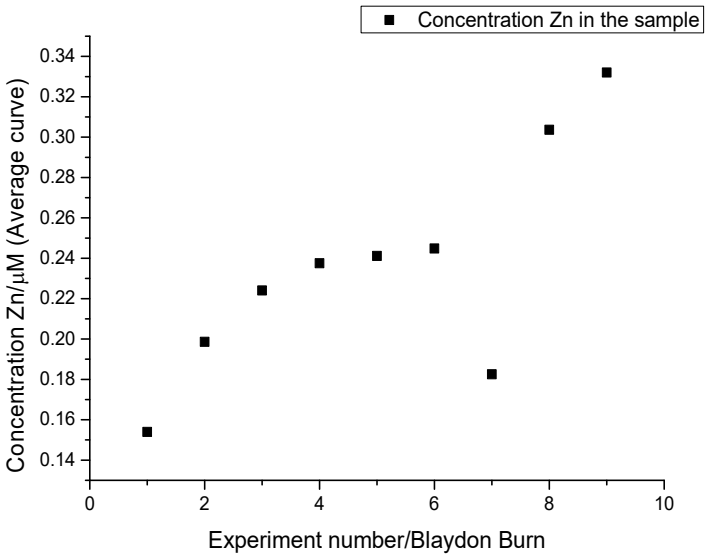

Figure 6.21: Concentration Zn (μM) in the original Blaydon Burn sample based on the average calibration curve. Variation of the concentration per experiment based on the Zn first calibration curve Blaydon Burn Water.

As the concentration in the original concentration (in µg/L) is utterly important to be estimated, the Figures 6.22 and 6.23 illustrate the referred values showing its highest 20.5 µg/L and 9.5 µg/L as the lowest based in the first calibration curve, for the average calibration curve the highest and the lowest value estimated are 10.1 µg/L and 21.7 µg/L respectively.

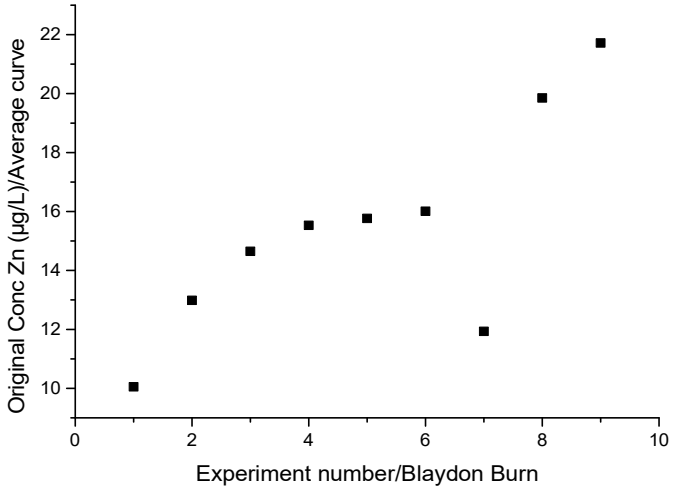

Figure 6.22: Concentration (µg/L) of Zn in the original Blaydon Burn sample based on the average calibration curve. Variation of the original concentration (µg/L) per experiment based on the Zn average calibration curve Blydon Burn sample.

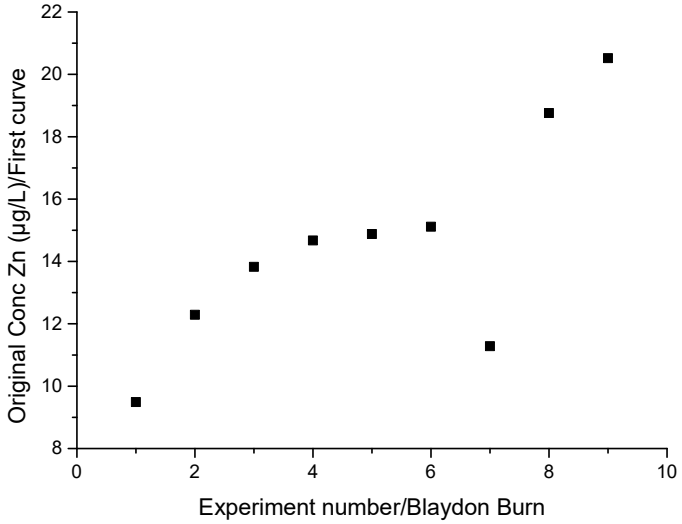

Figure 6.23: Concentration (µg/L) of Zn in the original sample Blaydon Burn based on the first calibration curve. Variation of the original concentration (µg/L) per experiment based on the Zn first calibration curve Blaydon Burn sample.

b) Blaydon Bridge

As referred earlier, another collection point was Blaydon bridge (54.965731, -1.688271) – Sample from the River Tyne at high flow due to heavy rainfall. Due to some circumstances, only two experiments could be executed, which means it is insufficient for statistics. The accessibility to the site has constituted an issue due to the limited knowledge of the region. On the other hand, a considerable part of the sample has been lost during failed experiments caused by equipment's and instrument's failures. This location is known for being a former industrial area, therefore, it was expected to contain a considerable amount of the metals in study. The sample was collected manually using sampling bottles attached to a cord as to reach a at least a metre of depth. Figure 6.24 shows the site where the sample was collected.

Figure 6.24: Blaydon bridge collection point

The Figure 6.25 below presents the stripping voltammogram of both experiments realized for the sample from Blaydon Bridge. These curves were integrated, and the concentration of Zn was also estimated using the calibration curves demonstrated in the previous chapter.

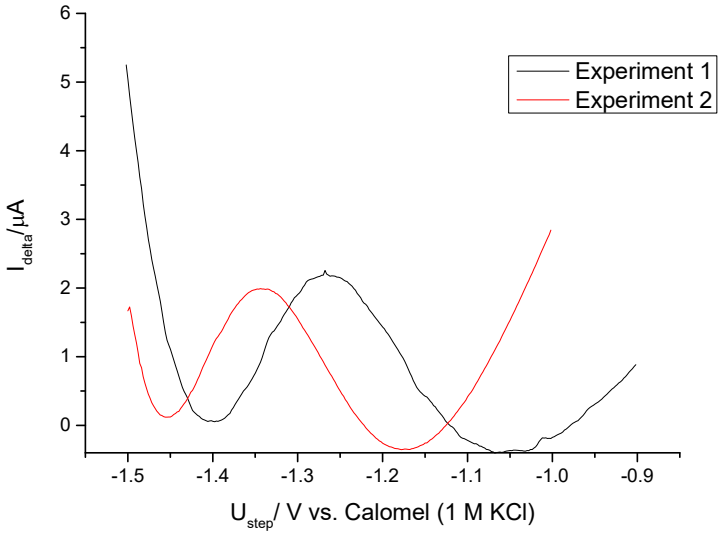

Figure 6.25: Stripping Zn peaks Blaydon Bridge sample, deposition potential= -1.4 V vs. Calomel (1 M KCl), deposition time: 10 min, quiet time: 20 s; DPV parameters: E_i= -1.6 V to E_v= -0.5 V vs. Calomel (1 M KCl), P_H (pulse height): 50 mV, P_W (pulse width): 50 ms, S_H (step height): 2 ms and S_T (step time): 200 ms.

c) Full results natural water

A closer look onto all the results of these experiments for natural water can be seen in the Table 6.2 below. The Blaydon Burn results are more reliable than the one from Blaydon Bridge due to a limited number of successful samples analysed, as numerous reasons such as accessibility constituted an issue. It can also be observed that the precision is higher than the result obtained from the tap water samples for reasons that are unclear. The closeness between the values observed is significant compared to tap water results, as it can be observed by the value of the standard deviation.

Table 6.2: Summary of Zn concentration in natural water samples

River Sample		Concentration Zn in the original sample	
Collection points	Number of experiments	First calibration curve (µg/L)	Average calibration curve (µg/L)
Blaydon Bridge	2	5.9±0.5	6.3±0.5
Blaydon Burn	9	14.5±3.5	15.4±3.7

6.3.3. ICP-MS and ICP-OES results

The electrochemical results through calibration curves needed to be compared to independent analytical measurements in order to assess the reliability of the technique and the approach developed in this work. Due to the high accuracy and sensitivity of the spectrometric techniques of mass and atomic spectrometry, ICP-MS and ICP-OES were chosen as comparison techniques. The samples filtered were taken to the analytical laboratory located in the Devonshire Building (Newcastle University) for analysis.

Figures 6.26 and 6.27 illustrate a comparison between ICPs (ICP-OES and ICP-MS) and the electrochemical results according to each calibration curve used. It can be observed that all the results are in the same order of magnitude. Even though, at some point, there is a small difference among three set of results.

However, ICP-OES and ICP-MS results have shown different trends compared to the electrochemical results. ICP-OES values obtained are lower than ICP-MS, as it is also known ICP-MS is extremely sensitive. Overall, electrochemical results are relatively higher than those from ICPs. Except for Stanton Street sample which is slightly lower in the electrochemical results than in ICP-MS results.

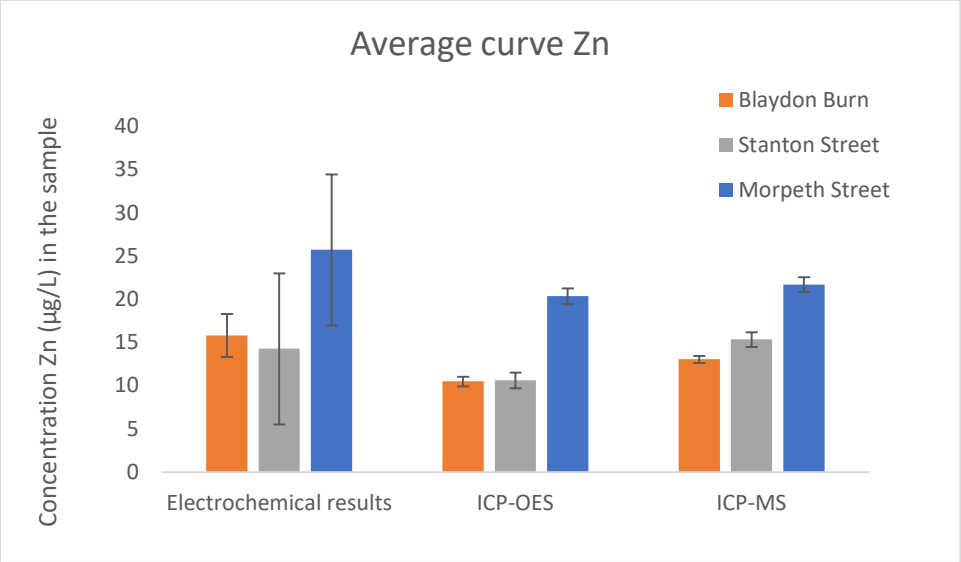

Figure 6.26: Comparison average calibration curve and ICP results (the error bars represent the standard deviation).

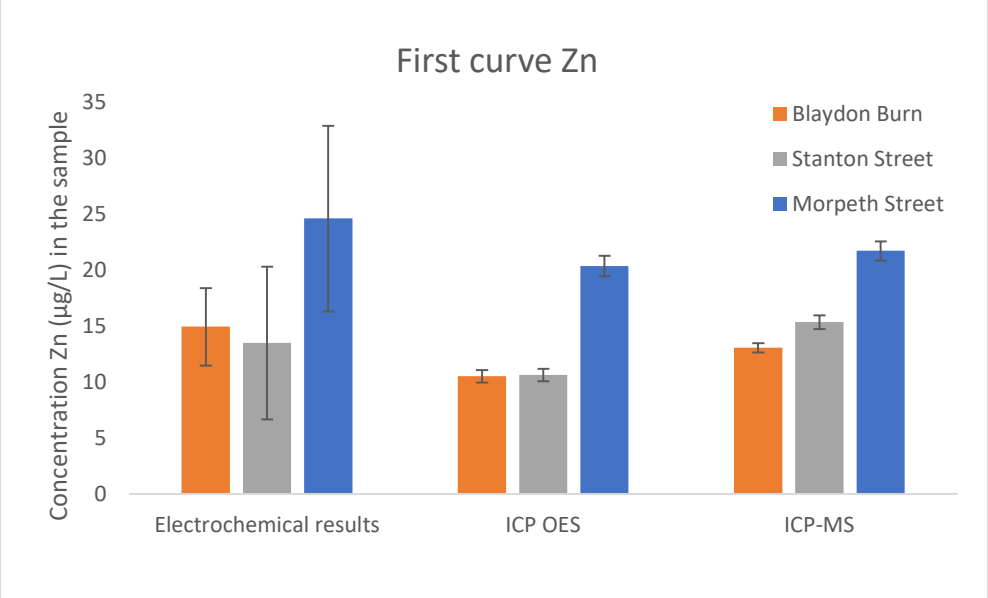

Figure 6.27: Comparison first calibration curve and ICP results (the error bars represent the standard deviation).

6.3.4. Standard Addition of Zn

The standard addition method is used alternatively to verify the results obtained using the calibration curve and to evaluate the matrix effect. This evaluation was only done based on the type of samples, that means natural and tap water. Two sample collection points were used: Blaydon Burn and Morpeth Street for natural and tap water, respectively. Due to time shortage, it wasn't possible to perform the standard addition for all the samples mentioned earlier.

As explained in Chapter 3, the standard addition procedure for this work was executed as follows: the aliquot taken was 50 mL from the sample. Six flasks were prepared, and crescent volumes of Zn (II) added into the flask. Each flask contained 50 mL of the sample alongside with crescent volume of Zn. Volumes added 100, 200, 300, 400 and 500 µL of 1 mM Zn (II) to each flask and then filled until the mark of the flask of 100 mL. The rest in the flask was filled with 0.1 M acetate buffer pH 4.5.

a) Morpeth Street Tap Water

The tap water sample collected from Morpeth Street located in Spital Tongues. The same sample used in calibration curve calibration method. Treatment sample is maintained the same as explained earlier. 50 mL are taken from the volumetric flask after preparation

mentioned earlier. A closer look at the voltammogram, Zn peak shift is smaller than observed in case of calibration curve, from nearly -1.37 V to -1.1 V versus calomel (1 M KCl). The Figure 6.28 and 6.29 present the stripping voltammogram for the sample of this collection point.

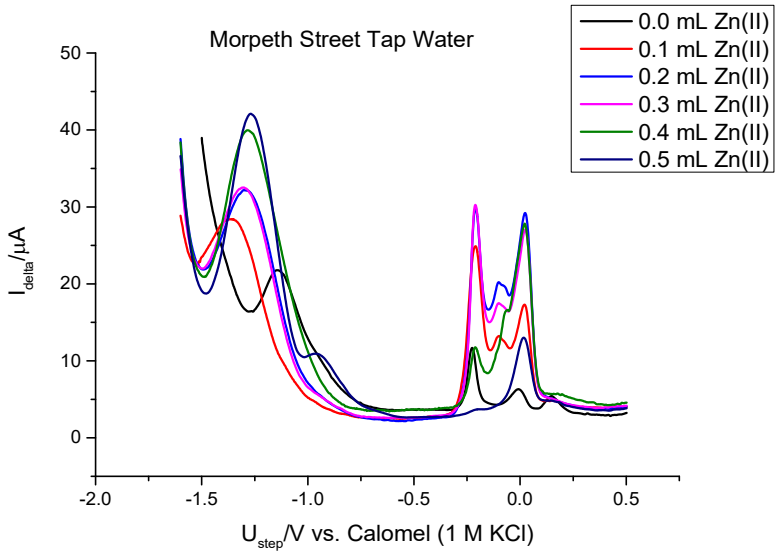

Figure 6.28: Stripping voltammograms of Morpeth Street tap water for standard addition, deposition potential= -1.4 V vs. Calomel (1 M KCl), deposition time: 10 min, quiet time: 20 s; DPV parameters: E_i= -1.6 V to E_v=-0.5 V vs. Calomel (1 M KCl), P_H (pulse height): 50 mV, P_W (pulse width): 50 ms, S_H (step height): 2 ms and S_T (step time): 200 ms.

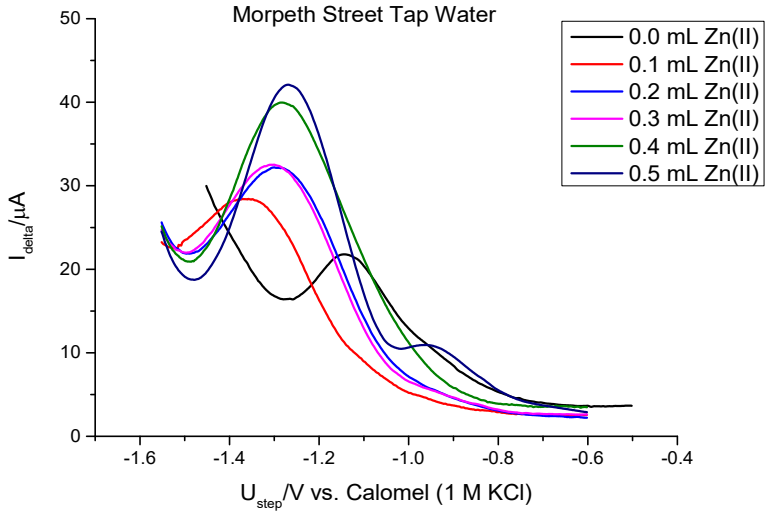

Figure 6.29: Stripping Zn peaks Morpeth Street tap water for standard addition. Deposition potential= -1.4 V vs. Calomel (1 M KCl), deposition time: 10 min, quiet time: 20 s; DPV parameters: E_i= -1.6 V to E_v= -0.5 V vs. Calomel (1 M KCl), P_H (pulse height): 50 mV, P_W (pulse width): 50 ms, S_H (step height): 2 ms and S_T (step time): 200 ms.

Zn peaks are normally expected to appear at -1.4 V, however in case of samples shifts are observed to roughly -1.1 V. As per the literature, the standard addition curve does not pass through the origin as it is required for standard addition. The curve generated from the charge obtained through integration of the stripping peak, the correlation obtained from this curve is 0.985 as seen in the Figure 30. It seems to be acceptable for analytical purposes.

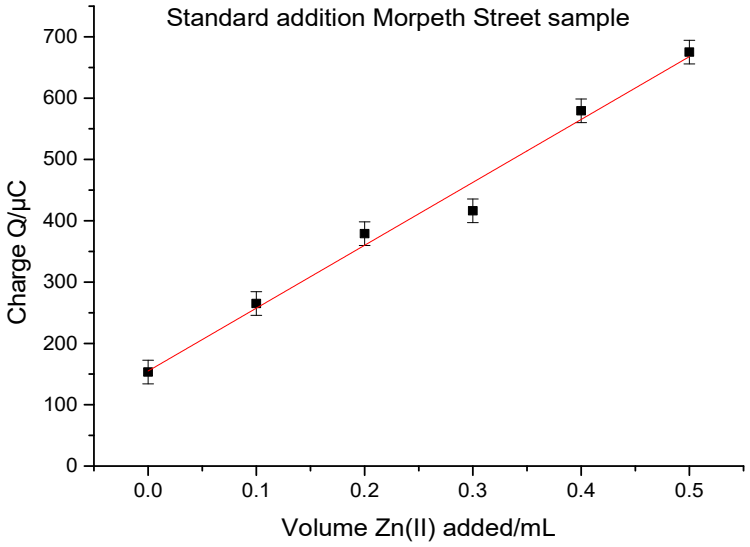

Figure 6.30: Standard addition curve for Morpeth Street sample (the error bars represent the standard error of the intercept).

b) Blaydon Burn

The second sample employed for the standard addition was a natural water sample from Blaydon Burn collection point, this natural water sample was used in calibration curve as well. Surprisingly, the charges registered are significantly higher than those registered for the calibration curve for both the Morpeth Street sample and Blaydon Burn. Moreover, Zn peak currents are also higher, which may be also evidence of a matrix effect. Although, the cell has been cleaned as well as the electrode to prevent any contamination. So, the Figures 6.31 and 6.32 show the stripping voltammograms for this sample. Remembering that the additional volumes added for the execution of the standard addition are small, then it was not expected for a significant difference in the values of the charges as observed.

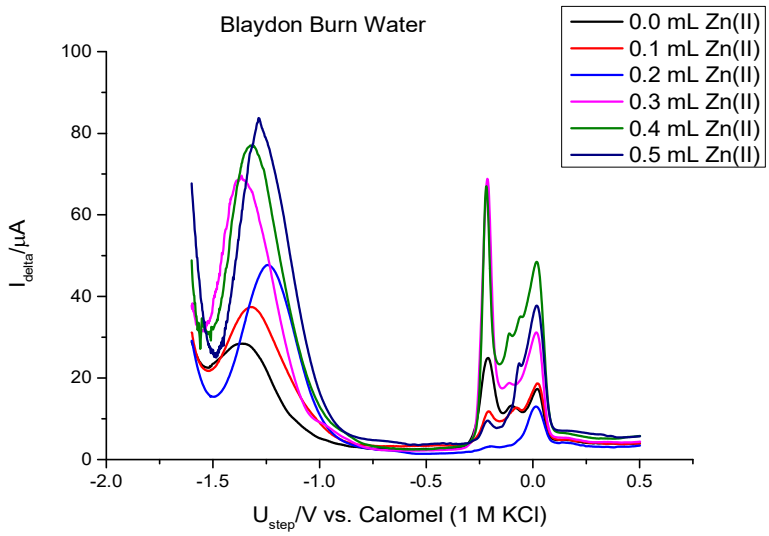

Figure 6.31: Stripping voltammogram Blaydon Burn water for standard addition. Deposition potential= -1.4 V vs. Calomel (1 M KCl), deposition time: 10 min, quiet time: 20 s; DPV parameters: E_i= -1.6 V to E_v= -0.5 V vs. Calomel (1 M KCl), P_H (pulse height): 50 mV, P_W (pulse width): 50 ms, S_H (step height): 2 ms and S_T (step time): 200 ms.

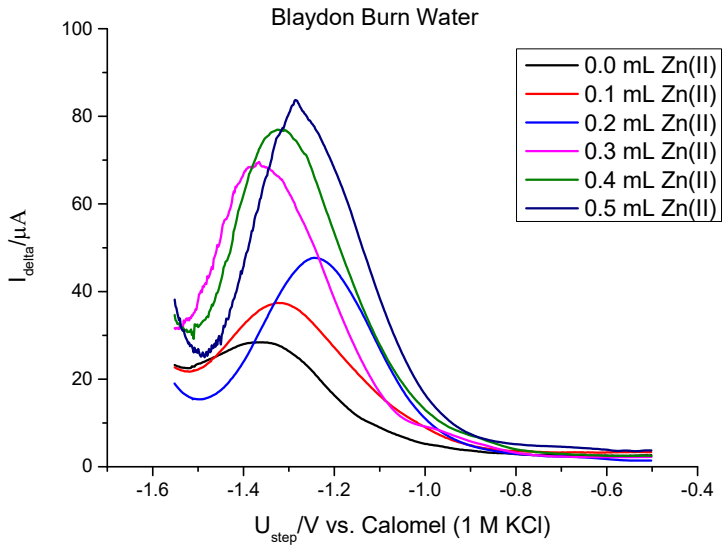

Figure 6.32: Stripping Zn peaks Blaydon Burn water for standard addition. Deposition potential= -1.4 V vs. Calomel (1 M KCl), deposition time: 10 min, quiet time: 20 s; DPV parameters: E_i= -1.6 V to E_v= -0.5 V vs. Calomel (1 M KCl), P_H (pulse height): 50 mV, P_W (pulse width): 50 ms, S_H (step height): 2 ms and S_T (step time): 200 ms.

The curve produced does not pass through the origin as it is in the case for standard addition graphs, a correlation of 0.982 is obtained as it can be observed in Figure 6.33.

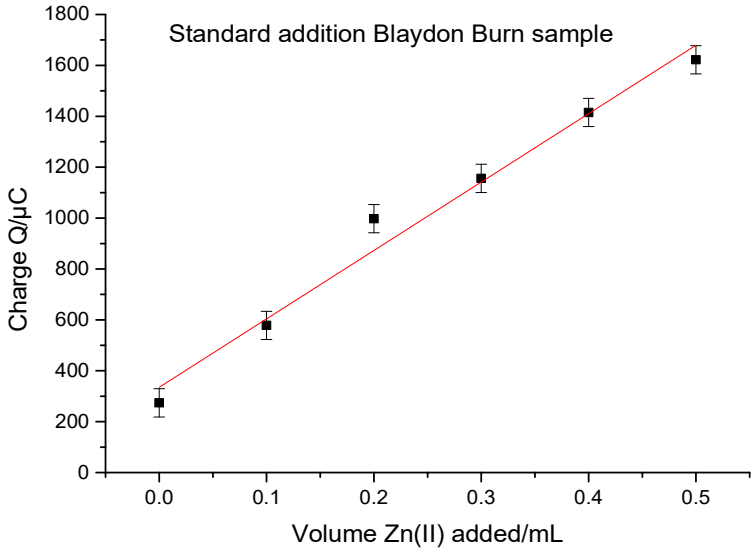

Figure 6.33: Standard addition curve Blaydon Burn sample (the error bars represent the standard error of the intercept).

C) Results Standard Addition

It was observed that the charges recorded for the standard addition are considerably higher than those from calibration curve. Despite the behaviour reported earlier, the concentration of Zn was estimated and was close to the values found in calibration curve as illustrated in Table 6.3. Another consideration is the fact of recording the slope of four digits and an intercept of a three figures value.

Table 6.3: Summary of Zn concentration in samples using standard addition

Sample	Concentration Zn (µg/L) in the original sample based on standard addition
Morpeth Street	19.8±1.59
Blaydon Burn	16.3±1.23

The standard addition experiments were done for only two samples, one of each type. Then, both standard addition curves obtained when compared as in Figure 6.34. Correlating both

curves for standard addition, it can be observed that natural water Zn peaks have showed higher values of charge than tap water, this may be due to the complexity of the matrix.

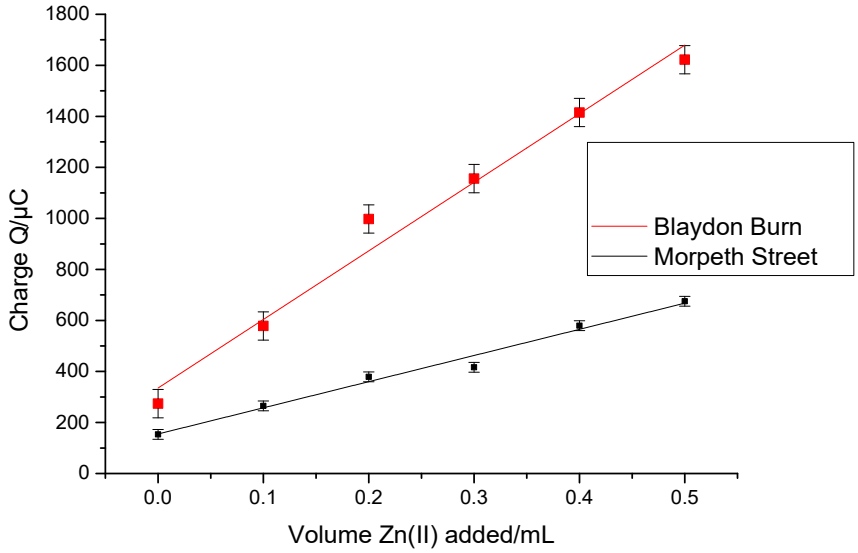

Figure 6.34: Standard addition curves Blaydon Burn and Morpeth Street. The error bars refer to the standard error of the intercept.

Besides, even the regression data follow the same tendency when looking at the values of the intercept and the slope as observed in Table 6.4.

Table 6.4: Regression analysis standard addition curves from Figure 6.34.

Equation	Y=a+bx			
	Blaydon Burn		Morpeth Street	
Residual Sum of squares	23530.8		2833.2	
Pearson's r	0.991		0.992	
Adj. R-Squares	0.977		0.981	
	Value	Standard Error	Value	Standard Error
Intercept	335.03	55.5	154.96	19.3
Slope	2688.4	183.3	1025.6	63.6

6.4. Comparison of the results from electrochemistry, ICP-OES and ICP-MS.

Throughout this work, the electrochemical results obtained through calibration curve has fulfilled the objective of the research. Because of the necessity to prove its reliability and accuracy, it is important to compare to other techniques such as ICP. Apart from that, standard addition is also necessary not only as a manner to compare with those obtained from calibration curve but also to assess the matrix effect.

The figures 6.35 and 6.36 illustrate the comparison between electrochemical results (either calibration curve or standard addition) and spectrometric techniques (ICP-OES and ICP-MS). These figures are represented in comparison based in the calibration curve used for the calculation. In both cases, it can be seen that all the results are in the same order of magnitude. Though, the values of Zn concentration vary between 11-26 µg/L.

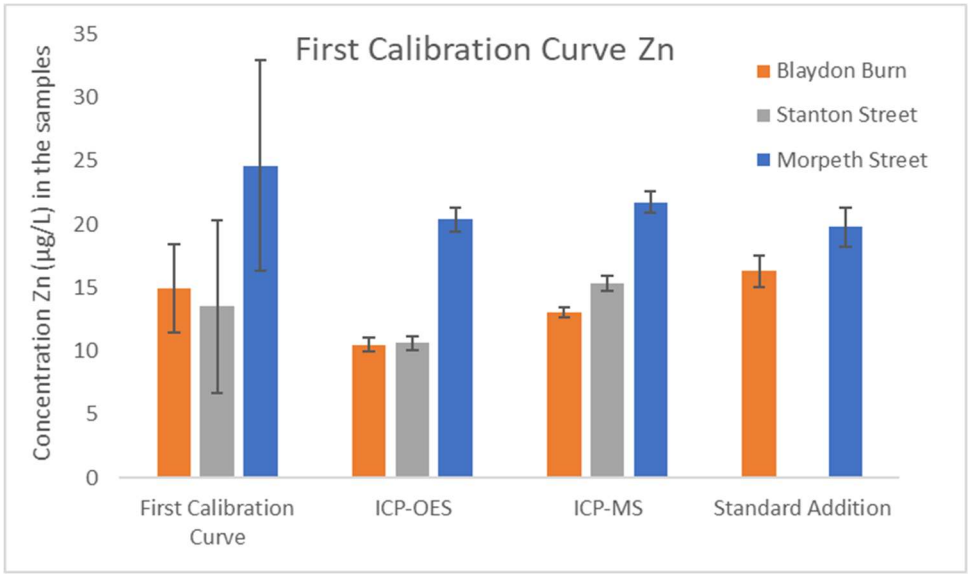

Figure 6.35: Comparison first calibration curve, standard addition and ICPs results. The error bars represent the standard deviation for calibration curve, ICP-OES and ICP-MS results, and standard error for standard addition results.

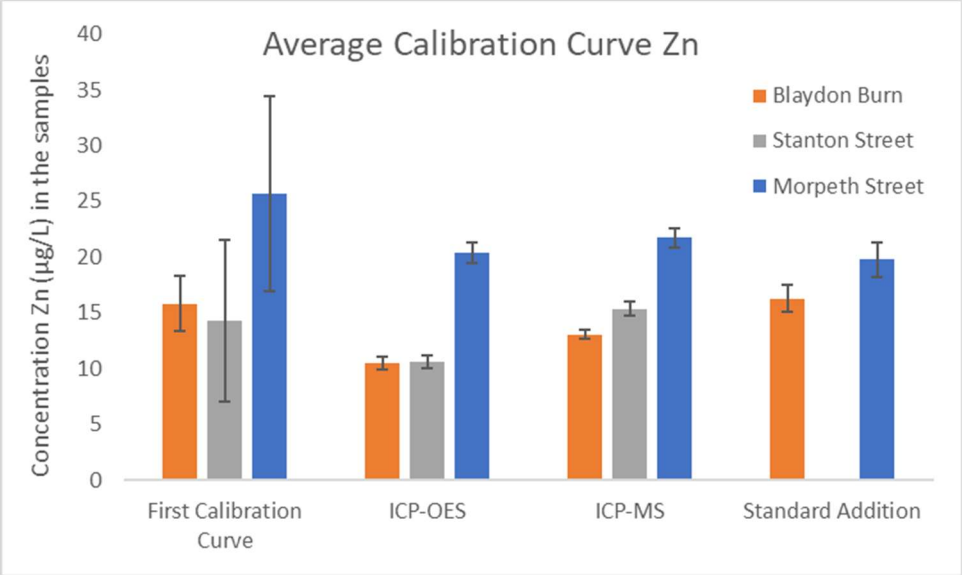

Figure 6.36: Comparison average calibration curve, standard addition and ICPs results. The error bars represent the standard deviation for calibration curve, ICP-OES and ICP-MS results, and standard error for standard addition results.

The t-test (Student's test) was used to compare statistically the electrochemical results (specifically from calibration curves) with ICPs. the test t (at 95% confidence) determine if there is a significant difference between the means of two groups of results. Concerning calibration curve results and ICP-MS, the full results of this test are found in the Appendix section, Appendix A and Table A.2; t-test value was estimated for both groups of results obtained from the first and average calibration curve, the t values obtained indicate that the difference is considered not significant, this observation refers to the results from all three samples mentioned throughout this work, namely Stanton Street, Morpeth Street and Blaydon Burn. On the other hand, the comparison between ICP-OES and electrochemical results (calibration curve results) has showed a slightly different direction (trend). In Appendix section of this work, Table A.1 illustrates t-test values estimated for the comparison of these two groups of results, calibration curve results from tap water samples (Stanton Street and Morpeth Street) have provided a t value that indicates the difference is considered to be not significant, while t-test value obtained from the first calibration curve result of Blaydon burn sample has revealed that the difference is not quite significant and with its average calibration curve result the difference is considered to be very significant.

6.5. Summary

In this chapter, samples results were examined based on Chapter 5 approach developed. In that chapter, two calibration curves were produced, then they are thought to be used for sample determination. Initially, the main target is to detect and quantify metals namely Zn (II) and Pb (II). However, a series of samples were collected from tap and natural water. As it is known, Pb was not expected to be found in tap water as it is harmful to humans and, it is probably removed during the treatment before reaching household. Thus, samples from the tap water have not shown any Pb peaks. Unexpectedly, samples from natural water collection points included in this work, also have not detected Pb peaks, it is unclear the reason for such situation, it may be due to the fact of Pb contained in the sample is lower than the range of concentration studied in this research. It may be thought that the concentration of Pb in the sample could be below 1.17 µg/L, which is the limit of detection established according to the conditions of this research.

The cleanliness of the surface is important as mentioned in the previous chapter. The extensive cleanliness implemented in that chapter is maintained for each sample stripping as well.

Moreover, the number of experiments executed for each sample was done according to the availability and accessibility. The pre-treatment of the samples by filtration is crucial as to remove any particle that can affect the analysis, as well as proportionate the appropriate medium to produce Bi film (pH adjustment to pH=4.5 with Acetate Buffer).

Zn peaks in the sample have reported shifts in their potential. Normally, Zn peaks should appear at -1.4 V vs. Calomel (1 M KCl). Accentuated shifts have been observed for tap water than in natural water. Bi peaks observed showed the same behaviour than in the case of the samples, that means, multiple peaks and variation in peak heights intensity.

The electrochemical results obtained through calibration curve are approximate to the those from ICPs, that were used as a comparative technique. All the results figure in the same order of magnitude. In addition to that, there is not a significant difference between calibration curve results and ICPs one which was confirmed by t-test values displayed in the Appendix section (Appendix A) of this work.

Unexpectedly, tap water results are greater than natural water. That means, overall Zn quantity determined in treated water (tap water) is relatively higher than in natural water. The greatest concentration was recorded with Morpeth Street samples, which is tap water. It was estimated 24.6±8.3 when used the first calibration curve and 25.7±8.7 when used the second calibration curve. This result contradicts the predictions, natural water was expected to present higher amount of Zn since the collection points selected are historically known to be an industrial area.

Standard addition was also used a complementary calculation method to compare with calibration curves. Although, it was only realized with one sample of each type. Morpeth Street and Blaydon Burn submitted to this method; the test t was also executed as confirmed in Appendix section, Table A.3, t-test values obtained from both groups of results, either from the first or the average calibration curve have demonstrated that the difference between the results is not significant. Standard addition intercept and slope are large compared to the calibration curve as well as the values of the peak currents. This may be considered as evidence of the matrix effect.

The precision of the technique is demonstrated by looking at the values of the standard deviation, which are acceptable. The coefficient of variation defined as a ratio of the standard deviation to the mean, shows the extent of variability in relation to the mean of the results, the higher the coefficient of variation greater the dispersion; thus, it can be used to evaluate the precision of the technique. The coefficient of variation estimated are 0.3, 0.5, 0.2 for Morpeth Street, Stanton Street and Blaydon Burn respectively for both first and average calibration curve results. A low variance is observed, then it can be reported that, despite having observed several irreproducibility issues, a good precision was attained. Besides, in the Appendix B, Figure B.1 and B.2 present the comparison of the calibration curve results with standard additions in which the errors bar are the standard deviation of each result for the calibration curve results and standard error for the standard addition results. In short, the results obtained through ASV can be considered reliable and accurate since similar results are obtained when using comparison techniques such as ICPs.

Chapter 7: Discussion

All the research realized throughout have as a purpose the detection and quantification of metals as Zn and Pb for environmental samples as water stream and tap water using Bi modified electrode through stripping voltammetry. The objective of choosing this technique is because of its cost effectiveness, the conventional techniques instruments such as AAS and ICP used for this purpose are extremely expensive. Another reason is the fact that many literatures suggest this technique (ASV with Bi-modified electrodes formation) due to its good reproducibility and low detection limit [50,94,99,181]. However, all through this work some of these advantages have not been observed for instance the reproducibility.

Glassy carbon was selected and employed as the working electrode material in this work. When the glassy carbon was characterized, some irregularities were revealed in terms of its roughness factor. The change in the electrode behaviour was consistently observed and several techniques employed to determine the roughness factor showed different apparent roughness values. The roughness factor was determined using two methods, both applying the Randles-Sevcik equation in the analysis of the data from cyclic voltammograms of hexacyanoferrate (II). However, the results of the first method which is the direct application of the Randles Sevcik equation, showed apparent roughness factor values below 1. On the other hand, when using a recalibration technique which consists in the application of the hydrogen adsorption/desorption at Pt to make accurate surface area and diffusion coefficient estimates, roughness factor values between 1 and 2 were found. The latter results are more reliable, and the magnitude of the roughness factors are of the expected order for glassy carbon electrodes. The electrodeposition of Bi was executed through chronoamperometry and potential cycling. In the first instance, during calibration curve trials, the electrodeposition potential was carefully chosen for each analyte separately, according to the reference electrode employed. Still, the Bi electrodeposited is characterized microscopically by optical microscopy, AFM, SEM and EDX as described in Chapter 5, Bi has exhibited a non-uniform distribution and a large amount of oxygen observed on the surface. Furthermore, this was validated while using XPS which demonstrated that the surface of the electrode is coated with a surface oxide, Bi_2O_3. Under the conditions applied in this work for the

electrodeposition, it was confirmed that although the elemental Bi is deposited, the surface layers showed Bi photoelectron spectra characteristic of the Bi(III) oxide, Bi_2O_3. Although the electrodeposition step was performed in a nitrogen atmosphere which was being purged throughout the experiments. The deposition step approach used in this work is similar to the one suggested in reference [102]; this procedure expects to have the elemental Bi deposited predominantly on the surface instead of Bi_2O_3, even though according to Wang in reference [181] the Bi-film is projected not to be homogeneous and with a range of morphologies present, this may be due to the impossibility of a solid surface to provide a defect free, pristine surface [24]. The non-homogeneous electrodes surfaces, adsorption, or interaction between two metals co-deposited on the surface of the solid electrode (glassy carbon in this case) can also be included as sources of irreproducibility [182].

The detection of both analyte Zn and Pb were both studied in this work, in Chapter 5 the stripping analysis of Zn was observed through deposition type used. At the beginning of the studies, different reference electrodes were tested, before reaching a conclusion and select the most appropriate for the calibration curve procedure. So, the first reference electrode to be used was MSE (1M H_2SO4), which provided the first impression (insight) on the deposition potential set up as -1.6 V, at this potential Zn peak could be observed. However, this reference electrode was found unsuitable due to the occurrence of a secondary reaction on account of the high protons' concentration, that included Zn being reduced to the metallic form and depositing on to the counter electrode (Au wire). Because of this behaviour, it was essential to replace with another reference electrode that would not produce such reaction. Then, MSE (K_2SO_4, sat'd) is selected for further analysis as well as Calomel (1 M KCl). Since the peak height is influenced by several factors, one of them is the addition of the electrolyte to increase the ionic strength, consequently, to enhance the peak height. Though, two mixtures of supporting electrolyte were prepared through the addition of 1 M Na_2SO4 and 1 M $NaClO_4$ respectively and, then used, reminding that the principal supporting electrolyte used from the beginning of this work was 0.1 M acetate buffer pH 4.5. In both cases, Bi is electrodeposited under ex-situ deposition using chronoamperometry and cycling potential in stirred and unstirred conditions. Normally, highest peaks mean the retention of considerable amount of the analyte on the electrode surface, then its stripping eventually. Another factor is the stirring conditions, as detailed in chapter 5, the literature explains that the convection

increase the mass transport of the species, therefore, the stirring has produced highest peaks, detecting large amount of the analyte over the case of unstirred conditions [12.182]. According to the results shown in Chapter 5, section 5.2.2.1.1. the mixture of acetate buffer with Na_2SO_4 showed consistent good performance over the one with $NaClO_4$, as the latter only proved to be a stripping peak enhancer (through the increase of the ionic strength) when the substrate was GC Bi-modified ex-situ using cycling potential under stirring conditions. Peak potential shifts have been reported during this study; this may be due to the dependence of the peak potential on the ion metal concentration in this case Zn(II) or the kind of intermetallic complex compound that may be produced on inert solid electrodes [144]. As a recommendation, this study is preferable to be done when the objective is to focus only on Zn detection and quantification in a sample, since it is not suitable for a simultaneous determination of Zn and Pb because of the formation of insoluble salts with Pb under the experimental conditions used in this work.

The behaviour of the electrode has been an issue during this research as the electrode has shown a large extent of irreproducibility problem. This irreproducibility problem affects the result in terms of precision of the technique, it could be observed from the calibration curve in the case of Zn where two calibration curves were produced. The first Zn calibration curve provided r = 0.979 (r: correlation coefficient), while the second curve showed r = 0.886, a loss of sensitivity can be confirmed. The stripping voltammogram for the second curve shows certain information that does raise an awareness, observing Figure 5.23 in Chapter 5, section 5.2.2.2.1, Zn peak height registered for 5 µM is higher than the one of 6 µM, its charge is bigger than the one of its predecessor as well. In the second Zn calibration curve, the charges of the standards are not well distributed, the difference between the charges expected and those obtained is quite significant. Though, there is a good peak distribution for the standards in the first Zn calibration curve than in the second as seen in Figure 5.20 in Chapter 5, section 5.2.2.2.1. This may indicate that during the procedure of the second Zn calibration curve, the sensitivity of the electrode was strongly affected. Observing the second Zn calibration curve regression data, a decline in terms of correlation coefficient is also observed. So, that means repeated measurements could not provide the approximate values of the charge, thus, affecting the precision of the results. Furthermore, this behaviour was observed in the samples evaluation, the variation of the charges values of the analyte peak (Zn) for each

sample illustrated in Chapter 6, has showed a noticeable degree of dispersion which may be confirmed by the values of the standard deviation reported, for example in the case of Morpeth Street sample, it was estimated 8.3 and 8.7 using the first and average Zn calibration curve respectively.

The real reasons of this irreproducibility problem are the main concern that need to be clarified. Economou [50], Pauliukaite, et al [144], and Krolicka, et al [110] have studied Bi_2O_3 modified electrodes, these electrodes exhibit some problems in ASV of metal ions. Some of those problems include the low linearity and shifts in stripping peaks to a less negative potentials, which occurs weakly with Pb and strongly with Zn as suggested in [144]. Besides, Bi_2O_3 modified electrodes are known to provide large non-zero intercepts (sometimes slightly negative intercepts as well) in the calibration plot. These findings may be considered the explanation to the behaviour reported in this research, and it may confirm the predominance of Bi_2O_3 layers and its influence on the results obtained.

At the beginning of the research the change in the behaviour of the electrode was observed, this may also be associated with the distribution of Bi on the surface. Bi distribution on the electrode is non uniform, although the conditions of the electrodeposition for instance the stirring rate, the deposition time and the deposition potential remained unchanged. This behaviour is reported in previous works such as [101].

Another probable reason that may be considered as a source of irreproducibility, observing stripping voltammograms in Chapter 5, Bi peaks showed different heights and consequently, its charges would also be different. In other words, the concentration of Bi electrodeposited on the surface may have varied randomly, reminding that the concentration of Bi spiked in the cell was the same for all the experiments as observed in Figure 5.31, section 5.2.3.2.1 in Chapter 5. However, the variation of the quantity of Bi deposited on the surface to form the alloy with Zn or Pb influence significantly in the result of the stripped peak. As per the literature, a large amount of Bi electrodeposited may lead to a higher amount of the alloy in the surface and consequently, a detection of larger amount of Pb or Zn [50,102]. So, if the concentration of Bi was constant in all the experiments, for each concentration of Pb/Zn standard solutions or for a sample, independently of the number of replicas, the results would be approximate, and the precision of the result would be higher, leading to a very low standard deviation.

Moreover, the electrolyte in which Bi solution was prepared, has also had an influence in the results obtained. The majority of supporting electrolytes tend to complex metal ions, this complexation can shift the potential along the potential axis. Though, the shift reported relies on the nature of the complex produced. Besides, a positive shift is also expected for higher concentrations of the analyte as the interaction with the electrode material, distribution on the surface determine and the amount plated the activity of the deposit [182]. In this research, two comparatives approaches are investigated, Bi solution prepared in 0.1 M acetate buffer pH 4.5 and 0.1 M HNO_3, observing the results, the analyte (Zn or Pb) peak heights are greater when Bi is prepared in 0.1M HNO_3. Such behaviour can be attributed to the incomplete dissolution (or complexation) of Bi in 0.1 M acetate buffer pH 4.5, which leads to a real low concentration than the expected when the solution was prepared. As a result of that, in the same conditions, the amount of Bi electrodeposited on the surface is lower in the case of Bi prepared in acetate buffer. Consequently, the detection of the analytes is greater using Bi in 0.1 M HNO_3 and the charges obtained are higher. On the other hand, the irreproducibility greatly affected analytes peaks when the plating solution was prepared in 0.1 M acetate buffer pH 4.5; as to obtain the best straight line from the method of least squares, it required to normalize the analyte peak charge to Bi peak charge. As referred earlier, Pb calibration curve study was done with two supporting electrolytes: acetate buffer pH 4.5 and HNO_3, apart from the multiple peaks issue, lower Pb peaks charges were obtained when Bi plating solution is prepared in acetate buffer pH 4.5. As an example, the solution containing 1 µM Pb(II) registered a charge of 44.6 µC in case of acetate buffer and 67.0 µC with 0.1 M HNO_3, that is a quite significant difference in charges. According to the literature, the microscopic structure of the Bi coating on glassy carbon consists of a porous three-dimensional structure, greatly depends on the plating potential and the composition of the plating solution; besides, it has been demonstrated that the thickness of the Bi film affects the peak height and shape in anodic stripping analysis, depending on the targeted metal ions [50,102].

The formation of metallic layers on bare solid electrode surfaces is a more complicated process. In practice, several surface phenomena and the difficulty of determining the activity of the metal film are responsible for the relatively poor theory-experiment correlation [24]. Generally, in a complicated solution, multiple peaks and irreproducible results may be

achieved. The emergence of extra stripping peaks can be attributed to the analyte and its concentration, and the deposition time [182]. However, in this work, multiple peaks were observed although glassy carbon was used as a working electrode unlike the recommendations of the literature. It was observed that lower concentrations of the analytes have produced multiple peaks especially in case of Pb, the details are explained in Chapter 5. The experimental data showed that concentrations below 10 µM Pb(II) present multiple peaks instead of a single one. Though, the reasons for such behaviour are unclear, it may be due to several processes that occur during the stripping which include the facile formation of intermetallic compounds on the surface of the electrode and the different oxidation (stripping) potentials associated with different states of the metal deposits [24]. The range of morphologies of the Bi coating on the electrode surface because of the heterogeneous composition of the solid surface after deposition results in different free energies required for the metal (or alloy) stripping from the electrode surface (source of changeable peak positions and broader peaks) [24,127]. Another probable reason is incomplete stripping which includes the deposition of a large extent of the metal on the electrode surface and in turn its incomplete removal during the stripping step [24]. Repeated deposition/stripping measurements using the same electrode and also the conversion of the deposited metal to a less electrochemically active form, such as metal oxide/hydroxide (as a result of a reaction with another specie such as oxygen/hydroxide in the solution) may also affect the stripping peak [24]. In this research, only Pb exhibited the multiple peaks behaviour; this may be attributed to the nature of Pb-Bi alloy produced under the conditions used in this work, the deposition potential chosen for this individual study was -0.6 V vs. Calomel (1 M KCl). Literature reports such as [102] and [203] have investigated Pb detection using Bi modified in carbon substrates, they have mainly focused on simultaneous determination of Pb with Cd and Zn, the deposition potential was more negative preferably -1.4 V when the determination includes Zn and around -1.1 V with Cd. Their results have not reported any multiple peaks behaviour. However, this study focused individually on Pb, and the deposition potential chosen seemed to be less negative (-0.6 V vs. Calomel (1M KCl)), this may also be the reason of the emergence of multiple peaks, although this was overcome by applying an extensive electrochemical cleaning.

Besides, low concentration of the analyte may also be affected by the impurities encountered on the surface, since an extensive electrochemical cleaning has greatly contributed to address this situation.

The samples were analysed in two groups namely natural and tap water. As described in Chapter 6, all the samples are treated applying the same procedure. The results have shown a low precision although, in the same order of magnitude. Two samples of each type were submitted to the analysis in order to evaluate the concentration of Pb or Zn in the sample. Normally, the natural water has a more complex matrix than the tap water, as the latter is treated before its distribution. The results of the samples, in short, for the tap water Morpeth Street and Stanton Street have an estimate of 24.6 and 13.5 µg/L, and its standard deviation 6.8 and 8.3 respectively when it was used the first Zn calibration curve for calculation. In the case of natural water, 14.5 and 5.9 µg/L are respectively estimated as the concentration of Zn for Blaydon Burn and Blaydon Bridge, and its standard deviation 3.5 and 0.5. Thus, the lowest standard deviation was recorded for natural waters, that means, the precision of the analysis is higher especially from Blaydon Burn, since the number of experiments is considerable unlike Blaydon bridge's which was submitted to only two experiments (this refers to successful experiments). A closer look at the results, contrary to the expectation, Zn concentration is higher in Morpeth Street which is a tap water instead of a natural water. This is also confirmed by ICP-MS and ICP-OES results. Reminding that, these two techniques were executed by an independent group based in Devonshire building at Newcastle University.

Additionally, the standard addition method was employed to compare the results of the calibration curve and ICPs, however, one of each type of samples was executed as described in Chapter 6, section 6.3.4. Two samples one of each type were submitted to this analysis, Morpeth Street for tap water and Blaydon Burn for natural water, the results are approximate to those obtained with calibration curve, 19.7 and 16.2 µg/L of Zn are estimated respectively. The volume of the standards incremented can be considered low, varying from 100 to 500 µL; nonetheless, the values of the charges reported are extremely higher for such low volumes added. This is also reflected in the values of the slope of each standard addition curve, 2688.4 for Blaydon Burn and 1025.6 for Morpeth Street. Despite that the results come in accordance with the calibration curve and ICPs, it may be thought that a contamination in the system or an influence of the matrix can have caused this condition. On the other hand, this matrix

effect is highly observed in natural water, since Zn peak charges for this type of sample are greater than in tap water, the complexity of the matrix can be the reason of such performance.

In terms of accuracy the results can be considered accurate, since they are comparable to others obtained using sophisticated techniques as ICPs (ICP-OES and ICP-MS). Nevertheless, this electroanalytical technique approach is not beneficial for routine analysis. The length of the experiment is beyond expectation, longer than estimated. On the other hand, the cleanliness of the electrode is fundamental as to ensure single and sharp peaks are obtained. This method is subject to constant change in the electrode behaviour, this is an inconvenience in the precision of the results and lead to some ambiguity.

In addition to that, the limit of detection (LOD) and quantitation (LOQ) were also estimated for Pb and Zn according to the regression data of its calibration curves obtained in Chapter 5, section 5.2.2.2.1 and 5.2.3.2.1. The limit of detection (LOD) is described as the minimum concentration of the analyte that can reliably be detected with a specified level of confidence, whereas the limit of quantitation (LOQ) is the lowest concentration of the analyte that can be determined with an acceptable level uncertainty [54,78]. For a linear calibration curve, it is expected that the instrument response *y* is linearly related to the standard concentration *x* for a limited range of concentration. The slope of the calibration graph defines correctly the sensitivity of the technique providing the plot is linear, and the measurement can be performed at any point in it. Therefore, the LOD and LOQ can be expressed as follow:

$$LOD = \frac{3.3s}{m} \qquad Equation\ 7.1$$

$$LOD = \frac{10s}{m} \qquad Equation\ 7.2$$

Where *s* is the standard deviation of the response and *m* is the slope of the calibration curve. the standard deviation of either y-residuals, or y-intercepts, of regression lines can be employed to estimate the standard deviation of the response [76,129]. The application of this method can be recommended for all cases, though, it is mostly applicable when the background noise is not involved in the analysis method. Using equations 7.1 and 7.2 alongside with the regression parameters and the samples conditions applied in this work,

the LOD and LOQ estimated for Pb as 1.17 µg/L and 3.56 µg/L, and for Zn 0.252 µg/L and 0.764 µg/L respectively.

Chapter 8: Conclusion

Throughout this work, it is demonstrated that Bi modified electrode on glassy carbon substrate shows a complex behaviour when employed. Constant changes in its behaviour have constituted an obstacle to the obtainment of accurate and reliable results. Consistent cleanliness control on the electrode is required, though, this has turned the procedure extremely extensive. The fact of being lengthy, discards it for routine works, unless necessary in case of financial limitations to obtain certified techniques as ICPs and AAS.

According to the literature consulted throughout this work such as references [4,50,102], glassy carbon is recommended to produce Bi modified electrodes. However, the results of this research showed a different perspective. A good reproducibility is one of the advantages mentioned in the literature while using glassy carbon, yet, the experimental results exhibit a low precision, although acceptable, in the results from standards to produce calibration curve to the samples in repeated trials.

Despite irreproducibility problems, the results are satisfactory as compared to certified techniques present similar results, the margin of difference between the two technique is not significant as confirmed by the values of t-test estimated (at 95% confidence), which can be found in the Appendix section (Appendix A).

The project brought some surprising outcomes such as the influence of oxygen on the deposition. Initially, it was expected that Bi would be in its fundamental state; however, in the working conditions of this work (room temperature), layers of Bi_2O_3 have covered the surface predominantly. The approach established in this research is essentially evaluating the performance of glassy carbon electrodes. The glassy carbon electrodes change in behaviour may have brought about irreproducibility problems, that affected the reliability of these results. The approach investigated in this work is not appropriate for routine analysis due to the length of time that a single experiment does take to be completed, though, real samples can be selected for the application of this approach. Even though the experiments were done in the presence of N_2 purging throughout, oxygen was not entirely suppressed in the system which may have led to the oxidation of Bi to Bi_2O_3, producing its layer on the surface.

Unfortunately, it was not possible to achieve the detection at lower deposition time for 10 minutes is such a long time for a range of 1-10 µM for both analytes Pb and Zn. Reminding that the issue reported as multiples peaks behaviour in the stripping peaks of Pb at lower concentration requires to be clarified, though, several reasons have been suggested.

Future works and recommendations

One of the perspectives for future works is to undergo the study of the interferences. Furthermore, the reduction of the deposition time for the range studied is also a prospect that needs to be looked into in order to reduce the analysis time per sample.

The presence of oxygen in the surface is also important factor that requires further studies, since N_2 purging throughout the procedure was insufficient to address this issue. As a probable reason for the emergence of multiple peaks in cases of Pb stripping for concentration below 10 µM is thought to be the fact of using a less negative potential as deposition potential which may have affected the composition of the alloy Pb-Bi formed during the deposition step. Thus, futures studies should also be directed to investigate the composition of this alloy formed in these working conditions and the implication of the deposition potential in this matter by variating it sequentially to more negative potential without the application of an extensive electrochemical cleaning.

Besides, since the working electrode selected for this research has constituted an issue and could be considered responsible of the irreproducibility issues reported. Therefore, future works should also aim the use of other reference electrodes (such as screen-printed electrodes, carbon paste electrodes…) preferably non solid electrodes.

Chapter 9: Bibliography

[1]. D. Agustini, A. S. Mangrich, M. F. Bergamini, L. H. Marcolino-Junior, *Talanta*, 2015, **142**, 221–227.

[2]. A. Alessandrini, P. Facci, *Meas. Sci. Technol*, 2005, **16,** 65–92.

[3]. G. M. S. Alves, L. S. Rocha and H. M. V. M. Soares, *Talanta*, 2017, **175**, 53–68.

[4]. F. Arduini, J. Q. Calvo. A. Amine, G. Palleschi and D. Moscone, *Trends in Analytical Chemistry*, 2010, **29,** 11, 1295-1304.

[5]. D. W. M. Arrigan, *Analyst*, 1994, **11**, 1953–1966.

[6]. G. Attard G and C. Barnes, *Surfaces*, Oxford Chemistry Primers, Seattle, 1998, p. 27.

[7]. P. Atkins and J. De Paula, *Atkin's Physical Chemistry*, Oxford University Press, Oxford, 2014.

[8]. R. Ayala, J. M. Martinez, R. R, Pappalardo, K. Refson and E. S. Marcos, *J. Phys. Chem. A,* 2018, **122**, 7, 1905–1915.

[9]. C. Baird and M. Cann, *Environmental Chemistry*. 5th ed., W. H. Freeman and Company, New York, 2012.

[10]. K. Bansod, T. Kumar, R. Thakur, S. Rana and I. Singh, *Biosens. Bioelectron.*, 2017, **94**, 443–455.

[11]. A. J. Bard, *Electroanalytical Chemistry, A Series of Advances*, M. Dekker, 1966.

[12]. A. J. Bard and L. R. Faulkner, *Electrochemical Methods*, John Wiley and Sons, Danvers, 2001.

[13]. J. Barón-Jaimez, M. R. Joya, J. Barba-Ortega, 2013, J. Phys.: Conf. Ser, **466**, 012025.

[14]. G. C. Barker and A. W. Gardner, *Analyst*, 1992, **117**, 1811– 1828.

[15]. G. C. Barker and I. L. Jenkins, *Analyst*, 1952, **77**, 685– 696.

[16]. G. E. Batley, *Mar. Chem.*, 1983, **12**, 107–117.

[17]. J. K. B. Bernadelli, F. R. Lapolli, C. M. G. d. S. Cruz and J. B. Floriano, *Material Research,* 2011, **14(3),** 366-371.

[18]. Z. Bi, C. S. Chapman, P. Salaün and C. M. G. Van Den Berg, *Electroanalysis*, 2010, **22**, 2897–2907.

[19]. G. Binnig, C. F. Quate, Ch. Gerber, *Physical Review Letters*, 1986, **56** (9), 930–933.

[20]. Biologic Science instruments, *Calculation of the Platinum's active surface (Fuel Cell ECSA)- Application note #11*, 2005. Available at: www.biologic.net.

[21]. Biologic Science instruments, EC-Lab and BT-Lab Software: Techniques and Applications, 2017.

[22]. A. Bobrowski, A. Królicka, J. Śliwa and J. Zarębski, *Electrochim. Acta*, 2017, **252**, 453–460.

[23]. J. O. M. Bockris, A. K. N. Reddy and M. Gamboa-Aldeco, *Modern Electrochemistry 2A*, Kluwer Academic Publisher, New York, 2002.

[24]. A. J. Borril, N. E. Reily and J. V. MacPherson, *Analyst*, 2019, **144(23)**, 6834-6849.

[25]. H. E. Bradl, *in Heavy Metals in the Environment: Origin, Interaction and Remediation*, ed. H. E. Bradl, Elsevier, Amsterdam, 2005, Chap. Sources and Origins of heavy metals, pp. 15-20.

[26]. K. Z. Brainina, *Talanta*, 1971, **18**, 513–539.

[27]. K. Brainina and E. Neyman, *Electroanalytical stripping method*, Wiley intersciences publications, New York, 1993.

[28]. M. Brand, I. Eshkenazi and E. Kirowa-Eisner, *Anal. Chem.*, 1997, **69**, 4660–4664.

[29]. C. M. A. Brett and A. M. Oliveira Brett, *J. Electroanal. Chem.*, 1989, **262**, 83–95.

[30]. D. A. C. Brownson and C. E. Banks, *The handbook of Graphene electrochemistry*, Springer, London, 2014.

[31]. P. J. Bryant, R. G. Miller, R. Yang, *Applied Physics Letters,* 1988, **52**(26), p. 2233–2235.

[32]. J. Caie, X. Zhou, Y. Tu, G. Feng, C. Huang, *Adv. Mat. Lett*, 2012, **3**(2), 87-91.

[33]. M.T. Castaneda, B. Perez, M. Numera, M. Del Valle, A. Merkoci, A. Alegret, *Analyst* (Cambridge, UK), 2005, **130**, 971.

[34]. S. Cerovac, V. Guzsvány, Z. Kónya, A. M. Ashrafi, I. Švancara, S. Roncevic, A. Kukovecz, B. Dalmacija, K. Vytras, *Talanta,* 2015, **134**, 640–649.

[35]. M. A. Chamjangali, H. Kouhestani, F. Masdarolomoor, H. Daneshinejad, *Sens Actuators B,* 2015, **216**, 384–393.

[36]. C. S. Chapman and C. M. G. Van Den Berg, *Electroanalysis*, 2007, **19**, 1347–1355.

[37]. S. J. Cobb and J. V. Macpherson, *Anal. Chem.*, 2019, **91**, 7935–7942.

[38]. M. Cole, P. Lindeque, C. Halsband and T. S. Galloway, *Marine Pollution Bulletin*, 2011, **62**(12), pp. 2588-2597.

[39]. T. R. Copeland, R. A. Osteryoung and R. K. Skogerboe, *Anal. Chem.*, 1974, **46**, 2093–2097.

[40]. T. R. Copeland and R. K. Skogerboe, *Anal. Chem.*, 1974, **46**, 1257A–1268A.

[41]. R. G. Compton and C. E. Banks, *Understanding Voltammetry*, Imperial College Press, 2010.

[42]. L. Cui, J. Wu and H. Ju, *Biosens. Bioelectron.*, 2015, **63**, 276–286.

[43]. Reversibility – Chemical vs. electrochemical, https://chem.libretexts.org/@go/page/61288, (accessed January 2018).

[44]. S. Dal Borgo, V. Jovanovski, B. Pihlar, S. B. Hocevar, *Electrochim Acta*, 2015, **155**, 196–200.

[45]. R. D. DeMars and I. Shain, *Anal. Chem.*, 1957, **29**, 1825.

[46]. V. J. M. Di Maio, *Forensic Pathology.* 2nd ed, CRC Press, Boca Raton, 2001.

[47]. A. Dekanski, J. Stevanovic, R. Stevanovic, B. Z. Nicolic and V. M. Jovanović, *Carbon*, 2001, **39**, 1195–1205.

[48]. J. Duay, J. E. Ortiz-Santiago and T. N. Lambert, *Electroanalysis*, 2017, **29**, 2685–2688.

[49]. P.J. Eaton and P. West, *Atomic force microscopy*, Oxford University Press, Oxford, 2014, Pp.23-24.

[50]. A. Economou, *Trends in Analytical Chemistry*, 2005, **24**(4), pp. 334-340.

[51]. A. Economou, Sensors, 2018, **18**, 1–23.

[52]. N. Elgrishi, K. J. Rountree, B. D. McCarthy, E. S. Rountree, T. T. Eisenhart and J. L. Dempsey, *J. Chem. Educ.*, 2018, **95**, 197–206.

[53]. W. D. Ellis*, J. Chem. Educ.*, 1973, **50**, A131.

[54]. S. L. Ellison, V. J. Barwick and T. J. D. Farrant, *Practical Statistics for the Analytical Scientist. A Bench Guide*, 2nd Edition, RSC Publishing, Cambridge, 2009.

[55]. R. C. Engstrom, *Anal. Chem.* 1982, **54**, 13, 2310–2314.

[56]. R. C. Engstrom and V. A. Strasser, *Anal. Chem.* 1984, **56**, 2, 136–141.

[57]. J. Emsley, *Nature''s Building Blocks*, Oxford university Press, Oxford, 2011.

[58]. L. Fang, Q. Tao, M. Li, L. Liao, D. Chen and Y. Chen, *Chin. J. Chem. Phys*, 2010, **23**, 5, 543-548.

[59]. T. M. Florence, *Analyst*, 1986, **111**, 5, 485-505.

[60]. T. M. Florence, *J. Electroanal. Chem.*, 1970, **27**, 273–281.

[61]. T. M. Florence, *Talanta*, 1982, **29**, 345–364.

[62]. T. M. Florence, *Water Res.*, 1977, **11**, 681–687.

[63]. T. M. Florence, G. E. Batley and P. Benes, *CRC Crit. Rev. Anal. Chem.*, 1980, **9**, 219–296.

[64]. W. T. Fonseca, R. M. Takeuchi, A. L. Santos, *Electroanalysis*, 2015, **27**, 1616–1624.

[65]. C. I. Fort, L. C. Cotet, A. Vulpoi, G. L. Turdean, V. Danciu, L. Baia, I. C. Popescu, *Sens Actuators B*, 2015, **220**, 712–719.

[66]. G. J. Fosmire, *The American Journal of Clinical Nutrition*, 1990, **51**(2), 225-227.

[67]. N. A. Geisse*, Materials Today, 2009*, **12** (7–8), 40–45*.*

[68]. A. Giacomino, A. Ruo Redda, S. Squadrone, M. Rizzi, M. C. Abete, C. La Gioia, R. Toniolo, O. Abollino and M. Malandrino, *Food Chem.*, 2017, **221**, 737–745.

[69]. F. Giessibl, *Reviews of Modern Physics*, 2003, **75** (3), 949–983

[70]. J. Goldstein, *Scanning Electron Microscopy and X-Ray Microanalysis*, Springer, Boston, 2003.

[71]. H. Greschonig and K. J. Irgolic, *Appl. Organomet. Chem.*, 1992, **6**, 565–577.

[72]. D. T. Grubb, in *Polymer Sciences: A comprehensive reference*, ed. K. Matyjaszewski and M. Moller, Elsevier, Amsterdam, 2012, Chapter 2.17, pp. 465-478.

[73]. N. I. Gumerova, A. Rompel, *Nature Reviews Chemistry,* 2018, **2** (2), 1–20.

[74]. M. B. Gumpu, S. Sethuraman, U. M. Krishnan and J. B. B. Rayappan, *Sens. Actuators, B*, 2015, **213**, 515–533.

[75]. C. Hao, Y. Shen, J. Shen, K. Xu, X. Wang, Y. Zhao, C. Ge, *Microchim Acta,* 2016, **183**, 1823–1830.

[76]. D. C. Harris, *Quantitative Chemical Analysis*, Freeman Palgrave Macmillan, New York, 2010.

[77]. D. Harvey, *Analytical Chemistry 2.0*, McGraw-Hill, San Francisco, 2000, Chap 5: Standardizing Analytical Methods, 153-202.

[78]. D. Harvey, *Modern Analytical Chemistry*, McGraw-Hill, Boston, 2000.

[79]. P. J. Harvey, H. K. Handley and M. P. Taylor*, Environmental Science and Pollution Research,* 2015, **22**(16), pp. 12276-12288.

[80]. M. Hävecker, S. Wrabetz, J. Kröhnert, L. Csepei, R. Naumann d'Alnoncourt, Y. V. Kolen'Ko, F. Girgsdies, R. Schlögl, A. Trunschke, *J. Catal, 2012,* **285**, 48–60*.*

[81]. A. B. M. Helaluddin, R. S. Khalid, M. Alaama and S. A. Abbas, *Trop. J. Pharm. Res.*, 2016, **15**, 427–434.

[82]. M. Hersey, S. N. Berger, J. Holmes, A. West and P. Hashemi, *Anal. Chem.*, 2019, **91**, 27–43.

[83]. D. B. Hibbert, *Analyst*, 2006, **131**(12), 1273-1278.

[84]. S. B. Hocevar, S. Daniele, C. Bragato, B. Ogorevc, *Electrochim Acta,* 2007, **53**,555–560.

[85]. S. B. Hočevar, B. Ogorevc, J. Wang and B. Pihlar, *Electroanalysis*, 2002, **14**, 1707–1712.

[86]. S.B. Hocevar, I. Svancara, K. Vytras, B. Ogorevc, *Electrochim. Acta*, 2005, **51**, 706.

[87]. S. B. Hocevar, J. Wang, R. P. Deo, B. Ogorevc, *Electroanalysis*, 2002, **14**,112–115.

[88]. R. Holze*, Experimental electrochemistry: a laboratory textbook*, Wiley-VCH, Weinheim, 2009.

[89]. S. Hüfner, *Photoelectron spectroscopy: principles and applications*, Springer Verlag, New York, 1995.

[90]. E. A. Hutton, S. B. Hočevar and B. Ogorevc, *Anal. Chim. Acta*, 2005, **537**, 285–292.

[91]. E. A. Hutton, S. B. Hocevar, B. Ogorevc, M. R. Smyth, *Electrochem Commun*, 2003, **5**,765–769.

[92]. E. A. Hutton, B. Ogorevc, S. B. Hocevar, F. Weldon, M. R. Smyth, J. Wang, *Electrochem Commun*, 2001, **3**, 707–711.

[93]. E. A. Hutton, J. T. Van Elteren, B. Ogorevc and M. R. Smyth, *Talanta,* 2004, **63**, 849–855.

[94]. G. H. Hwang, W. K. Han, J. S. Park and S. G. Kang, *Talanta*, 2008, **76**(2), 301-308.

[95]. L. Jarup, Hazards of heavy metal contamination. *British Medical Bulletin,* 2003, **68**(1), p. 168.

[96]. R. A. Jenkins, J. L. De Vries, *Practical X-Ray Spectrometry*. Springer, Eindhoven, 1969.

[97]. C. L. Jost, L. M. di Martos, L. Ferraz, P. C. do Nascimento, *Electroanalysis*, 2016, **28**, 287–295.

[98]. P. Jothimuthu, R. A. Wilson, J. Herren, X. Pei, W. Kang, R. Daniels, H. Wong, F. Beyette, W. R. Heineman and I. Papautsky, Electroanalysis, 2013, 25(2), 401-407.

[99]. V. Jovanoski, S. B. Hocevar and B. Ogorevc, *Current Opinion in Electrochemistry*, 2017, **3** (1), 114–122.

[100]. W. Kang, X. Pei, C. A. Rusinek, A. Bange, E. N. Haynes, W. R. Heineman and I. Papautsky, *Anal. Chem.*, 2017, **89**, 3345–3352.

[101]. G. Kefala, A. Economou and A. Voulgaropoulos, *Analyst,* 2004, **129**(11), 1082-1090.

[102]. G. Kefala, A. Economou, A. Voulgaropoulos and M. Sofonious, *Talanta*, 2003, **61**(5), 603-610.

[103]. J. Kim, W. R. De Araujo, I. A. Samek, A. J. Bandodkar, W. Jia, B. Brunetti, T. R. L. C. Paixão, J. Wang, *Electrochem Commun*, 2015, **51**, 41–45.

[104]. P. Kissinger and W. Heineman, *Laboratory techniques in electroanalytical chemistry*, Marcel Dekker, New York, 1996.

[105]. C. Kokkinos, A. Economou, *Curr. Anal. Chem.*, 2008, **4**, 183.

[106]. C. Kokkinos, A. Economou, I. Raptis, C.E. Efstathiou, *Electrochim. Acta*, 2008, **53**, 5294.

[107]. S. J. Konopka and McDuffie, *Analytical Chemistry*, 1970, **42**(14), 1741-1746.

[108]. A. Królicka, A. Bobrowski, A. Kowal, *Electroanalysis,* 2006, **18**, 1649–1657.

[109]. A. Królicka, A. Bobrowski, *Electrochim Acta*, 2016, **187**,224–233.

[110]. A. Krolicka, R. Pauliukate, I. Svancara, R. Metelka, A. Bobrowski, E. Norkus, K. Kalcher, K. Vytras, *Electrochemistry Communications*, 2002, **4**, 193-196.

[111]. J. Kruusma, C. E. Banks, R. G. Compton, *Anal Bioanal Chem*, 2004, **379**,700–706.

[112]. W. W. Kubiak and J. Wang, *Talanta*, 1989, **36**, 821– 824.

[113]. B. Kyeyune, *Thesis, AIMS African Institute of mathematical Sciences*, 2017. Available at https://www.researchgate.net/publication/322294428_Atomic_Force_Microscopy.

[114]. R. V. Lapshin, in *Encyclopaedia of Nanoscience and Nanotechnology.* Vol 14, ed. H. S. Nalwa, American Scientific Publishers, USA, 2011, Chap. Feature-oriented scanning probe microscopy, pages 105-115.

[115]. K. Y. Lee, A. Ambrosi and M. Pumera, *Electroanalysis*, 2017, **29**, 2444–2453.

[116]. N. Lezi, V. Vyskocil, A. Economou and J. Barek, *Sensing in Electroanalysis*, 2012, **7**, 71-78.

[117]. Y. Li, Y. He, J. Qiu, J. Zhao, Q. Ye, Y. Zhu, J. Mao, *Materials Research*, 2018, **21** (6).

[118]. G. Liang, L. Pan and X. Liu, *Int. J. Environ. Res. Public Health*, 2017, **14**, 1–10.

[119]. J. J. Lingane, *J. Am. Chem. Soc*.,1945,**67**,1916.

[120]. G.G. Long, L.D. Freedman, G.O. Doak, in: Encyclopedia of Chemical Technology, ed. M. Grayson, Wiley, New York, USA, 1978, Chap. Bismuth and bismuth alloys pp. 912–937.

[121]. W. Lund and R. Eriksen, *Anal. Chim. Acta*, 1979, **107**, 37– 46.

[122]. P. J. Mafa, A. O. Idris, N. Mabuba, O. A. Arotiba, *Talanta*, 2016, **153**, 99–106.

[123]. P. Manisankar, G. Selvanathan, S. Viswanathan and H. Gurumallesh Prabu, *Electroanalysis*, 2002, **14**, 1722– 1727.

[124]. R. María-Hormigos, M. J. Gismera, J. R. Procopio, M. T. Sevilla, *J Electroanal Chem*, 2016, **767**,114–122.

[125]. R. L. McCreery, *Chem. Rev,* 2008, **108**, 7, 2646–2687.

[126]. E. A. McGaw and G. M. Swain, Anal. Chim. Acta, 2006, **575**, 180–189.

[127]. D. Menshykau and R. G. Compton, *J. Phys. Chem. C*, 2009, **113**, 15602–15620.

[128]. R. A. Meyers, D. T. Sawyer, U. J. Krull and M. Thompson, *Encyclopedia of Physical Science and Technology-Analytical Chemistry*, American Press, San Diego, 2002.

[129]. J. N. Miller, J. C. Miller and R. D. Miller, *Statistics and Chemometrics for Analytical Chemistry*, 7th Edition, Pearson, Harlow, 2018.

[130]. O. Mikkelsen and K. H. Schroder, *Electroanalysis*, 2003, **15**, 679–687.

[131]. B. Molinero-Abad, D. Izquierdo, L. Pérez, I. Escudero and M. J. Arcos-Martínez, *Talanta*, 2018, **182**, 549–557.

[132]. P. M. S. Monk, *Fundamental of electroanalytical chemistry*, John Wiley and Sons, Chichester, 2001.

[133]. S. M. Moosavi and S. Ghassabian, in *Calibration and validation of Analytical methods: A sampling at current approaches*, ed. M. Stauffer, IntechOpen, London, 2018, Chap 6:A review of Criteria for Assessment of Methods reliability, 109-127.

[134]. J. F. Moulder, W. F. Stickle, P. E. Sobol and K. D. Bomben, *Handbook of X-ray photoelectron Spectroscopy*, Perkin Elmer Corporation, Eden Prairie, 1992.

[135]. R. Naumann d'Alnoncourt, L. I. Csepei, M. Hävecker, F. Girgsdies, M. E. Schuster, R. Schlögl, A. Trunschke, *Journal of Catalysis,*2014, **311,** 369–385.

[136]. R. S. Nicholson and I. Shain, *Anal. Chem.*, 1964, **36**, 706– 723.

[137]. M. A. Nolan and S. P. Kounaves, *Anal. Chem.*, 1999, **71**, 3567–3573.

[138]. F. Ohnesorge, *Science, 1993, **260** (5113), 1451–6.*

[139]. J. W. Olesik, *Anal. Chem.*, 1991, **63**, 12A–21A.

[140]. J. G. Osteryoung and R. A. Osteryoung, *Anal. Chem.*, 1985, **57**, 101A–110A.

[141]. R. A. Osteryoung and J. Osteryoung, *Philos. Trans. R. Soc. A*, 1981, **302**, 315–326.

[142]. C. Paluszkiewicz, N. Piergies, P. Chaniecki, M. Rękas, J. Miszczyk, W. M. Kwiatek, *Journal of Pharmaceutical and Biomedical Analysis*, 2017, **139**, 125–132.

[143]. E. P. Parry, R. A. Osteryoung, *Anal. Chem*, 1964, **37**, 1634.

[144]. R. Pauliukaite, C. M. A. Brett, *Electroanalysis*, 2005, **17**, 15-16. (1354-1359).

[145]. R. Pauliukaite, S. B. Hocevar, B. Ogorevc, J. Wang, *Electroanalysis,* 2004, **16**,719–723.

[146]. K. Pecková, J. Musilová and J. Barek, *Crit. Rev. Anal. Chem.*, 2009, **39**, 148–172.

[147]. J. Perry and E. L. Vanderklein, *Water Quality: Management of a Natural Resource,* Blackwell Science, Cambridge, 1996.

[148]. G. D. Pierini, M.F. Pistonesi, M. S. Di Nezio, M. E. Centurión, *Microchem J*, 2016, **125**, 266–272.

[149]. M. Protasowicki, in *Toxins in Food*, ed. W. M. Dabrowski and Z. E. Sikorski, CRC Press, Boca Raton, 2004, Chap. 10, 237-249.

[150]. Rahmayeni; A. Alfina, Y. Stiadi, H. J. Lee, Zulhadjri, *Materials Research*, 2019, **22** (5).

[151]. Z. Rasic-Milutinovic and D. Jovanovic, in *Health Effects of Metals and Related Substances in Drinking Water*, eds. M. Ferrante, G. Oliveri Conti, Z. Rasic-Milutinovic & D. Jovanovic, IWA Publishing, London, 2013, Chap Toxic Metals, p. 6.

[152]. S. Ray and A.G. Shard, *Analytical Chemistry*, 2011, **83**(22), p. 8659-8666.

[153]. C. Reimann, U. Siewers, H. Skarphagen and D. Banks, *Sci. Total Environ.*, 1999, **239**, 111–130.

[154]. D. T. Richens, *The Chemistry of Aqua Ions. Synthesis, structure and reactivity. A tour through the periodic table of elements*, John Wiley and Sons, Chichester,1997.

[155]. M.A.G. Rico, M. Olivares-Marín, E.P. Gil*, Electroanalysis (NY*), 2008, **20,** 2608.

[156]. T. Romih, S. B. Hocevar, V. Kononenko, D. Drobne, *Sens Actuators B*, 2016.

[157]. D. E. Rusyniak, A. Arroyo, J. Acciani, B. Froberg, L. Kao and B. Furbee, in *Molecular, Clinical and Environmental Toxicology*. vol 2, ed. A. Luch, Birkhäuser Verlag, Basel, 2010, Chap. Heavy metal poisoning: Management of intoxication and antidotes, pp. 365–396.

[158]. A. Sani and I. L. Abdullahi, *Toxicol. Rep.*, 2017, **4,** 72–76.

[159]. F. Scholz, *Electroanalytical methods: Guide to experiments and applications*, Springer, Berlin, 2010.

[160]. K. Shiraishi, *Drug delivery System*, 2014, **29**(1), 83-85.

[161]. D. A. Skoog, D. M. West, F. J. Holler and S. R. Crouch*, Skoog and West'sFundamenta's of Analytical Chemistry*, Cengage, Boston, 2014.

[162]. H. Sopha, J. Roche, I. Švancara, A. Kuhn, *Anal Chem 2014*, **86**,10515–10519.

[163]. S. Stankovic and A. R. Stankovic, in *Green materials for energy, products and depollution*, eds. E. Lichtfouse, J. Schwarzbauer and D. Robert, Springer, Dordrecht, 2013, Chap. Bioindicators of toxic metal, pp. 151-228.

[164]. D. J. Stokes, *Principles and Practice of Variable Pressure Environmental Scanning Electron Microscopy (VP-ESEM)*, John Wiley & Sons, Chichester, 2008.

[165]. Z. Stojek and Z. Kublik, *J. Electroanal. Chem.*, 1979, **105**, 247–259.

[166]. I. Svancara, L. Baldrianova, E. Tesarova, S.B. Hocevar, S.A.A. Elsuccary, A. Economou, S. Sotiropoulos, B. Ogorevc, K. Vytras, *Electroanalysis (NY)*, 2006, **18**, 177.

[167]. I. Švancara, C. Prior, S. B. Hocevar, J. Wang, *Electroanalysis,* 2010, **22**, 1405–1420.

[168]. E. Suzuki, *Journal of Microscopy*, 2002, 208 (*3): 153–157.*

[169]. M. G. Tamba and N. Vantini, *J. Electroanal. Chem.*, 1970, **25**, 235–244.

[170]. W. Tang, J. Bin, W. Fan, Z. Zhang, Y. Yun, Y. Liang, *Anal Methods,* 2016, **8**,5475–5486.

[171]. R. J. Taylor and A. A. Humffray, *Journal of electroanalytical chemistry and interfacial electrochemistry*,1975, **64**, 95-105.

[172]. E. Tesarova, L. Baldrianova, S. B. Hocevar, I. Svancara, K. Vytras and B. Ogorevc, *Electrochim. Acta*, 2009, **54**, 1506–1510.

[173]. R. Trouillon and D. O'Hare, *Electrochim. Acta*, 2010, **55**, 6586–6595.

[174]. C. Van der Horst, B. Silwana, E. Iwuoha and V. Somerset, *Analytical Letters*, 2015, **48**(8), 1311-1332.

[175]. J. F. Van Staden and M. C. Matoetoe, *Anal. Chim. Acta*, 2000, **411**, 201–207.

[176]. N. Vashishtha and S. Sapate, *Materials Research,* 2019, **22** (1).

[177]. D. Voiry, H. S. Shin, K. P. Loh, M. Chhowalla, *Nature Reviews Chemistry,* 2018, **2** (1).

[178]. D. E. Van der Linden and J. W. Dieker, *Analitica Chimica Acta*, 1980, **119**(1), 1-24.

[179]. J. Wang, *Analytical Electrochemistry*, John Wiley and Sons, New Jersey, 2006.

[180]. J. Wang, Electroanalysis, 2001, **13**,1153–1156.

[181]. J. Wang, *Electroanalysis*, 2005, **17**(15-16),1341-1346.

[182]. J. Wang, *Stripping Analysis: Principles, instrumentation and applications*, VCH Publishers, Florida, 1985.

[183]. J. Wang, J. Lu, S. B. Hocevar and P. A. M. Farias, *Anal. Chem,* 2000, **72**, 14, 3218–3222.

[184]. J. Wang, J. Lu, Ü. A. Kirgöz, S. B. Hocevar and B. Ogorevc, *Anal. Chim. Acta*, 2001, **434**, 29–34.

[185]. J. Wang and T. Peng, *Analytical Chemistry*, 1986, **58**(8), 1787-1790.

[186]. J. Wang and J. M. Zadeii, *J. Electroanal. Chem.*, 1988, **246**, 297–305.

[187]. Ian M. Watt, *The Principles and Practice of Electron Microscopy*, Cambridge University Press, Cambridge, 1997.

[188]. M. J. Watt-Smith, J. M. Friedrich, S. Rigby, T. R. Ralph and F. C. Walsh, Journal of Physics (D): Applied Physics, 2008, 41(17). 8 pp.

[189]. D. E. Weisshaar and T. Kuwana, *Analytical Chemistry,* 1985, **57**(1), 378-379.

[190]. Weller, Overton, Rourke and Armstrong, *Inorganic Chemistry*, Oxford University Press, Oxford, 2014.

[191]. M. A. A. Wijayawardena, M. Megharaj, R. Naidu, in *Advances in Agronomy*, ed. D. L. Sparks, Academic Press, London, 2016, Chap. Exposure, Toxicity, Health impacts, and Bioavailability of Heavy Metal Mixtures, pp. 175-234.

[192]. WHO, Guidelines for drinking water quality, WHO, Geneva, 2003.

[193]. WHO, *Lead in drinking water-Guidelines for drinking water quality*, World Health Organization, Geneva, 2011.

[194]. WHO, *Trace elements in human nutrition and health*, 1996.

[195]. S. H. Wu, Z. Y. Zheng, J. F. Zhang, Z. W. Song, L. Fang, J. J. Sun, *Electroanalysis,* 2015, **27**, 1610–1615.

[196]. Y. Xin and Z. Zhang, Analytical Chemistry, 2018, 90, 1068-1071.

[197]. H. Xu, L. Zeng, D. Huang, Y. Xian and L. Jin, *Food Chemistry*, 2008, **109**(4), 834-839.

[198]. X. Xuan, M. D. F. Hossain, J. Y. Park, *J Nanosci Nanotechnol*, 2016, **16**, 11421–11424.

[199]. M. Yang and Z. Hu, *Journal of electroanalytical chemistry*, 2005, **583**, 46-55.

[200]. E. Yeager*, Electrochim. Acta*, 1984, **29**, 1527–1537.

[201]. W. Zhang, S. Zhu, R. Luque, S. Han, L. Hu and G. Xu, *Chem. Soc. Rev.*, 2016, **45**, 715–752.

[202]. D. Zhao, X. Guo, T. Wang, N. Alvarez, V. N. Shanov and W. R. Heineman, *Electroanalysis*, 2014, **26**, 488–496.

[203]. L. Zhu , L. Xu, B. Huang, N. Jia, L. Tan and S. Yao, *Electrochimica Acta*, 2014, **115**, 471-477.

[204]. C. G. Zoski, *Handbook of electrochemistry*, Elsevier Sciences, Amsterdam, 2007.

[205]. P. Zuman, *Crit. Rev. Anal. Chem.*, 2001, **31**, 281–289.

Appendix A: Statistic Test t values

Table A.1: Statistic test t values ASV vs. ICP-OES

Teste t values ASV vs. ICP-OES		
	First curve	Average curve
Stanton Street		
T value	0.704	0.876
Confidence interval	-12.83 to 7.097	-14.32 to 6.77
df	6	6
Standard error of difference	4.072	4.309
P value	0.5078	0.4146
	The difference is considered not significant.	The difference is considered to be not significant
Morpeth Street		
T value	0.8629	1.036
Confidence interval	-14.65 to 6.17	-16.34 to 5.61
df	16	16
Standard error of difference	4.911	5.178
P value	0.401	0.3157
	The difference is to be considered not significant	The difference is to be considered not significant
Blaydon Burn		
T value	2.147	3.577
Confidence interval	-9.054 to 0.167	-8.63 to -2.006
df	10	10
Standard error of difference	2.069	1.487
P value	0.0573	0.005
	The difference is considered to be not quite significant	The difference is considered to be very significant

Table A.2: Statistic test t values ASV vs. ICP-MS

Test t ASV vs ICP-MS		
	First curve	Average curve
Stanton Street		
T	0.457	0.249
confidence interval	-8.105 to 11.83	-9.47 to 11.62
df	6	6
standard error of difference	4.073	4.31
P value	0.664	0.811
	The difference is considered to be not statistically significant	The difference is considered to be not statistically significant
Morpeth Street		
T	0.5879	0.775
confidence interval	-13.29 to 7.52	-14.99 to 6.96
df	16	16
standard error of difference	4.91	5.177
P value	0.5648	0.4497
	The difference is to be considered not significant	The difference is to be considered not significant
Blaydon Burn		
t	0.9154	1.866
confidence interval	-6.49 to 2.71	-6.07 to 0.537
df	10	10
standard error of difference	2.066	1.482
P value	0.3815	0.0916
	This difference is considered to be not statistically significant	The difference is considered to be not quite statistically significant

Table A.3: statistic test t values ASV Calibration curve vs. Standard Addition

Test t ASV Calibration curve vs. Standard Addition		
	First curve	Average curve
	Morpeth Street	
t	1.318	1.126
confidence interval	-15.5 to 3.58	-13.92 to 4.23
df	17	17
standard error of difference	4.529	4.301
P value	0.2049	0.2757
	the difference is to be considered not significant	the difference is to be considered not significant
	Blaydon Burn	
t	0.7007	0.3233
confidence interval	-2.901 to 5.610	-2.79 to 3.75
df	11	11
standard error of difference	1.934	1.486
P value	0.498	0.7525
	This difference is considered to be not statistically significant	the difference is considered to be not statistically significant

Appendix B: Comparison of Zn electrochemical results in the sample: calibration curve and standard addition.

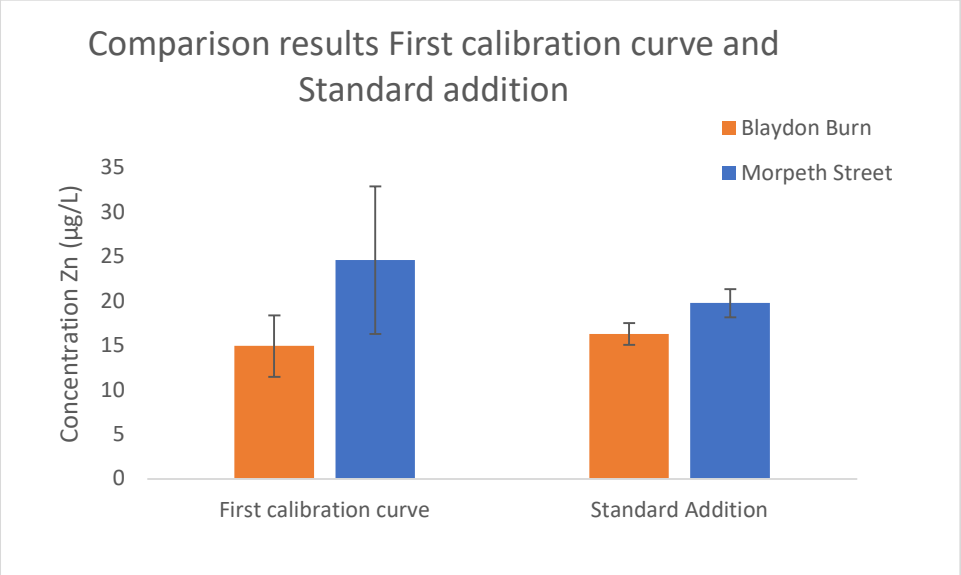

Figure B.1: Figure B2: Comparison results of the concentration of Zn from the first calibration curve and Standard Addition, the error bars on calibration curve columns represent the standard deviation and the standard error on the standard addition columns.

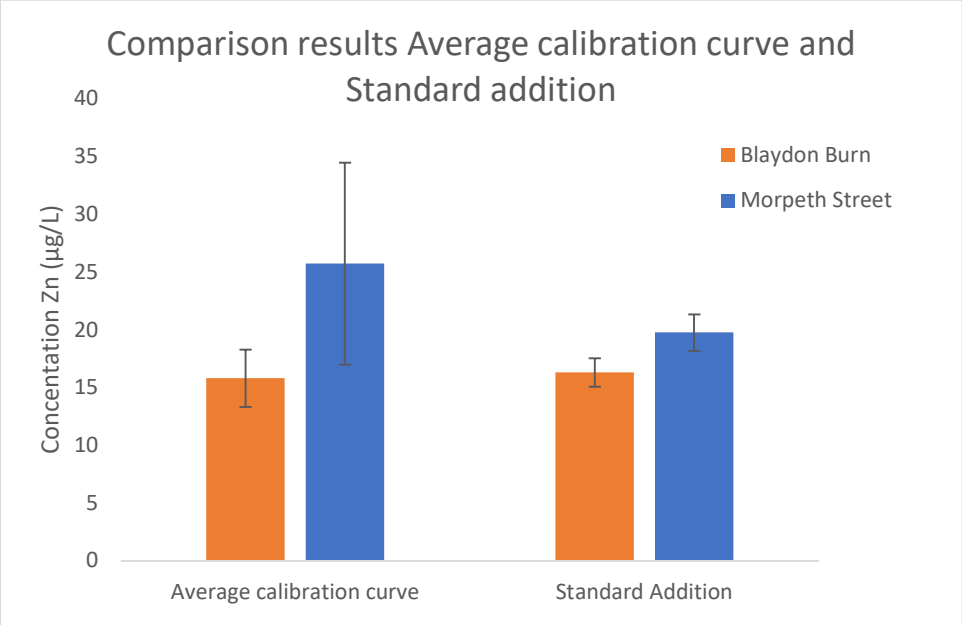

Figure B.2: Comparison results of the concentration of Zn from the Average calibration curve and Standard Addition, the error bars on calibration curve columns represent the standard deviation and the standard error on the standard addition columns.

Appendix C: Thickness of Bi-film under stirred and unstirred conditions from Figures 5.2 and 5.3

Table C.1: Thickness of Bi-film from CA electrodeposition under stirred and unstirred conditions

	Q (Charge)/ mC	N (mol)	*M* (Bi)/ (g)	*d* (cm)	*h* (nm)
CA electrodeposition 250 ppm (1.2 mM) Bi(III) stirred	32.4	1.12E-07	2.34E-05	0.5	121.9
CA electrodeposition 5 mM Bi(III) unstirred	5.8	2.00E-08	4.19E-06	0.5	21.82